universität wien

DISSERTATION / DOCTORAL THESIS

Titel der Dissertation /Title of the Doctoral Thesis

„Evaluation of drug effects regarding novel metal-based as well as natural anticancer compounds by means of bottom-up label-free LC-MS/MS-based proteome profiling“

verfasst von / submitted by

Mag.[a] Dominique Kreutz

angestrebter akademischer Grad / in partial fulfilment of the requirements for the degree of

Doktorin der Naturwissenschaften (Dr.rer.nat.)

Wien, 2018 / Vienna 2018

Studienkennzahl lt. Studienblatt / degree programme code as it appears on the student record sheet:	A 796 605 419
Dissertationsgebiet lt. Studienblatt / field of study as it appears on the student record sheet:	Chemie
Betreut von / Supervisor:	Univ.-Prof. Dr. Christopher Gerner

Acknowledgements

I would like to express my sincere gratitude to

My supervisor Univ.-Prof. Dr. **Christopher Gerner** for giving me the opportunity to perform my thesis in his group on this interesting topic and for his support at all times. The enthusiasm he presents for his research was contagious, motivating and gave rise to great discussions.

Dr. **Astrid Slany** for giving advices where needed, taking care that we stay focused and having a friendly ear at all times.

Dr. **Samuel M. Meier-Menches** for willingly sharing his knowledge about metallodrugs, correcting thus many written pages over and over and always giving valuable inputs.

Dr. **Andrea Bileck** for taking me around the first weeks, introducing me to cell culture, listening, discussing, laughing together - simply for becoming and being such a great friend.

All my former PhD colleagues - Dr. **Rupert L. Mayer**, Dr. **Denise Wolrab**, Dr. **Besnik Muqaku**, Dr. **Ammar Tahir** – for their support, especially when I needed it the most, and all the fun we had.

The next generation of PhD students - **Lukas Janker**, MSc, **Laura Niederstätter**, MSc, **Benjamin Neuditschko**, MSc, and **Julia Brunmair**, MSc - for welcoming me back with open arms and offering help at all times.

Mag. **Günter Walder**, **Peter Frühauf** and DI Dr. **Johanna Mader** for technical support and lab assistance.

Andrea Hilbert for all the administrative help and her positive presence.

My family and friends, especially to my mother **Momo** and my sister **Denise** for always being there and making almost everything possible in particular during the last year. Last, but not least, I want to thank **Werner** for all his support, reminding me that life is not as serious as I sometimes believe and above all I'm grateful for having our son **Alexander** who makes every day a special day.

This doctoral thesis is based on the following publications and manuscripts:

Response Profiling Using Shotgun Proteomics Enables Global Metallodrug Mechanisms of Action To Be Established

Dominique Kreutz, Andrea Bileck, Kerstin Plessl, Denise Wolrab, Michael Groessl, Bernhard K. Keppler, Samuel M. Meier and Christopher Gerner

Chemistry - A European Journal, **2017**, 23 (8), 1881-1890, doi:10.1002/chem.201604516

Curcumin exerts its antitumor effects in a context dependent fashion

Dominique Kreutz, Chomdao Sinthuvanich, Andrea Bileck, Lukas Janker, Astrid Slany, Christopher Gerner

Journal of Proteomics, **2018**, 182, 65-72, doi:10.1016/j.jprot.2018.05.007

Comprehensive assessment of proteins regulated by dexamethasone reveals novel effects in primary human peripheral blood mononuclear cells

Andrea Bileck, Dominique Kreutz, Besnik Muqaku, Astrid Slany, Christopher Gerner

Journal of Proteome Research, **2014**, 13 (12), 5989-6000, doi:10.1021/pr5008625

An Organoruthenium Anticancer Agent Shows Unexpected Target Selectivity For Plectin

Samuel M. Meier, Dominique Kreutz, Lilli Winter, Matthias H. M. Klose, Klaudia Cseh, Tamara Weiss, Andrea Bileck, Beatrix Alte, Johanna C. Mader, Samir Jana, Annesha Chatterjee, Arindam Bhattacharyya, Michaela Hejl, Michael A. Jakupec, Petra Heffeter, Walter Berger, Christian G. Hartinger, Bernhard K. Keppler, Gerhard Wiche and Christopher Gerner

Angewandte Chemie - International Edition, **2017**, 56 (28), 8267-8271, doi:10.1002/anie.201702242

Further contributions enabled the following co-authored publications:

Proteome profiling of breast cancer biopsies reveals a wound healing signature of cancer-associated fibroblasts

Michael Groessl, Astrid Slany, Andrea Bileck, Kerstin Gloessmann, Dominique Kreutz, Walter Jaeger, Georg Pfeiler, Christopher Gerner

Journal of Proteome Research, **2014**, 13(11), 4773–82, doi:10.1021/pr500727h

Quantification of cytokines secreted by primary human cells using multiple reaction monitoring: evaluation of analytical parameters

Besnik Muqaku, Astrid Slany, Andrea Bileck, Dominique Kreutz, Christopher Gerner

Analytical and Bioanalytical Chemistry, **2015**, 407(21), 6525–36, doi:10.1007/s00216-015-8817-9

Proteomic and metabolomic analyses reveal contrasting anti-inflammatory effects of an extract of mucor racemosus secondary metabolites compared to dexamethasone

Samuel M Meier, Besnik Muqaku, Ronald Ullmann, Andrea Bileck, Dominique Kreutz, Johanna C Mader, Siegfried Knasmüller, Christopher Gerner

PLoS One, **2015**, 10(10), e0140367, doi:10.1371/journal.pone.0140367

Contribution of human fibroblasts and endothelial cells to the hallmarks of inflammation as determined by proteome profiling

Astrid Slany, Andrea Bileck, Dominique Kreutz, Rupert L Mayer, Besnik Muqaku, Christopher Gerner"

Molecular and Cellular Proteomics, **2016**, 15(6), 1982–97, doi:10.1074/mcp.M116.058099

Coffee consumption modulates inflammatory processes in an individual fashion

Besnik Muqaku, Ammar Tahir, Philip Klepeisz, Andrea Bileck, Dominique Kreutz, Rupert L Mayer, Samuel M Meier, Marlene Gerner, Klaus Schmetterer, Christopher Gerner

Molecular Nutrition and Food Research, **2016**; 60(12), 2529–2541, doi:10.1002/mnfr.201600328

Evaluation of inflammation-related signaling events covering phosphorylation and nuclear translocation of proteins based on mass spectrometry data

Andrea Bileck, Rupert L Mayer, Dominique Kreutz, Tamara Weiss, Sabine Taschner-Mandl, Samuel M Meier, Astrid Slany, Christoher Gerner

Journal of Proteomics, **2017**, 152, 161–171, doi: 10.1016/j.jprot.2016.11.008

Combined proteome and eicosanoid profiling approach for revealing implications of human fibroblasts in chronic inflammation

Ammar Tahir, Andrea Bileck, Besnik Muqaku, Laura Niederstaetter, Dominique Kreutz, Rupert L Mayer, Denise Wolrab, Samuel M Meier, Astrid Slany, Christopher Gerner

Analytical Chemistry, **2017**, 89(3), 1945–1954, doi: 10.1021/acs.analchem.6b04433

Table of Contents

1. Introduction

1.1. Carcinogenesis

Cancer is among the leading causes of death nowadays, with prostate and breast cancer as the most frequent types among men and women, respectively.[1] Genetic mutations in cells can lead to the transformation of healthy cells to cancerous ones and their proliferation results in the development of tumors.[2] These abnormal cells can infiltrate surrounding tissues and make use of the blood and lymph system to invade distant tissues.

In 2000 Hanahan *et al.*[2] proposed the hallmarks of cancer and expanded them in 2011.[3] They defined eight acquired biological capabilities and their enabling characteristics to characterize the pathogenesis of tumors:

(i) *Resisting cell death* can be realized *via* various strategies; most commonly tumor cells lose the tumor suppressor function of the tumor protein 53 (TP53). Induction of autophagy can contribute to their survival, as can cell death by necrosis through recruiting tumor promoting immune inflammatory cells and release of stimulating factors for neighboring cells.

(ii) *Sustaining proliferative signaling* can be achieved through growth factors that where either produced in an autocrine-fashion or supplied by stimulated tumor-associated stromal cells. Growth factor receptor alterations (structural or in numbers) or downstream signaling activation can contribute to continuous proliferation of cancer cells.

(iii) *Evading growth suppressors* like retino-blastoma-associated and TP53 proteins enable cancer cells to avoid senescence and apoptosis. Contact inhibition can be circumvented and TGF-β signaling might be redirected to epithelial-to-mesenchymal transition (EMT).

(iv) *Enabling replicative immortality* in cancer cells is accomplished by the expression of telomerase, a telomere repeat segment adding enzyme, which is absent in normal cells.

(v) *Activation of invasion and metastasis* can be realized through downregulation of cell-to-cell or cell-to-extracellular matrix (ECM) adhesion molecules, especially E-cadherin. EMT and secreted factors from stromal cells are further contributing to this process. Multiple

steps are succeeded during invasion and metastasis – local invasion, intravastation into and transit through the hematogenous and lymphatic system, extravastation, micrometastation and finally "colonization".

(vi) *Induction of angiogenesis* is an early process in tumor development consecutively depending also on the stromal microenvironment. Regulating factors are not only deriving from the cancer cells themselves, also immune inflammatory cells can contribute. The resulting blood vessels' structure is, however, not fully intact since they show excessive sprouting, enlargements and leakiness.

(vii) *Deregulating cellular energetics* gives cancer cells the possibility to survive in the hypoxic conditions within tumors. Instead of relying on mitochondrial oxidative phosphorylation, the cells may use the less efficient glycolysis to produce ATP, while the secreted lactate can be used by another subpopulation of cancer cells in the tumor microenvironment.

(viii) *Avoiding immune destruction* has become an emerging hallmark since the immune system is supposed to eliminate cancer cells and thus suppresses tumor development.

(ix) *Genome instability and mutation*, as already mentioned, are critical in the development of tumors. Acquisition of various advantageous genetic alterations enables the adaption of the hallmark capabilities discussed above. Cancer cells suppress at least one of the DNA repair pathways giving rise to even more mutations.

(x) *Tumor-promoting inflammation* is an effect coming from cells of the innate as well as the adaptive immune system infiltrating the tumor tissue. These cells can supply the stromal cells with various important molecules like growth and survival factors consecutively leading to tumor progression. Furthermore, the release of reactive oxygen species (ROS) accelerates the acquisition of mutations in cancerous cells.

In addition to the interplay of cancer cells with the immune system, the tumor microenvironment also strongly influences cancer development and progression.[4,5] Furthermore, drug responses are affected by tumor-stroma interactions.[6,7] Healthy stromal cells presumably prevent tumor development; however, signal proteins and proteolytic enzymes secreted by the cancer cells alter the stromal cells into tumor-supporting cells (Figure 1).[8] For example, cancer-associated fibroblasts (CAFs) are more aggressive than naïve fibroblasts. They are an integral part of the tumor microenvironment and influence the initiation of angiogenesis, tumor promotion and invasiveness.

Stromal cells secrete growth factors and other signal molecules to which the tumor becomes addicted. Therefore, novel therapeutic strategies targeting the tumor microenvironment are of great interest.[9] Co-culture models of cancer and stromal cells may hold great potentials to investigate drug effects *in vitro* and may serve as a good model for the *in vivo* situation.[9] Proteome profiling is a powerful tool enabling comprehensive cellular analysis and thus, qualified to investigate tumor-CAF interactions.[10-13]

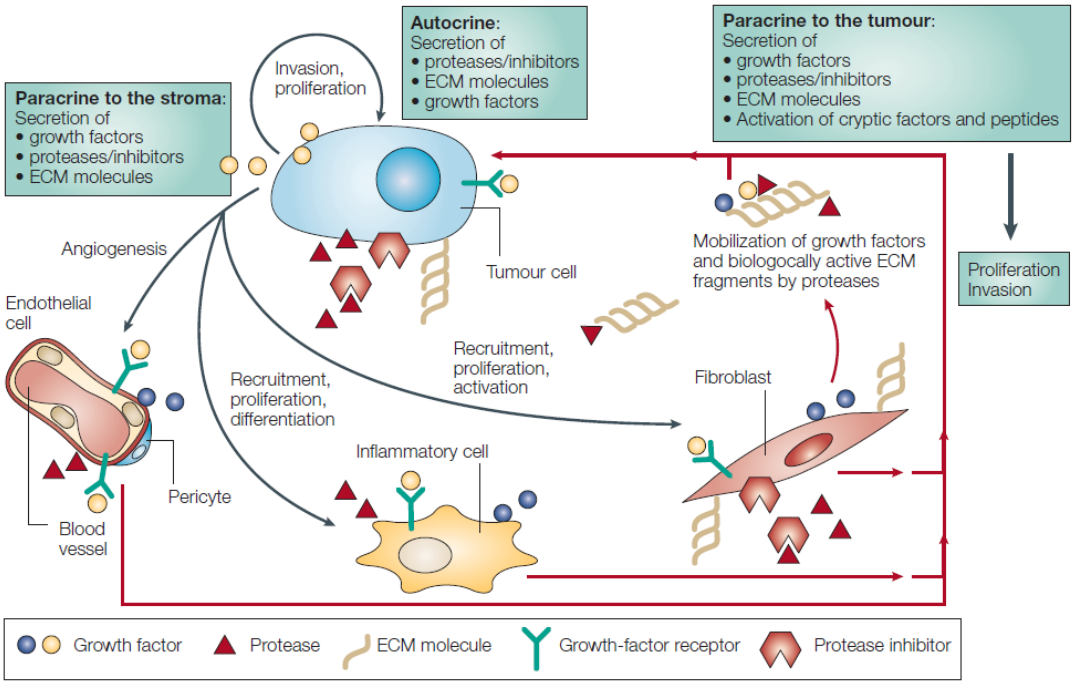

Figure 1 Crosstalk between tumor and activated stromal cells (Reprinted with permission from Mueller & Fusenig, Copyright © 2004 Springer Nature)[8]

1.2. Cancer Therapy

Classical cancer treatments are surgery, chemotherapy and radiotherapy, which are often used in combination.[14] Nitrogen mustards were the first cytotoxic agents introduced in cancer therapy in the 1940s.[15] In the 1960s, combination therapy was implemented and improved patient survival rates tremendously and the application of drug cocktails is still common nowadays.[16,17] Current cytotoxic agents in therapeutic use can be classified according to their mode of action, including

antimetabolites that mimick DNA precursors or hinder DNA synthesis (*e.g.* 5-Fluorouracil, methotrexate), direct DNA-interacting agents that alkylate DNA bases (*e.g.* dacarbazine) or form inter- or intra-strand crosslinks (*e.g.* cisplatin, oxaliplatin, nitrogen mustards), antitubulin agents (*e.g.* taxanes, vinca alkaloids), hormones and monoclonal antibodies.[15,18] Inhibition of kinases and the cell cycle checkpoint have also become interesting targeted strategies for cancer therapy.[19,20] However, the precise mechanisms that would explain drug effectiveness and selectivity (towards cancer rather than normal cells) of many widely applied chemotherapeutics are still not fully elucidated.[14]

Major problems in cancer treatment are innate and acquired resistance, the latter can occur rapidly due to the high tumor heterogeneity and is often responsible for treatment failure.[14] Genetic alterations as well as variations on protein level, like elevated expressions of drug export pumps, can account to their occurrence. Unfortunately resistance is often not only distinct toward a single drug, but to various agents, which is explained by the concept of multidrug resistance (MDR). Consequently, multidrug therapies applying drugs with complimentary modes of action were implemented in cancer therapies. However, toxicity remains a major challenge.

The discovery and development of novel drugs is a long and costly endeavor.[21] Therefore, strategies are becoming more popular that provide a more comprehensive picture of the effects induced upon drug treatment, *e.g.* 'omics' approaches. The gained information gives rise to a better understanding of the drug's behavior and clinical prospective, thereby potentially accelerating the process of drug discovery. Such 'omics' investigations might also enable the discovery of patient stratification parameters for targeted and hence more effective therapies in the clinics. Metal-based compounds and natural products were in the focus of the research projects of this PhD-thesis and will be detailed below.

1.2.1. Metal-based anticancer drugs

The most prominent inorganic anticancer drug is cisplatin (cis-diamminedichloroplatinum(II), CDDP, Figure 2), which was introduced as a potential antitumor agent in 1969[22] and which was followed by next-generation platinum compounds that reduced side effects or overcame resistance, *e.g.* carboplatin and oxaliplatin. Due to their broad anticancer activity these drugs are administered in approximately 50–70% of all cancer therapies to patients and thus, are among the most successful

anticancer agents.[23-25] However, their molecular mechanisms of action are still controversially discussed and not fully understood.

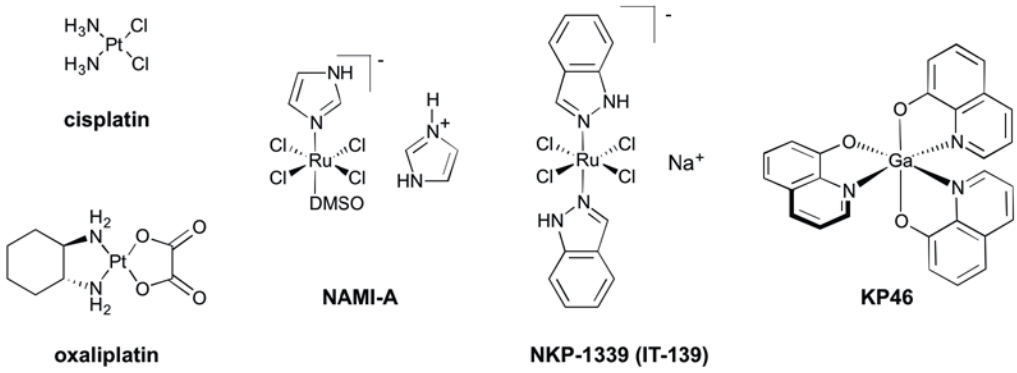

Figure 2 Chemical structures of cisplatin, oxaliplatin, NAMI-A, NKP-1339 and KP46

The mechanism of action of cisplatin generally involves three steps: accumulation, activation and cellular processing.[26] Whether cisplatin enters the cells via passive diffusion or through active transport, is still under discussion, most likely there are multiple pathways.[27] Once inside the cell cisplatin is activated by aquation due to the drop of chloride concentration and subsequently, can react with DNA, forming coordinative covalent (mainly intra-strand) crosslinks with the nucleobases.[26,28] The distortion of the three dimensional DNA structure leads to inhibition of transcription and DNA replication. Specifically, binding of high mobility group proteins shields the DNA-cisplatin adducts from nucleotide excision repair and prevents DNA-repair processes, which usually leads to activation of apoptotic cell death.[26,29] Even though DNA is considered as the main target of cisplatin, there is emerging interest in other possible molecular targets, like proteins, within the cell. Next to the mitochondrial genome the mitochondrial transcription factor A has been proposed as potential target of cisplatin.[30] Furthermore this metallodrug might aim for 3-phosphoinositide-dependent protein kinase 1[31] and long noncoding RNAs.[32]

Cisplatin treatment comes along with severe side effects, over 90% of the patients suffer from nausea and vomiting.[33] Nephrotoxicity is a frequent dose limiting factor in therapy.[34] Neuro- and ototoxicity were also reported adverse effects upon cisplatin treatment. Moreover,

myelosuppression may occur and liver, respiratory system and skin functions may be affected.[33-35] There have been several successful attempts to reduce the toxicity of cisplatin, especially with saline diuresis,[34] but also supplementation with sodium salicylate[36] or glutathione[37] improved the patient's quality of life. In 1992, the cisplatin analogue carboplatin was approved for clinical practice, functioning *via* a similar mode of action.[38] Importantly, carboplatin displays reduced toxicity probably resulting from slower hydrolysis in the circulatory system.[38,39]

Besides adverse effects, resistance phenomena are a major drawback of cisplatin therapy.[26] Various mechanisms can be responsible for their occurrence. Loss of transporter molecules reducing the incorporation of the platinum drug into the cell and enhanced abundances of proteins involved in DNA repair processes can be one reason. Defective mismatch repair pathway, activated survival pathways, *e.g.* through paxillin overexpression, and higher abundances in extracellular matrix proteins enabling reorganization of the matrix are further mediators of cisplatin resistance.[40]

Oxaliplatin (Figure 2) showed promising activity towards colorectal cancer, with intrinsic or acquired resistance against cisplatin or carboplatin. Similarly to cisplatin, DNA damage is considered to be the main cytotoxic effect of oxaliplatin. However, the diaminocyclohexane ligand is more bulky and single-strand breaks occur more often than with cisplatin. Differential cell sensitivity towards oxali- and cisplatin is not fully understood yet. Interaction with mismatch repair proteins, postreplicative bypass mechanisms, downstream transcription pathways and Pt-DNA damage recognition proteins as well as their distinct reaction to DNA adducts seem to contribute to this difference.[25,29]

The challenges of intrinsic and acquired resistance and severity of the side effects of cytotoxic platinum(II) anticancer agents led to the discovery of [[(1R,2R,4R)-4-methyl-1,2-cyclohexanediamine] oxalatoplatinum(II) (KP1537).[41] Besides displaying activity against oxaliplatin resistant cells, this methylated oxaliplatin derivative is depending less on immunogenic cell death and side effects are distinctly reduced. Moreover, research also focused on inorganic anticancer compounds with alternative metal centers. These included compounds based on ruthenium (*e.g.* NAMI-A,[42] KP1019/NKP-1339,[43] or plecstatins[44]), gallium (*e.g.* KP46[45] or gallium maltolate[46]) and lanthanum (*e.g.* KP772[47]). The benefits of using different metal centers are potentially novel modes of actions and reduced side effects compared to the platinum-based drugs. For example, instead of a square-planar geometry as observed for platinum(II) drugs, ruthenium(III) forms octahedral complexes and display altered physicochemical properties, *e.g.* hydrolysis behavior, and may exhibit

potentially novel modes of action.[24] Furthermore, the resemblance to iron and the 'activation by reduction' mechanism are probably responsible for the minor toxicity of ruthenium(III)-based drugs.[24,48,49] Insufficient blood supply in solid tumors results in a hypoxic milieu. The reduced oxygen enables the reduction of the ruthenium(III) to the ruthenium(II) species, which is kinetically more labile. This process was introduced as the 'activation by reduction' theory.[50]

A metallodrug that is already in clinical use is arsenic trioxide (As_2O_3), which displays substantial efficacy in patients with acute promyelocytic leukemia.[51] Furthermore, several not platinum-based metallodrugs have entered clinical trials, namely NKP-1339 (IT-139), NAMI-A, KP46, TDL1433, auranofin and ferroquine.[52-54]

Currently, ruthenium and gallium compounds showed promising results in clinical trials with good tolerability since only mild dose-limiting toxic effects were experienced by the patients.[24,43] Imidazolium trans-[tetrachloro(dimethylsulfoxide)(1H-imidazole)ruthenate(III)] (NAMI-A) (Figure 2) was the first Ru-based drug candidate to enter clinical trials with encouraging efficacy against development and growth of metastases in preclinical trials.[42,55] It affects the interaction between tumor and stroma cells, influencing matrix degradation,[56] cell adhesion,[57,58] invasiveness and migration.[55,56] Bergamo *et al.* investigated regulations in the whole transcriptome of non-tumorigenic and invasive carcinogenic mammary cells by RNA-sequencing, supporting the hypothesis of metastasis inhibition by NAMI-A.[59] There was, however, no effect observable for the drug on the growth of primary tumors.[55] Clinical phase I/II studies on primary tumors had poor outcomes, both as monotherapy and in combination with gemcitabine.[60] However, it would be worthwhile testing NAMI-A in a clinical setting that would directly evaluate the anti-metastatic activity, but such endpoints are not implemented in clinical investigations so far.[61] A promising ruthenium-based drug in clinical trials is sodium trans-[tetrachlorobis(1H-indazole)ruthenate(III)] (NKP-1339) (Figure 2), which features enhanced solubility compared to the indazolium analogue KP1019.[62] The compound is predominantly active against primary tumors, especially on colon cancers in preclinical studies.[62,63] Adverse effects in clinical phase trials were minor and promising results were observed especially for neuroendocrine tumors.[43,64] The mode of action of NKP-1339 is not fully elucidated yet (Figure 3). Once administered intravenously it is believed to bind preferentially to albumin and transferrin in the bloodstream.[65] Due to a higher demand on iron, cancer cells overexpress the transferrin receptor which can lead to accumulation of the Ru compound in these cells. Inside the cells the above mentioned 'activation by reduction' process

takes place. Observed effects upon drug treatment include the induction of reactive oxygen species (ROS) probably via Fenton-like reactions,[64,66] endoplasmic reticulum stress with the glucose-regulated protein of 78 kDa (GRP78) as potential NKP-1339 target,[64] cell cycle arrest in the G2/M phase[67,68] and induction of apoptosis by caspase 8 and the mitochondrial pathway.[66,68]

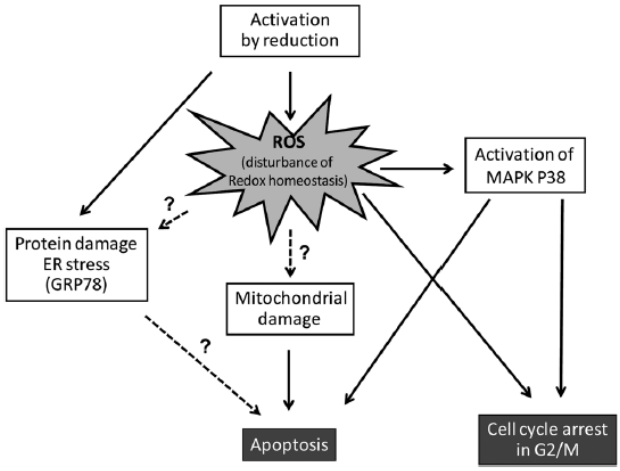

Figure 3 Proposed mechanism of NKP-1339 (Reprinted in accordance with Creative Commons Attribution-NonCommercial 3.0 Unported Licence from Trondl *et al*. Copyright © 2014 - published by The Royal Society of Chemistry)[64]

Furthermore, the coordination complex tris(8-quinolinolato)gallium(III) (KP46) (Figure 2) was undergoing clinical trials.[69] Similarly to ruthenium, the gallium compound was postulated to hijack the transferrin receptor as the main route of cellular accumulation.[70] However, in contrast to the Ru compounds, KP46 is orally bioavailable and targets preferentially bone tissue,[45] displaying activity against osteosarcoma.[71] Due to the interference with cellular iron uptake, the inhibition of the iron depending enzyme ribonucleotide reductase is believed to be responsible for the anticancer activity of KP46.[72] The drug candidate induced loss of cell adhesion, cell cycle arrest in S-phase, apoptosis and autophagy, where the latter is probably a protective reaction of the cells.[71,73] Clinical phase I tests yielded promising results for patients with renal cancer, recommending phase II studies.[70] Another gallium metallodrug that has reached clinical evaluation is gallium maltolate (tris(3-hydroxy-2-methyl-4H-pyran-4-onato)gallium(III)), which was designed to dissemble the iron(II)-maltol complex catering a bioavailable form of iron.[70] Even though gallium maltolate displayed

anticancer activity *in vitro*[74,75] as well as in a patient with hepatocellular carcinoma,[76] clinical studies focused primarily on its antimicrobial activity.[77]

1.2.2. Anticancer drugs from natural sources

Since the beginning of drug screening strategies, natural products were investigated for their anticancer activity. The natural product colchicine isolated from autumn crocus plants was one of the first substances identified as potential anticancer drug inducing cell cycle arrest in mitosis and causing genomic damage in cell cultures. However, high toxicity prevented further trials.[78] Nowadays, the interest in potential anticancer efficacy of dietary phytochemicals like curcumin and resveratrol is increasing due to their effects in cancer patient, which include anti-proliferative, -metastatic, -angiogenic and pro-apoptotic properties as well as alterations of ROS.[79] Moreover, they provoke only minimal side effects. A clinically approved natural product is Paclitaxel (Taxol).[80] This chemotherapeutic agent was isolated from the Pacific yew *Taxus brevifolia* and is used to successfully treat various types of cancer today.[80,81] The naturally occurring compound curcumin is an interesting candidate (Figure 4) and its effects on tumor-stroma interactions in co-culture model systems was investigated in this thesis.

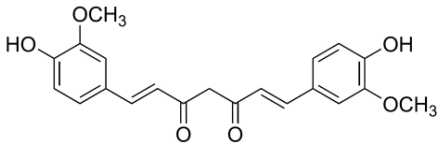

Figure 4 Chemical structure of curcumin

Curcumin is the active agent in turmeric, a dietary spice as well as a herbal agent in traditional Chinese and Indian medicine.[82] The diarylheptanoid displays many valuable characteristics for cancer therapies including anti-inflammatory, antioxidant, chemopreventive, -therapeutic and -sensitizing properties. Reduction of oxidative stress, inhibition of gene transcription regulating oxidative stress and inflammatory response, radioprotective and -sensitizing features were demonstrated for curcumin treatment.[83,84] Chirnomas *et al.* screened for compounds sensitizing resistant cancer cells to chemotherapeutics and found curcumin as a promising sensitizer for

cisplatin treatment.[85] This natural compound served as sensitizer for various drugs in (MDR-)resistant breast cancer cells.[84] Curcumin does not solely act on cancer cells directly, but on the tumor microenvironment as well by inhibiting angiogenesis through downregulation of various proangiogenic proteins, e.g. vascular endothelial growth factor, basic fibroblast growth factor and matrix metalloproteinases.[86]

1.3. Proteome profiling

Proteins are the active players within a cell determining cellular fate and function, and are nowadays frequent drug targets.[87,88] Tracing their regulation upon stress stimuli comprises large amounts of information concerning the involved processes. The comprehensive analysis of proteins within a cell, tissue or organism, the so called proteome, under defined conditions is referred to as proteomics. Since its introduction around 20 years ago,[89] the development of compatible analytical techniques, especially in the field of mass spectrometry (MS), enable nowadays the analysis of thousands of proteins in single sample injections.[90]

1.3.1. Analytical methods in proteomics

Proteins can be identified and quantified by analytical methods that rely either on the use of antibodies (*e.g.* ELISA, Western blot), two-dimensional gel electrophoresis (2-DE) or MS. Also, combinations thereof have been developed, like mass spectrometric immunoassays,[91] where antibodies are first used to target specific analytes, and subsequently MS analysis is performed for identification and quantification. Sensitivity and specificity are more independent from external factors during MS measurements than antibody-based methods, where the quality of the antibodies is the decisive factor. The issue of cross-reactivities due to unspecific binding and poor reproducibility common to antibody assays do not interfere with MS approaches.[92] MS-based proteomics can involve the measurement of intact proteins referred to as top-down proteomics.[93] Conversely, in a bottom-up approach the proteins are first enzymatically digested to peptides, which are then identified by MS and assigned to the respective proteins by algorithms.[94] The analysis of peptides has the advantage that their mass range and fragmentation properties are better compatible with MS instruments than that of intact proteins.[95] In the field of proteomics, liquid chromatography in combination with tandem mass spectrometry (MS/MS) has become the most

powerful strategy of analysis enabling untargeted proteome profiling, *i.e.* detecting not a single or few selected analytes, but all peptides as comprehensively as possible. The bottom-up approach was applied throughout the research projects of this thesis and will be discussed here in more detail.

Nowadays, proteomic studies concentrate on characterizing protein regulations upon stress stimuli, which include changes in their abundance, activity and post-translational modifications. The high complexity and the large dynamic range of proteins in the samples, *e.g.* cell lysates or tissue material, make this a challenging task. Approaches for protein identification and quantification need to be considered carefully.[95] Before the dawn of online MS-based proteomics, 2-DE based on poly acrylamide (2D-PAGE) was a routinely applied protein separation technology.[96] The separation is based on the differences in charge and molecular weight of the proteins. In the first dimension isoelectric focusing enables the separation according to their respective isoelectric point. Then, they are orthogonally separated in a second dimension by their molecular weight resulting in distinct protein spots. The spots are stained, cut out and the protein content is enzymatically digested for subsequent MS-analysis, usually by matrix-assisted laser/desorption ionization – time of flight (MALDI-TOF). Two dimensional – gel electrophoresis is a robust method. Unfortunately, low abundant as well as hydrophobic proteins are challenging to investigate.[89] It enables the identification of around a thousand proteins, however, it is a powerful, but time-consuming method since every single protein has to be prepared and analyzed separately. Furthermore, a cell's proteome comprises a couple of thousands of proteins. Currently almost 16.000 proteins are covered in the ProteomicsDB[97,98] and over 20.000 human proteins (considering only reviewed entries) are listed at UniProt.[99] Identification of such a large number of analytes requires appropriate, high-performance approaches covering large dynamic ranges and also hydrophobic proteins.

Besides in-gel digestion,[100] preparation of proteomics samples often relies on in-solution digestion procedures. Advantages of the latter approach include reduced sample handling and the possibility of automatization, however, they may be more prone to impurities.[101] Filter-aided sample preparation (FASP) allows using detergents for in-solution digestions, increasing the solubility of proteins.[101] Currently, peptide identification of in-solution digested samples is in many cases achieved by LC-MS/MS analysis, where they are first separated on a reversed phase (RP) column according to their hydrophobicity, ionized by electrospray ionization and then analyzed by MS. The peptide sequences are determined via MS/MS fragmentation. Peptide separation by liquid

chromatography prior to fragmentation enhances the accuracy of protein identifications especially in complex samples that are usually investigated in the field of proteomics.[102] The LC performance benefits from applying higher pressure, increasing column length in combination with longer gradients and reduction of particle size of the stationary phase.[90,103] Nowadays, nano-LC systems are routinely used in proteome profiling studies.[104] The main advantage of this technique is the possibility to run flow rates in the nano scale, usually between 200 and 300 nL min^{-1}.[105] This enables the analysis of small sample volumes with little dilution thus enhancing sensitivity, which is especially important for low abundant proteins.[106] Furthermore, the small inner diameter of the nanoLC column (75 µm) requires fewer mobile phase volumes for elution, hence costs for solvents and waste production are reduced, and it facilitates temperature control since heat transfer occurs fast and efficiently.[102,106] The reduced particle size of the stationary phase enhances peak capacity and separation efficiency.[107,108] However, these benefits come at the cost of analysis time, consequently sample throughput, and the operational robustness of the system is lower compared to capillary LC. In order to increase the loading capacity and simultaneously decrease the time needed for sample injection precolumns (also referred to as trapping columns) are inserted prior to the analytical column enabling flow rates between 5 and 20 µL min^{-1} (Figure 5).[105,109] The installation of a switching valve enables the usage of two flow circuits with autonomous pumps.[105] This way samples are desalted, cleaned and preconcentrated online on the trapping column, which otherwise needs to be done off-line with microcolumns.[105,110] A gradient with increasing amounts of organic solvent is employed to elute the peptides from the columns.[104,105] Furthermore, an ion-pairing reagent is added to the mobile phases, trifluoroacetic acid (TFA) and formic acid are the modifiers of choice. TFA, although it has the higher ion pairing strength, interferes with the ionization by ESI and should therefore only be used for sample loading.[105] Nano columns integrated into microfluidic devices (HPLC-Chip) are also applied in proteomic studies.[111] Two dimensional LC has been introduced for proteome profiling analysis under the name multidimensional protein identification technology (MudPIT).[112] It combines two complementary separation techniques, including strong cation exchange (SCX) and RP chromatography, coupled to ESI multiple-stage mass spectrometry (MS^n). By increasing the salt concentration stepwise the peptides are eluted according to their isoelectric points and subsequently separated by RP chromatography with an acetonitrile gradient.

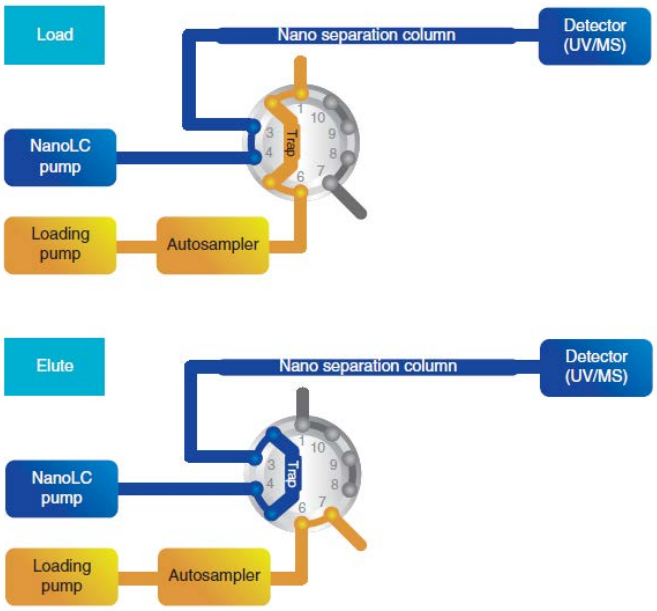

Figure 5 Flow paths for loading over trapping column and elution over separation column in a nanoLC system(Reprinted with permission from Köcher *et al.* Copyright © 2012 Springer Nature)[105]

For MS data acquisition three main approaches have evolved in the field of proteomics: Shotgun proteomics (data dependent acquisition, DDA), targeted proteomics (selected reaction monitoring, SRM, and MS/MS^{ALL}) and SWATH (data independent acquisition, DIA).[95] DDA and DIA both provide a comprehensive analysis of the proteins in a sample, while following distinct data acquisition processes. The former selects specific peptides based on measured MS^1 signals for fragmentation whereas the latter fragments all ions in defined m/z ranges. Targeted analysis is often used for validating shotgun results.

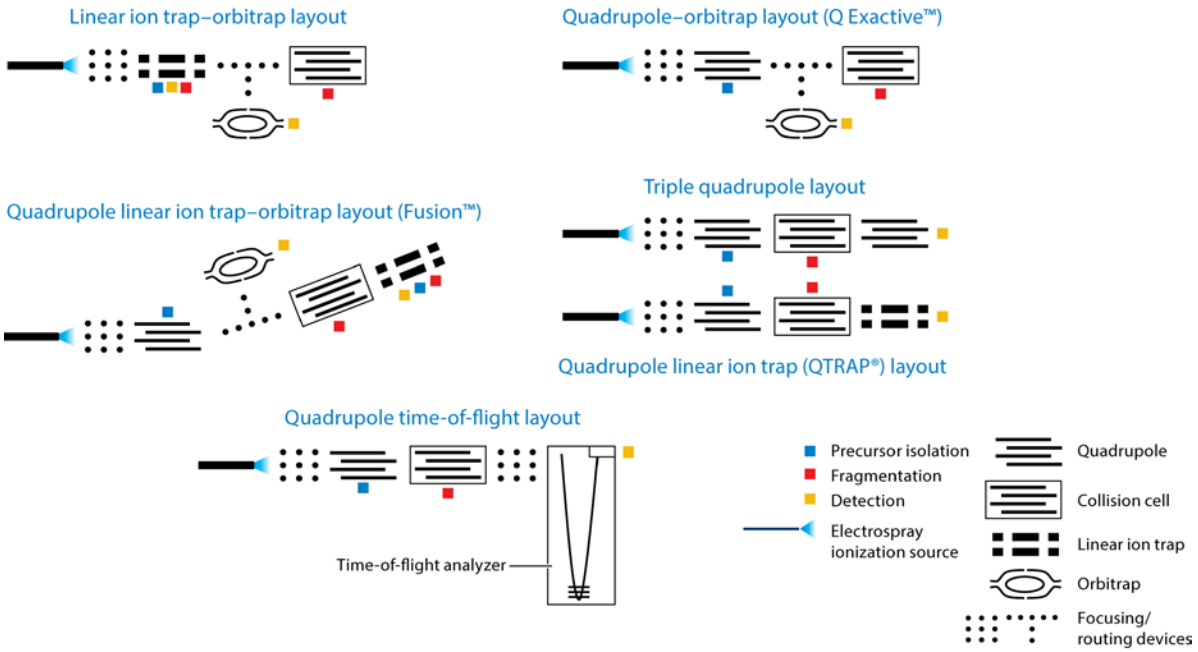

Figure 6 Different designs of mass spectrometers (Reprinted with permission from Gillet *et al.* Copyright © 2016 Annual Reviews)[95]

In **shotgun analysis** precursor ions are selected for fragmentation according to predetermined criteria.[95] Usually, the most intense signals of a full mass spectrum are selected, and can then be excluded for a certain period of time to additionally acquire data for less abundant analytes. Furthermore, only certain charge states are selected, *e.g.* +2, +3, +4. Singly-charged ions are most likely corresponding to potential contaminants or redundant small peptides. Higher charges indicate incomplete digestion of the protein and their resulting spectra would be difficult to interpret via bioinformatics. Based on the parameter settings, instruments can modulate the conditions for fragmentation to achieve the best results.[113] Even though the isolation windows for a precursor ion can already be set very narrowly, ranging from 1 to 3 m/z, co-isolation of peptides with similar m/z ratios cannot be excluded, which brings certain disadvantages. The resulting chimeric spectra complicate the identification and can falsify quantification of samples with isobaric tags.[95] These shotgun approaches enable the identification of thousands of proteins within one run covering a dynamic range of several orders of magnitude. Major challenges are sufficient sensitivity and reproducibility.[114] Predominantly Orbitrap and TOF mass spectrometers are in use in the field of shotgun proteomics, where ion isolation is achieved with quadrupoles or linear ion traps (different

layouts are presented in Figure 6).[95] For this thesis the QExactive Orbitrap by Thermo Fisher Scientific was the main instrument in use and will be discussed in more detail (Figure 7).

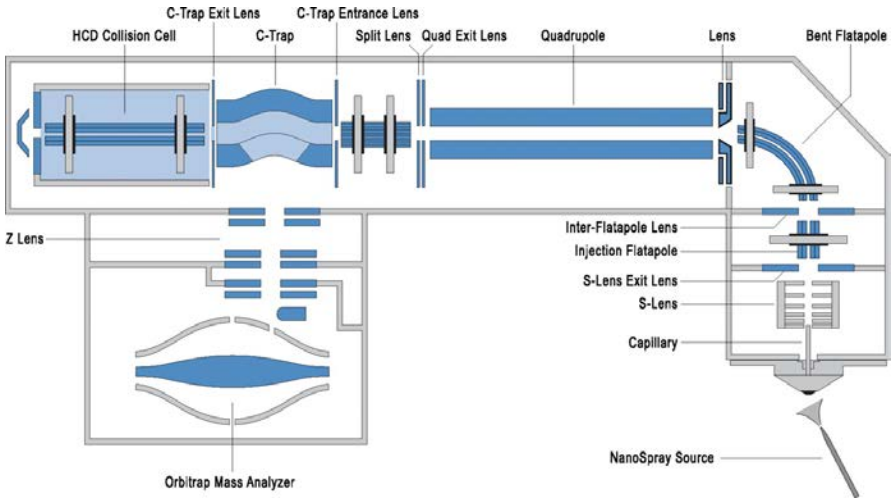

Figure 7 Layout of the QExactive (Reprinted in accordance with Creative Commons Attribution License from Michalski *et al.* Copyright © 2011)[115]

Upon separation by nanoLC, the peptides are ionized via nano electrospray ionization.[115] The generated ions then enter the mass spectrometer through a heated capillary. The ion cloud passes through the S-lens where the ion beam is being focused and is further transmitted to the bent flatapole. This change of direction eliminates neutral species. In the subsequently integrated quadrupole either a wide or narrow m/z range is filtered for full MS^1-scans or for fragmentation of a specific peptide to obtain MS^2-spectra, respectively. The C-trap brings the ion beam either into the HCD cell or to the orbitrap. Inside the HCD cell, which is gas-filled, fragments of the selected peptides are generated at their optimum collision energy. For high-resolution and accurate mass analysis the ions are trapped inside the oribtrap, where they orbit around the inner spindle-like electrode in trajectories specific for their m/z ratio. The frequency of the generated harmonic oscillation is acquired and Fourier transformed into a high resolution mass spectrum.[116] The resolution of orbitrap detectors is proportional to the time of analysis, which is thus a determining factor for analyzing complex samples, *e.g.* cell lysates.[117]

Highly precise and reproducible quantification even in plasma samples can be achieved by **targeted proteomic** methods.[118] Therefore, it has evolved as the preferred method of validating shotgun

data. Here, in contrast to DDA, the instrument does not select precursor ions, but consistently and repeatedly fragments user-defined ions. Although precise, this method comes at the cost of the number of peptides determinable in one measurement. For SRM, also known as multiple reaction monitoring (MRM), triple quadrupole mass spectrometers (QqQ) or quadrupole linear ion traps (QTRAP), used as QqQ, are the instruments of choice (Figure 6).[95] The first quadrupole isolates the selected precursor, which is then fragmented in the second quadrupole, functioning as collision cell. Subsequently, specific fragments for the selected peptide (transitions), which were predefined by the user, typically 3 to 5, are isolated in the third quadrupole and subsequently detected.[119] Some effort in preliminary work is required to achieve accurate measurements. Next to the most promising peptide for each protein, their most intense transitions need to be selected. Best sensitivity can only be ensured when instrument parameters are optimized, *e.g.* the collision energy. If a certain mass is only analyzed when eluted, more peptides can be measured in one run, therefore retentions times of the targets need to be predetermined as well.[95,119] Next to SRM, MS/MS^{ALL} or parallel reaction monitoring (PRM) was introduced as quantification tool for proteomics.[120] Instead of a third quadrupole a mass analyzer with high accuracy and resolution (Orbitrap or TOF) is utilized recording complete target product ion spectra.

DIA aims at acquiring data for multiple analytes in certain m/z ranges at once instead of selecting specific precursor ions for fragmentation (Figure 8).[121] Highly multiplexed MS/MS spectra of the fragment ions of all the peptides falling in the isolation window at a given time point are recorded. This way presumably all analytes above the limit of detection will be acquired. A widely applied DIA method is SWATH (sequential windowed acquisition of all theoretical mass spectra) MS, where repeatedly m/z isolation windows of typically 25 Da are sequentially analyzed (Figure 9). The time needed to cover the whole m/z range to be analyzed with those windows is defined as cycle time. A so called ‘swath’ refers to one isolation window measured throughout the whole LC.

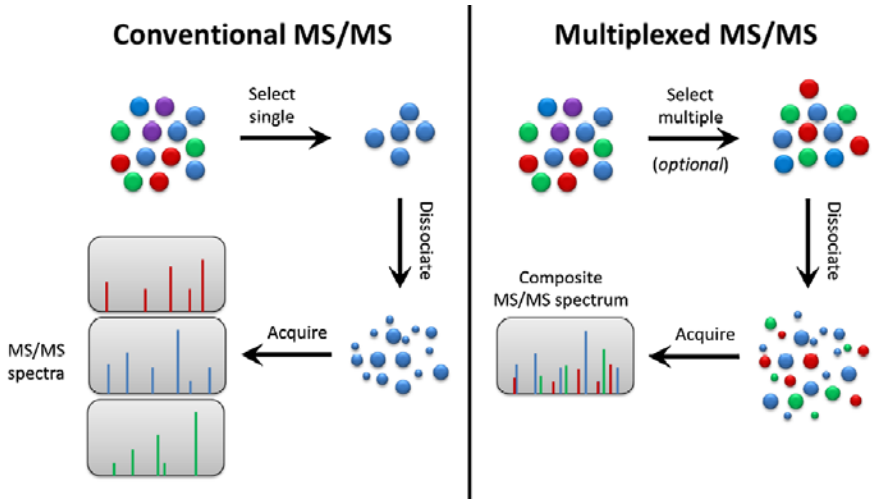

Figure 8 Comparison of conventional and multiplexed tandem mass spectrometry (Reprinted with permission from Chapman *et al.* Copyright © 2013 John Wiley and Sons)[121]

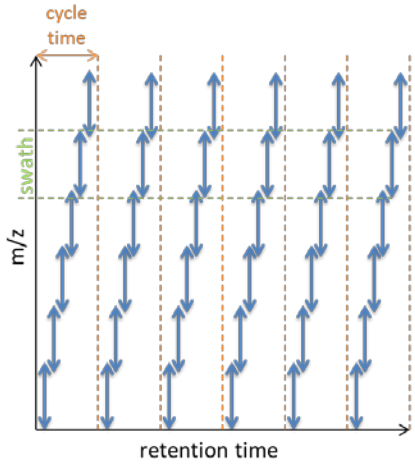

Figure 9 Representation of SWATH data acquisition mode

Several quantification approaches have emerged in the field of proteomics, which include label-free methods, metabolic labeling using stable isotopes or chemical labeling using isobaric tags after proteolysis (Figure 10).[122] Label-free quantification (LFQ) in proteome profiling experiments is realized by comparing signal intensities of the identified peptides or the number of MS^2 spectra that were matched to peptides and proteins, the latter is referred to as spectral counting.[123-125] Applying LFQ proteomics in the investigation of regulatory effects brings many advantages.[126] In contrast to label-based methods like iTRAQ (isobaric tag for relative and absolute quantitation) or SILAC (stable isotope labelling with amino acids) there is no sample modification needed prior to analysis.

Furthermore, label-free approaches enable protein identification most comprehensively.[122] Additionally, LFQ proteomics allows the comparison of large sample numbers with highly diverse protein profiles.[126] Less sample preparation steps and no requirement for special labeling reagents also reduce the material costs of such investigations significantly.[127] The main advantage of label-based approaches on the other hand is the minimization of non-systematic errors, since samples are combined and hence processed identically, giving the most accurate results for peptide quantification. Label-free approaches require normalization and chromatographic alignment for accurate quantification.[95] However, not all cell types are easily labeled, for some it is even impossible, a label-free approach makes such model systems accessible.[128,129]

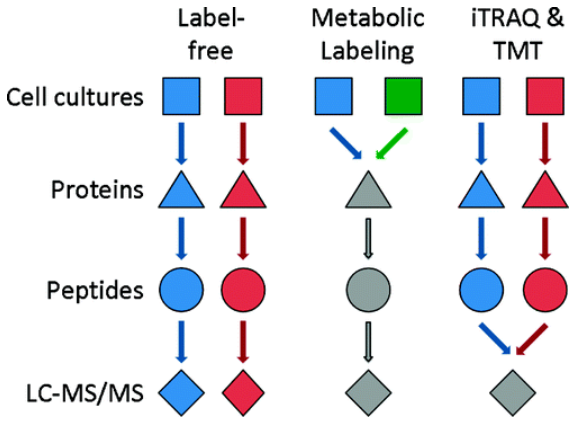

Figure 10 Procedure of label-free and label-based quantification in proteomics (Reprinted with permission from Li *et al.* Copyright © 2012, American Chemical Society) [122]

1.3.2. Data analysis in proteomics

In shotgun proteomics, the peptides are identified and assigned to their corresponding proteins from raw MS data. MS^2 spectra are characteristic for a specific peptide and are therefore used for their identification by comparison to database spectra. Several search engines have been developed for that purpose, like the freely available Adromeda[130] or the commercially sold Mascot.[131] Corresponding chromatographic peaks, *i.e.* the intensity of a peptide with a certain m/z in MS^1 plotted over its retention time, can be employed for quantification as done by the MaxQuant software,[132] which has the Andromeda search engine integrated. Peptides are then assigned to corresponding proteins. Some peptide sequences uniquely identify a protein, while others may refer

to more than one protein. Therefore, proteins with homologous sequences and/or isoforms are frequently consolidated into protein groups avoiding redundancies and inaccurate data interpretation.[133] Statistical evaluation can be utilized with further software packages like Perseus,[134] which is compatible with MaxQuant outputs and which was used throughout this thesis.

Since the peptides are predefined in SRM approaches and the fragments are monitored over time, chromatographic peaks of the fragment ions can be reconstructed and taken for quantification. Spiking with isotopically labelled standard peptides enables absolute quantitation and determination of post translational modifications.[135]

For peptide identification of SWATH MS data the chromatographic features of their fragment ions are considered, *e.g.* co-elution or peak shape. They are compared to library data containing MS^2 spectra that uniquely identify a peptide. Subsequently, like in targeted approaches, the chromatographic peaks resulting from the MS^2 spectra are used for quantification, which is possible over four orders of magnitude. The sensitivity of the method lies between that of SRM and shotgun analysis, but it achieves consistent and accurate result comparable to SRM.[136]

Once the proteins are identified and quantified, basal differences in protein abundances or regulatory effects triggered by stress stimuli like drug exposure can be investigated. Gene Ontology (GO)[137] terms for each protein can be implemented and enrichment analysis can be performed. Several software options are available to gain a deeper insight into the involved cellular processes for further data interpretation.[114] For example, a list of regulated proteins can be analyzed by the Database for Annotation, Visualization and Integrated Discovery (DAVID),[138,139] providing GO enrichment, pathway mapping and other features. Pathway analyses are possible with respective databases like KEGG,[140] Ingenuity Pathway Knowledge Base, or Reactome.[141] They comprise a large set of interaction maps, enabling a deeper insight into possibly affected biological processes. Protein-protein interactions networks can be searched using the STRING (Search Tool for the Retrieval of Interacting Genes/Proteins)[142] database, which implements literature data mining. These software solutions for data interpretation provide suitable starting points, however, detailed evaluations of protein lists manually represents still the bottleneck of the whole workflow in many cases.

1.4. Proteomics in drug investigations

During the process of drug discovery and development the evaluation of a drug candidate's prospects of success is crucial. Phenotypic assays to determine cell cycle, viability and death are well established and commonly used methods for a first evaluation. In *in vitro* preclinical toxicity tests adequate human cell line systems are employed to investigate organ-specific drug reactions. Common investigated endpoints for cytotoxicity screenings are (i) membrane integrity (*e.g.* Annexin V and propidium iodide staining to distinguish apoptotic and necrotic cells), (ii) mitochondrial function (*e.g.* MTT assay for half maximal inhibitory concentration (IC_{50})-determination), (iii) cellular metabolite content (*e.g*. ATP by luciferin-luciferase assay), (iv) lysosomal function (*e.g.* estimation of cell viability by neutral red uptake assay) and (v) apoptosis (*e.g.* determination of increasing caspase activity using high-throughput screening assays).[143] Also genotoxicity, embryotoxicity, carcinogenicity, endocrine disruption and reprotoxicity are investigated in high-throughput screening assays. These tests are important in the pharmaceutical industry to reduce toxicity-based attrition rates.[144]

Approaches for further development of such methods are for example attempted with microfluidic-devices. The miniaturization enables high throughput at low costs and even allows mimicking cell-cell interactions with interconnected chambers, representing living organisms and their complexity more appropriately.[145,146] Fast first screenings of drug combinations are examinable as well.[147]

However, all of these tests give little information about a drug's molecular mechanism of action within the cell. This understanding is, however, of great importance to predict a compound's prospect of success in drug development. Since proteins are determining cellular fate and function, proteome profiling represents a powerful screening method, which may allow identifying specific cell responses to drugs. Toxicoproteomics aims to predict adverse drug effects as well as (organ specific) toxicity and to discover novel biomarkers.[148] Particularly, metal-based anticancer research requires novel methods that help establishing drug effects in an unbiased profiling manner to generate hypotheses about potentially novel modes of action. For a long time they were believed to act in a very unspecific way. Since cisplatin was shown to induce direct DNA lesions,[149] the same mechanism was suspected for other metallodrugs as well. However, this view changed drastically during recent years.[54] An investigation on the two ruthenium compounds [(η^6-p-cymene)Ru(ethylene-diamine)Cl]PF_6 (RAED-C) and [(η^6-p-cymene)Ru(1,3,5-triaza-7-

phosphaadamantane)Cl_2] (RAPTA-C) revealed contrasting binding sites and selectivity for proteins in the crystal structure of the nucleosome core particle containing DNA and histones.[150] While RAED-C was observed to directly coordinate to nucleobases, RAPTA-C was preferentially bound to surface-exposed nucleophilic amino acid side chains of histone H2A/B. As a consequence, alternative molecular targets to DNA, such as proteins, were brought into focus as potential targets for non-platinum metallodrugs. Complicating research on metal-based compounds is the fact that under physiological conditions they are prone to reduction and ligand exchange reactions,[151] which needs to be accounted for in the experimental set-up.

Classical proteomic approaches with 2-DE and MS analysis were combined with photo-activatable fluorescent probes[152] or photoaffinity-click chemistry[153] to identify possible targets of metallodrugs. The proteins HSPA, HSPB, NAPA and TSAA were proclaimed as potential targets for the antiulcer compound colloidal bismuth subcitrate (CBS) in *Helicobacter pylori*, investigated by comparative 2-DE based proteomics and immobilized-metal affinity chromatography (IMAC).[154] Furthermore, MudPIT seemed to enable the analysis of metals bound to their targets.[112] It required a characteristic isotopic distribution of the metal and a kinetically inert binding site, but no drug derivatizations are needed for this approach. Cisplatin[155,156] and [(η^6-p-cymene)$RuCl_2$(DMSO)][157] targets in *Escherichia coli* cells were investigated this way. The Ru(II) compound was mainly bound to stress regulating proteins and helicases.[157] High-dose cisplatin treatment revealed 31 potential targets, where the interaction with low abundant proteins seemed very specific.[156] Treatment with a medically more relevant dose resulted in 18 cisplatin-bound proteins.[155] Additionally, regulatory effects upon exposure to the drug were observed for 46 proteins. A chemical proteomics approach was employed based on affinity-purification to investigate potential molecular targets of a derivative of the organometallic Ru-based compound RAPTA.[158] First, the drug was modified with biotin and immobilized on streptavidin resins. The immobilized drug was then exposed to whole cell lysates of untreated and treated (competitive) cells, respectively. In a subsequent LFQ proteomics analysis, potential binding partners were identified by subtracting the non-specific interactors obtained from the competitive pull-down. This way 18 potential RAPTA-targets were identified, albeit with low enrichment factors, including extracellular growth factors, cell cycle-regulating, cancer-related, histone-related and ribosomal proteins. A similar approach was employed to investigate target proteins of the naturally occurring compound curcumin. Affinity enrichment combined with an iTRAQ-based proteomics approach revealed 197 potential interaction partners.[159]

Ingenuity Pathway Analysis revealed various affected pathways, including mitochondrial dysfunction and mTOR signaling.

Proteome profiling was also applied to gain mechanistic insights of drug activity and identify potential marker proteins of efficacy and resistance, respectively. Lawrence *et al.* employed a label-free LC-MS/MS-based proteomics approach to investigate 16 triple negative breast cancer cell lines.[160] They combined their data with IC_{50}-values and publicly available data of 160 drugs to identify protein markers for sensitivity and resistance mechanisms. Regression analysis and hierarchical clustering were used to reveal sensitivity patterns, *e.g.* for drugs depending on mitochondrial proteins, these proteins were enriched in sensitive cells. In the additional analysis of primary tumor samples 73% of the proteins were overlapping with the prior obtained *in vitro* data and quantifiable as well. This clearly demonstrated the clinical relevance of such investigations. Comparison of protein abundances in oxaliplatin sensitive and resistant colon cancer cell lines by 2-DE combined with LC-MS/MS analysis associated resistance with decreased expression of pyruvate kinase M2.[161] The findings were confirmed in patients indicating a potential clinical marker for resistance. In 2017, a SILAC based proteomic approach investigated early events induced by oxaliplatin treatment in T-lymphoblastic leukemia-derived cells identifying 107 regulated proteins.[162] Functional annotation clustering by DAVID and STRING analysis correlated them to four distinct clusters – centromere and G2/M checkpoint, secreted proteins, ribosomal and nucleolar proteins. Immunoblotting and ELISA assays were performed for verifications, also with oxaliplatin-treated osteosarcoma and colorectal cancer cells, revealing differential regulations in the latter. Another label-free proteomic study of oxaliplatin effects in three colon cancer cell lines revealed up to 57 regulated proteins analyzed by 2-DE and subsequent MALDI-TOF-MS.[163] An overlap of 21 differentially expressed proteins was observed in all three cells, influencing various cellular processes including signal transduction, structural organization and apoptosis. Also, cisplatin resistance has been investigated by proteomic approaches, especially with 2-DE and MALDI-TOF analysis.[164-167] A LFQ proteome profiling approach identified a potential cisplatin resistance signature comprising 47 proteins important for survival, cell adherence and lysosomal function.[168] These observations point out that resistance cannot be correlated to regulations of single proteins, but effects occurring in groups of proteins need to be considered.

A SILAC-based phosphoproteomics approach observed alterations induced by curcumin treatment in head and neck cancer.[169] Affected pathways included actin cytoskeleton reorganization and focal

adhesion kinase signaling. Another phosphoproteomic study on curcumin effects in colon cancer used a phosphoprotein purification kit to enrich phosphorylated proteins, which were subsequently fluorescence labelled, separated by 2-DE and spots of interests were analyzed by LC-MS/MS.[170] Thirty-nine differentially expressed proteins were identified, displaying the p53 as well as the mTORC1 signaling pathways. Anti-metastatic effects of 3 chemotherapeutics (oxaliplatin, 5-fluorouracil, sorafenib) and 3 naturally occurring compounds (curcumin, ginsenoside 20(s)-Rg_3, lutelion) were investigated by a shotgun proteomics approach.[171] Oxaliplatin and curcumin down-regulated histone H4 and fatty acid synthase, two proteins with important roles in cancer metastasis. In another LC-MS/MS-based proteomics approach effects of paclitaxel, cisplatin, and 3 ruthenium-based RAPTA-compounds on breast cancer cells were compared, revealing possible targets and potential insights into their modes of action.[172]

Nano-LC orbitrap analysis was also employed to investigate differential protein regulations in tissue samples upon drug exposure.[173] Rats were treated with anti-inflammatory corticosteroids, sacrificed at 11 time points over 66 hours and their livers were proteomically analyzed identifying 451 differentially expressed proteins. These could be assigned to six functional clusters that are clinically relevant for corticosteroids' effects, like energy metabolism and cellular stress, showing diverse time-dependent varieties of proteins with similar functions. Affinity chromatography was employed to identify potential targets of curcumin in mouse brain.[174] The drug was immobilized and exposed to the tissue lysates, subsequently 2-DE MALDI-TOF-MS analyses were performed showing that the biphenol binds to a wide range of proteins.

Proteomics can also be combined with other 'omics' strategies, *i.e.* multi-omics research, to investigate drug effects. Proteogenomics was employed to discover potential biomarkers of drug resistance in cancer.[175] Proteomic, epigenomic and transcriptomic data were combined to study modes of resistance to methotrexate in colon cancer cells.[176] Identified regulators of resistance were then used to suggest compounds that possibly revert resistance. Proteomics and transcriptomics were employed to elucidate the antimicrobial effects of berberine.[177] Nucleic acids were found as potential targets, membrane transport was affected by the treatment and a general down-regulation of metabolism was observed. The mechanism of the naturally occurring compound geniposide was investigated by an approach integrating proteomics, metabolomics and miRNAomics.[178] Various metabolic pathways were affected including the citric cycle. Applying proteomics and metabolomics the effects of coffee consumption and caffeine were observed in *ex*

vivo and *in vitro* experiments, demonstrating individual pro- and anti-inflammatory effects.[179] A similar study revealed a possible metabolic shift due to changes in the citric acid and urea cycle upon coffee consumption.[180] Proteomics was combined with metabolomics to examine the effects of the ruthenium compound RAPTA-T employing size exclusion chromatography, inductively coupled plasma MS and MudPIT.[181] Both approaches revealed an important impact of histones to its mechanism of action. Also the anti-inflammatory effects of a secondary metabolite of *Mucor racemosus* and dexamethasone were investigated by changes in proteome and metabolome.[182] Profiling of proteins and eicosanoids represent another powerful combination giving a better insight into regulatory effects upon drug exposure and highlighted once again the importance of stromal cells in chronic diseases.[183]

1.5. General Overview of Applied Methods in this Doctoral Thesis

1.5.1. Cell culture

For this thesis cell lines as well as primary cells were investigated, which differ in handling and function. While cell lines are immortalized, primary cells can only be cultivated over short periods of time. A better representation of the *in vivo* situation can be achieved with cells directly isolated from tissue. Cancer cell lines display many mutations, can therefore lose tissue-specific functions and change their phenotype. Proteomes of cell lines can be altered dramatically compared to the respective primary cells as observed in several proteome profiling studies.[184-186] Culturing of cell lines is easier since they are already well adapted to the cell culture conditions. Primary cells are stressed by the introduction to a new, artificial environment and require adding of essential nutrients and growth factors if cultured in classical media, increasing costs as well. Not all cells can be cultured and cell lines are the only opportunity for investigations over longer periods of time as needed for example for the observation of drug effects and acquired resistance.

All cell lines (SW480, HCT116, MCF-7, ZR-75-1) and primary cells (human mammary fibroblasts) investigated in this thesis were cultivated in their recommended media including the respective supplements, fetal calf serum, penicillin and streptomycin. Drug treatment concentrations in the experiments should not induce apoptosis to explore primary drug effects. Programmed cell death is a cataclysmic process and once started it will be the protein readout of the cell state, while other

regulations will be masked. Therefore, the half maximum inhibitory concentrations (IC_{50}) of the investigated drugs were determined with the colorimetric MTT (3-(4,5-dimethylthiazol-2-yl)-2,5-diphenyltetrazolium bromide) assay.[187] Only viable cells convert the yellow MTT reagent to the purple-colored and insoluble formazan (Figure 11) since active mitochondria are required for this process.[188] After dissolution in DMSO, absorbance is measured at 570 nm, which is proportional to the amount of proliferating cells (Figure 12). First, an appropriate number of cells is seeded per well. While the absorbance should be high enough (around 0.75–1.25), the cells should still be in the exponential growth phase.[189] Therefore, a confluence of not more than approximately 80% at the end point is recommendable. The cells are then exposed to drug concentrations between 0.01 and 100 µM (range as tested by the National Cancer Institute), or even higher if lower toxicity of the investigated compound is expected, *e.g.* in the case of NKP-1339. For our experiments the results of the most sensitive cells were utilized to decide on an appropriate concentration for drug treatment. Between one to two thirds of the respective IC_{50}-values of were usually selected to minimize apoptosis induction.

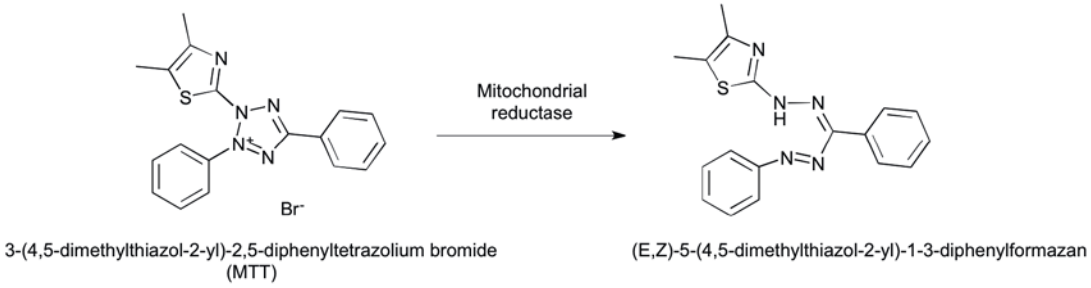

Figure 11 MTT reaction

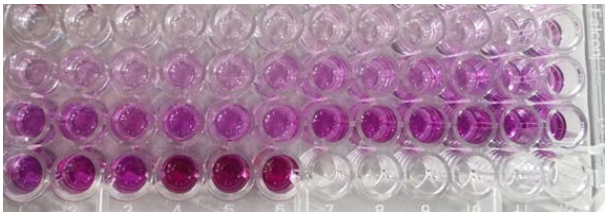

Figure 12 MTT assay

Cytoplasmic and nuclear fractions were obtained by cellular fractionation, which were separately analyzed. This step allowed the observation of intracellular translocation events and by reducing the complexity of the single samples analyzed, it enabled a more comprehensive detection of low abundant proteins.[190] A fractionation buffer containing Triton X-100, which leads to permeabilization of the outer cell membrane,[191] was added to the cells and shear stress was applied by means of a syringe. This combination permitted the lysis of the cells with intact nuclei. Cytoplasmic and nuclear fractions were separated by centrifugation. A 500 mM NaCl solution was used to disrupt the nuclei. The proteins of the cytoplasmic and nuclear extracts were precipitated in ice-cold ethanol. The protein pellets were denatured and solubilized in sample buffer with addition of urea for subsequent in-solution digestion.

Since the microenvironment plays an important role in tumor progression[7] and drug response,[6] the implementation of tumor/stroma co-culture models represents great potential for the investigation of drug effects.[9] Human mammary fibroblasts were first treated with TGF-β to display a wound healing signature as predominantly observed in breast cancer microenvironment.[192] These cancer-associated fibroblast (CAF)-like cells were then co-cultivated with breast cancer cell lines, *i.e.* MCF-7 and ZR-75-1, respectively, in a ratio of 1:10, representative for the *in vivo* situation.[192] Due to a higher need of nutrients and growth factors of primary cells and the fast uptake of these by cancer cells the media were mixed 1:1 for co-cultivation. Prior to drug treatment the co-cultures were incubated for 24 h. Treatment concentrations were decided from the IC_{50}-values of the single cell types. The proteome of the co-cultures experiments was assessed by obtaining whole cell lysates. After washing with PBS, sample buffer (7.5 M urea, 1.5 M thiourea, 4% 3-[(3-cholamidopropyl)dimethylammonio]-1-propanesulfonate (CHAPS), 0.05% sodium dodecyl sulfate (SDS), 100 mM dithiothreitol (DTT)) was added and cells were scraped off. To disrupt the cells an ultrasonic treatment was applied. A spatula tip of urea was added for denaturation and sufficient solvation of the proteins. Samples were put on 4 °C overnight prior to in-solution digestion.

Differential regulations of integrins, which are cell adhesion receptors,[193] observed in the response profiling study of the metallodrugs, suggested differences in cell adhesion after drug exposure. To verify this finding, cell adhesion assays were conducted in 96-well-plates with laminin, collagen I, gelatin, matrigel, fibronectin, poly-D-lysin as positive and bovine serum albumin as negative control. Twenty thousand cells were seeded per well after drug treatment. After 1 hour incubation in serum-

free media wells were washed with PBS twice and viable adherent cells were determined by the MTT assay as described above.

1.5.2. Sample Preparation for LC-MS/MS Analysis

After concentration determination *via* Bradford photometric assay 20 or 25 µg protein from each sample were pre-concentrated on 10 kDa spin-off filters and washed with an ammonium bicarbonate buffer. For the disruption and subsequent prevention of reformation of covalent disulfide bonds, the proteins were first reduced with DTT and then cysteine groups were carbamidomethylated with iodoacetamide (IAA). Finally, proteins were digested over night at 37°C with a mixture of trypsin and lys-C, cleaving at the sides of the amino acids arginine and lysine. Trypsin is commonly used in the field of bottom-up proteomics, due to its relatively good specificity, robustness, comparatively low price and generation of peptides compatible with LC-MS/MS performances, ranging from 500 – 3000 Da in mass and with reasonable ionization and fragmentation properties.[95] Additionally lys-C compensates for the deficiency of trypsin to efficiently digest proteins at lysine sites.[194] Cytoplasmic and nuclear fraction samples were dried after elution and stored at -20°C until further analysis, whereas samples of whole cell lysates were first purified with C-18 spin columns.

1.5.3. Liquid chromatography – Tandem Mass Spectrometry

For in-depth proteome profiling an UltiMate 3000 RSLCnano chromatography system (Thermo Fisher Scientific) was hyphenated to a QExactive orbitrap mass spectrometer (Thermo Fisher Scientific). The peptide samples were reconstituted in 30% formic acid (FA) and diluted with eluent A (98% H_2O, 2% acetonitrile (ACN), 0.1% FA). The solution also contained four synthetic peptides with a range of hydrophobicity as internal standards to monitor the performance of the analysis, enabling immediate recognition of problems in the LC-MS system, like retention time shifts or intensity issues.

With a flow rate of 10 µL min^{-1} of eluent A, samples were loaded on the 2 cm C-18 precolumn. Peptides were separated on a 50 cm C-18 column with an inner diameter of 75 µm at a flow rate of 300 nl min^{-1}, the amount of eluent B (80% CAN, 20% H_2O, 0.1% FA) was increased over a 90 min gradient from 8–40%. Overall, including washing and equilibration steps, the LC method was 135 min long. The MS method was 115 min long, scanning over 400 to 1.400 m/z in MS^1 at a resolution

of 70.000 (at m/z = 200). For MS^2 the 8 most abundant peptides were further fragmented with HCD at 30% normalized collision energy and measured with a resolution of 17.500 (at m/z = 200).

Targeted analysis as well as measurements of oxidized glutathione, which were both required for verification of the shotgun data, were performed on an Agilent 6490 triple quadrupole mass spectrometer combined with a chip-based nano-LC or a ultra-high performance LC system, respectively.

1.5.4. Data Analysis

For protein identification and label-free quantification the MaxQuant[132] software with the Andromeda search engine was employed. For a positive identification at least two peptides had to be identified, at least one needed to be unique for the respective protein. Only the curated Swiss-Prot entries were used as references, which are non-redundant and without isoforms. The false discovery rate (FDR) enables the control of incorrect identifications.[195] For the investigations conducted during this thesis the FDR was set to 0.01 on peptide and protein level. Statistical analysis was performed with the MaxQuant compatible software package Perseus.[134] The permutation-based FDR, which was set to 0.05 for the Student's t-test, permits the labeling of multi-parameter significant changes and differences, respectively. Such a multi-parameter correction is of great importance in the evaluation of large data sets as obtained in proteomics experiments improving the accuracy of the received results.[196]

1.6. Research Justification

The advent of mass spectrometry-based shotgun proteomics enabled a comprehensive characterization of a large fraction of the cellular proteome in one experiment.[90] This holds great promise for the analysis of drug effects at a molecular level. Such approaches are potentially ideally suited to generate hypotheses about unknown or novel modes of action of emerging therapeutic drugs. Especially, the classes of next-generation metal-based anticancer agents and natural products would benefit tremendously from an improved understanding of their cellular effects not only by observing changes of single proteins, but protein signatures. Importantly, MS-based proteomics methods were rarely applied to study these drug classes.

Novel anticancer metallodrugs as well as naturally occurring compounds hold great potential for the treatment of cancer. Comparative proteome profiling of untreated and drug challenged cancer cells will be evaluated as a strategy to obtain detailed information about drug effects. Furthermore, target identification is a challenging task that is required for the discovery of improved and mechanism-based anticancer drugs.[54] Recently, proteins emerged as potential targets for next-generation metal-based anticancer agents and thus, affinity-purification strategies will be evaluated to determine potential targets of a selected metal-based anticancer agent.

Therefore, the aim of this thesis is to explore the suitability of label-free shotgun proteomics to characterize drug effects of next-generation metal-based anticancer agents and natural products in cell culture model systems of increasing complexity. Not only cultures of single cell types, but also co-culture models of tumor cells and cancer-associated fibroblast-like cells will be employed to account more realistically for *in vivo* situations of the tumor microenvironment and thus, the context-dependency of drug treatments. Drug effects will be evaluated at subcytotoxic doses according to prior determined IC_{50}-values. The entire proteomics workflow from sample preparation to data acquisition, evaluation and visualization will be optimized so that such experiments can be conducted in a reproducible and efficient manner. Finally, the results of the shotgun proteomics experiments will be validated by biochemical, metabolic and/or targeted proteomics assays.

1.7. List of Abbreviations

2-DE, two-dimensional gel electrophoresis; **ACN**, acetonitrile; **CAFs**, cancer-associated fibroblasts; **DDA**, data dependent acquisition; **DIA**, data independent acquisition; **DTT**, dithiothreitol; **ECM**, extracellular matrix; **EMT**, epithelial-to-mesenchymal transition; **ESI**, electrospray ionization; **FA**, formic acid; **FDR**, false discovery rate; **GO**, Gene Ontology; **HMF**, human mammary fibroblasts; **IAA**, iodoacetamide; **IC_{50}**, half maximal inhibitory concentration; **iTRAQ**, isobaric tag for relative and absolute quantitation; **LC**, liquid chromatography; **LFQ**, label-free quantification; **MALDI**, matrix assisted laser desorption-ionization; **MDR**, multidrug resistance; **MRM**, multiple reaction monitoring; **MS**, mass spectrometry; **MS/MS** or **MS^2**, tandem mass spectrometry; **MS^n**, multiple-stage mass spectrometry; **MTT**, 3-(4,5-dimethylthiazol-2-yl)-2,5-diphenyltetrazolium bromide; **MudPIT**, multidimensional protein identification technology; **QqQ**, triple quadrupole; **ROS**, reactive oxygen species; **RP**, reversed phase; **SILAC**, stable isotope labelling with amino acids; **SRM**, selected reaction monitoring; **SWATH**, sequential windowed acquisition of all theoretical mass; **TOF**, time-of-flight; **TP53**, tumor protein 53

1.8. References

1. R. L. Siegel, K. D. Miller and A. Jemal, Cancer Statistics, 2017, *CA Cancer Journal for Clinicians*, 2017, **67**, 7-30.
2. D. Hanahan and R. A. Weinberg, The hallmarks of cancer, *Cell*, 2000, **100**, 57-70.
3. D. Hanahan and R. A. Weinberg, Hallmarks of cancer: The next generation, *Cell*, 2011, **144**, 646-674.
4. N. A. Bhowmick, E. G. Neilson and H. L. Moses, Stromal fibroblasts in cancer initiation and progression, *Nature*, 2004, **432**, 332-337.
5. A. Klein-Goldberg, S. Maman and I. P. Witz, The role played by the microenvironment in site-specific metastasis, *Cancer Letters*, 2014, **352**, 54-58.
6. M. R. Junttila and F. J. De Sauvage, Influence of tumour micro-environment heterogeneity on therapeutic response, *Nature*, 2013, **501**, 346-354.
7. E. Nakasone*, et al.*, Imaging Tumor-Stroma Interactions during Chemotherapy Reveals Contributions of the Microenvironment to Resistance, *Cancer Cell*, 2012, **21**, 488-503.
8. M. M. Mueller and N. E. Fusenig, Friends or foes - Bipolar effects of the tumour stroma in cancer, *Nature Reviews Cancer*, 2004, **4**, 839-849.
9. A. Slany*, et al.*, Targeting breast cancer-associated fibroblasts to improve anti-cancer therapy, *Breast*, 2015, **24**, 532-538.
10. D. Drev*, et al.*, Proteomic profiling identifies markers for inflammation-related tumor-fibroblast interaction, *Clinical Proteomics*, 2017, **14**, 33.
11. V. Paulitschke*, et al.*, Entering a new era of rational biomarker discovery for early detection of melanoma metastases: Secretome analysis of associated stroma cells, *Journal of Proteome Research*, 2009, **8**, 2501-2510.
12. A. Slany*, et al.*, Extracellular matrix remodeling by bone marrow fibroblast-like cells correlates with disease progression in multiple myeloma, *Journal of Proteome Research*, 2014, **13**, 844-854.
13. A. Slany*, et al.*, Myofibroblasts are important contributors to human hepatocellular carcinoma: Evidence for tumor promotion by proteome profiling, *Electrophoresis*, 2013, **34**, 3315-3325.
14. R. A. Weinberg, *The biology of cancer. - Second edition.*, Garland Science, Taylor & Francis Group, 2014.
15. D. S. Shewach and R. D. Kuchta, Introduction to cancer chemotherapeutics, *Chemical Reviews*, 2009, **109**, 2859-2861.
16. B. Al-Lazikani, U. Banerji and P. Workman, Combinatorial drug therapy for cancer in the post-genomic era, *Nature Biotechnology*, 2012, **30**, 679-692.
17. V. T. DeVita Jr and E. Chu, A history of cancer chemotherapy, *Cancer Research*, 2008, **68**, 8643-8653.
18. S. Nussbaumer*, et al.*, Analysis of anticancer drugs: A review, *Talanta*, 2011, **85**, 2265-2289.
19. J. Benada and L. Macurek, Targeting the checkpoint to kill cancer cells, *Biomolecules*, 2015, **5**, 1912-1937.
20. T. M. Pitts*, et al.*, Targeting nuclear kinases in cancer: Development of cell cycle kinase inhibitors, *Pharmacology and Therapeutics*, 2014, **142**, 258-269.
21. R. Tonkens, An overview of the drug development process, *Physician executive*, 2005, **31**, 48-52.
22. B. Rosenberg*, et al.*, Platinum compounds: A new class of potent antitumour agents, *Nature*, 1969, **222**, 385-386.
23. C. G. Hartinger*, et al.*, Application of mass spectrometric techniques to delineate the modes-of-action of anticancer metallodrugs, *Chemical Society Reviews*, 2013, **42**, 6186-6199.
24. M. A. Jakupec*, et al.*, Antitumour metal compounds: More than theme and variations, *Dalton Transactions*, 2008, 183-194.
25. E. Raymond*, et al.*, Cellular and molecular pharmacology of oxaliplatin, *Molecular Cancer Therapeutics*, 2002, **1**, 227-235.
26. S. Dhar and S. J. Lippard, Current Status and Mechanism of Action of Platinum-Based Anticancer Drugs in *Bioinorganic Medicinal Chemistry*, 2011, pp. 79-95.
27. D. P. Gately and S. B. Howell, Cellular accumulation of the anticancer agent cisplatin: A review, *British Journal of Cancer*, 1993, **67**, 1171-1176.

28. D. Wang and S. J. Lippard, Cellular processing of platinum anticancer drugs, *Nature Reviews Drug Discovery*, 2005, **4**, 307-320.
29. S. Ahmad, Platinum-DNA interactions and subsequent cellular processes controlling sensitivity to anticancer platinum complexes, *Chemistry and Biodiversity*, 2010, **7**, 543-566.
30. K. Kohno*, et al.*, Mitochondrial transcription factor a and mitochondrial genome as molecular targets for cisplatin-based cancer chemotherapy, *International Journal of Molecular Sciences*, 2015, **16**, 19836-19850.
31. A. L. Stark*, et al.*, Identification of Novel Protein Expression Changes Following Cisplatin Treatment and Application to Combination Therapy, *Journal of Proteome Research*, 2017, **16**, 4227-4236.
32. H. Chen*, et al.*, Cisplatin and paclitaxel target significant long noncoding RNAs in laryngeal squamous cell carcinoma, *Medical Oncology*, 2014, **31**, 246.
33. L. Astolfi*, et al.*, Correlation of adverse effects of cisplatin administration in patients affected by solid tumours: A retrospective evaluation, *Oncology Reports*, 2013, **29**, 1285-1292.
34. K. Barabas*, et al.*, Cisplatin: A review of toxicities and therapeutic applications, *Veterinary and Comparative Oncology*, 2008, **6**, 1-18.
35. U. B. Chaudhary and J. R. Haldas, Long-term complications of chemotherapy for germ cell tumours, *Drugs*, 2003, **63**, 1565-1577.
36. G. Li*, et al.*, Salicylate protects hearing and kidney function from cisplatin toxicity without compromising its oncolytic action, *Laboratory Investigation*, 2002, **82**, 585-596.
37. J. F. Smyth*, et al.*, Glutathione reduces the toxicity and improves quality of life of women diagnosed with ovarian cancer treated with cisplatin: results of a double-blind, randomised trial, *Annals of Oncology*, 1997, **8**, 569-573.
38. J. Lokich and N. Anderson, Carboplatin versus cisplatin in solid tumors: An analysis of the literature, *Annals of Oncology*, 1998, **9**, 13-21.
39. M. Sooriyaarachchi, A. Narendran and J. Gailer, Comparative hydrolysis and plasma protein binding of cis-platin and carboplatin in human plasma in vitro, *Metallomics*, 2011, **3**, 49-55.
40. D. A. Fennell*, et al.*, Cisplatin in the modern era: The backbone of first-line chemotherapy for non-small cell lung cancer, *Cancer Treatment Reviews*, 2016, **44**, 42-50.
41. U. Jungwirth*, et al.*, Anticancer activity of methyl-substituted oxaliplatin analogs, *Molecular Pharmacology*, 2012, **81**, 719-728.
42. G. Sava*, et al.*, Na[trans-RuCl4(DMSO)Im], a metal complex of ruthenium with antimetastatic properties, *Clinical & Experimental Metastasis*, 1992, **10**, 273-280.
43. C. G. Hartinger*, et al.*, KP1019, a new redox-active anticancer agent - Preclinical development and results of a clinical phase I study in tumor patients, *Chemistry and Biodiversity*, 2008, **5**, 2140-2155.
44. S. M. Meier*, et al.*, Novel metal(ii) arene 2-pyridinecarbothioamides: A rationale to orally active organometallic anticancer agents, *Chemical Science*, 2013, **4**, 1837-1846.
45. P. Collery, J. L. Domingo and B. K. Keppler, Preclinical toxicology and tissue gallium distribution of a novel antitumour gallium compound: Tris (8-quinolinolato) gallium (III), *Anticancer Research*, 1996, **16**, 687-692.
46. L. R. Bernstein*, et al.*, Chemistry and pharmacokinetics of gallium maltolate, a compound with high oral gallium bioavailability, *Metal-Based Drugs*, 2000, **7**, 33-47.
47. P. Heffeter*, et al.*, Anticancer activity of the lanthanum compound [tris(1,10-phenanthroline) lanthanum(III)]trithiocyanate (KP772; FFC24), *Biochemical Pharmacology*, 2006, **71**, 426-440.
48. M. A. Jakupec*, et al.*, Redox-active antineoplastic ruthenium complexes with indazole: Correlation of in vitro potency and reduction potential, *Journal of Medicinal Chemistry*, 2005, **48**, 2831-2837.
49. P. Schluga*, et al.*, Redox behavior of tumor-inhibiting ruthenium(III) complexes and effects of physiological reductants on their binding to GMP, *Dalton Transactions*, 2006, **6**, 1796-1802.
50. M. J. Clarke, Ruthenium metallopharmaceuticals, *Coordination Chemistry Reviews*, 2002, **232**, 69-93.
51. Z. X. Shen*, et al.*, Use of arsenic trioxide (As2O3) in the treatment of acute promyelocytic leukemia (AFL): II. Clinical efficacy and pharmacokinetics in relapsed patients, *Blood*, 1997, **89**, 3354-3360.
52. C. Artner*, et al.*, DNA or protein? Capillary zone electrophoresis-mass spectrometry rapidly elucidates metallodrug binding selectivity, *Chemical Communications*, 2017, **53**, 8002-8005.

53. Ö. Karaca*, et al.*, On the binding modes of metal NHC complexes with DNA secondary structures: Implications for therapy and imaging, *Chemical Communications*, 2017, **53**, 8249-8260.
54. S. M. Meier-Menches*, et al.*, Structure-activity relationships for ruthenium and osmium anticancer agents-towards clinical development, *Chemical Society Reviews*, 2018, **47**, 909-928.
55. G. Sava*, et al.*, Dual action of NAMI-A in inhibition of solid tumor metastasis: Selective targeting of metastatic cells and binding to collagen, *Clinical Cancer Research*, 2003, **9**, 1898-1905.
56. S. Pacor*, et al.*, Intratumoral NAMI-A treatment triggers metastasis reduction, which correlates to CD44 regulation and tumor infiltrating lymphocyte recruitment, *Journal of Pharmacology and Experimental Therapeutics*, 2004, **310**, 737-744.
57. F. Frausin*, et al.*, Free exchange across cells, and echistatin-sensitive membrane target for the metastasis inhibitor NAMI-A (imidazolium trans-imidazole dimethyl sulfoxide tetrachlororuthenate) on KB tumor cells, *Journal of Pharmacology and Experimental Therapeutics*, 2005, **313**, 227-233.
58. G. Sava*, et al.*, Actin-dependent tumour cell adhesion after short-term exposure to the antimetastasis ruthenium complex NAMI-A, *European Journal of Cancer*, 2004, **40**, 1383-1396.
59. A. Bergamo*, et al.*, RNA-seq analysis of the whole transcriptome of MDA-MB-231 mammary carcinoma cells exposed to the antimetastatic drug NAMI-A, *Metallomics*, 2015, **7**, 1439-1450.
60. S. Leijen*, et al.*, Phase I/II study with ruthenium compound NAMI-A and gemcitabine in patients with non-small cell lung cancer after first line therapy, *Investigational New Drugs*, 2015, **33**, 201-214.
61. R. Pazdur, Endpoints for assessing drug activity in clinical trials, *Oncologist*, 2008, **13**, 19-21.
62. C. G. Hartinger*, et al.*, From bench to bedside - preclinical and early clinical development of the anticancer agent indazolium trans-[tetrachlorobis(1H-indazole)ruthenate(III)] (KP1019 or FFC14A), *Journal of Inorganic Biochemistry*, 2006, **100**, 891-904.
63. A. Bergamo*, et al.*, Inhibitory effects of the ruthenium complex KP1019 in models of mammary cancer cell migration and invasion, *Metal-Based Drugs*, 2009, **2009**, 681270.
64. R. Trondl*, et al.*, NKP-1339, the first ruthenium-based anticancer drug on the edge to clinical application, *Chemical Science*, 2014, **5**, 2925-2932.
65. M. Sulyok*, et al.*, Two dimensional separation schemes for investigation of the interaction of an anticancer ruthenium(III) compound with plasma proteins, *Journal of Analytical Atomic Spectrometry*, 2005, **20**, 856-863.
66. S. Kapitza*, et al.*, The heterocyclic ruthenium(III) complex KP1019 (FFC14A) causes DNA damage and oxidative stress in colorectal tumor cells, *Cancer Letters*, 2005, **226**, 115-121.
67. P. Heffeter*, et al.*, The ruthenium compound KP1339 potentiates the anticancer activity of sorafenib in vitro and in vivo, *European Journal of Cancer*, 2013, **49**, 3366-3375.
68. B. Schoenhacker-Alte*, et al.*, Sensitivity towards the GRP78 inhibitor KP1339/IT-139 is characterized by apoptosis induction via caspase 8 upon disruption of ER homeostasis, *Cancer Letters*, 2017, **404**, 79-88.
69. P. Collery*, et al.*, Preclinical and early clinical development of the oral Gallium complex KP46 (FFC11), *Metal Ions in Biology and Medicine*, 2006, **9**, 521-524.
70. A. R. Timerbaev, Advances in developing tris(8-quinolinolato)gallium(iii) as an anticancer drug: Critical appraisal and prospects, *Metallomics*, 2009, **1**, 193-198.
71. B. Kubista*, et al.*, Distinct activity of the bone-targeted gallium compound KP46 against osteosarcoma cells - Synergism with autophagy inhibition, *Journal of Experimental and Clinical Cancer Research*, 2017, **36**.
72. N. Wilfinger*, et al.*, Novel p53-dependent anticancer strategy by targeting iron signaling and BNIP3L-induced mitophagy, *Oncotarget*, 2016, **7**, 1242-1261.
73. U. Jungwirth*, et al.*, Calpain-mediated integrin deregulation as a novel mode of action for the anticancer gallium compound KP46, *Molecular Cancer Therapeutics*, 2014, **13**, 2436-2449.
74. C. R. Chitambar*, et al.*, Development of gallium compounds for treatment of lymphoma: Gallium maltolate, a novel hydroxypyrone gallium compound, induces apoptosis and circumvents lymphoma cell resistance to gallium nitrate, *Journal of Pharmacology and Experimental Therapeutics*, 2007, **322**, 1228-1236.
75. M. S. Chua*, et al.*, Gallium maltolate is a promising chemotherapeutic agent for the treatment of hepatocellular carcinoma, *Anticancer Research*, 2006, **26**, 1739-1743.

76. L. R. Bernstein, J. J. M. van der Hoeven and R. O. Boer, Hepatocellular carcinoma detection by gallium scan and subsequent treatment by gallium maltolate: Rationale and case study, *Anti-Cancer Agents in Medicinal Chemistry*, 2011, **11**, 585-590.
77. C. R. Chitambar, The therapeutic potential of iron-targeting gallium compounds in human disease: From basic research to clinical application, *Pharmacological Research*, 2017, **115**, 56-64.
78. B. C. Baguley and D. J. Kerr, *Anticancer Drug Development*, Academic Press, 2002.
79. A. K. Singh*, et al.*, Emerging importance of dietary phytochemicals in fight against cancer: Role in targeting cancer stem cells, *Critical Reviews in Food Science and Nutrition*, 2017, **57**, 3449-3463.
80. R. C. Alves*, et al.*, Characteristics, Properties and Analytical Methods of Paclitaxel: A Review, *Critical Reviews in Analytical Chemistry*, 2018, **48**, 110-118.
81. M. C. Wani*, et al.*, Plant Antitumor Agents.VI.The Isolation and Structure of Taxol, a Novel Antileukemic and Antitumor Agent from Taxus brevifolia2, *Journal of the American Chemical Society*, 1971, **93**, 2325-2327.
82. S. Prasad and B. B. Aggarwal, Turmeric, the Golden Spice: From Traditional Medicine to Modern Medicine in *Herbal Medicine: Biomolecular and Clinical Aspects*, eds. nd, I. F. F. Benzie and S. Wachtel-Galor, CRC Press/Taylor & Francis Llc., Boca Raton (FL), 2011.
83. H. Hatcher*, et al.*, Curcumin: From ancient medicine to current clinical trials, *Cellular and Molecular Life Sciences*, 2008, **65**, 1631-1652.
84. Y. Wang*, et al.*, Curcumin in Treating Breast Cancer: A Review, *Journal of Laboratory Automation*, 2016, **21**, 723-731.
85. D. Chirnomas*, et al.*, Chemosensitization to cisplatin by inhibitors of the Fanconi anemia/BRCA pathway, *Molecular Cancer Therapeutics*, 2006, **5**, 952-961.
86. S. S. Bhandarkar and J. L. Arbiser, Curcumin as an inhibitor of angiogenesis, *Advances in experimental medicine and biology*, 2007, **595**, 185-195.
87. L. H. Hartwell*, et al.*, From molecular to modular cell biology, *Nature*, 1999, **402**, C47-C52.
88. O. T. Schubert*, et al.*, Quantitative proteomics: Challenges and opportunities in basic and applied research, *Nature Protocols*, 2017, **12**, 1289-1294.
89. N. L. Anderson and N. G. Anderson, Proteome and proteomics: New technologies, new concepts, and new words, *Electrophoresis*, 1998, **19**, 1853-1861.
90. S. S. Thakur*, et al.*, Deep and highly sensitive proteome coverage by LC-MS/MS without prefractionation, *Molecular and Cellular Proteomics*, 2011, **10**, M110.003699.
91. R. W. Nelson*, et al.*, Mass Spectrometric Immunoassay, *Analytical Chemistry*, 1995, **67**, 1153-1158.
92. M. G. Weller, Quality Issues of Research Antibodies, *Analytical Chemistry Insights*, 2016, **2016**, 21-27.
93. N. L. Kelleher, Top-down proteomics, *Analytical Chemistry*, 2004, **76**, 196 A-203 A.
94. Y. Zhang*, et al.*, Protein analysis by shotgun/bottom-up proteomics, *Chemical Reviews*, 2013, **113**, 2343-2394.
95. L. C. Gillet, A. Leitner and R. Aebersold, Mass Spectrometry Applied to Bottom-Up Proteomics: Entering the High-Throughput Era for Hypothesis Testing, *Journal*, 2016, **9**, 449-472.
96. T. Rabilloud*, et al.*, Two-dimensional gel electrophoresis in proteomics: Past, present and future, *Journal of Proteomics*, 2010, **73**, 2064-2077.
97. T. Schmidt*, et al.*, ProteomicsDB, *Nucleic Acids Research*, 2018, **46**, D1271-D1281.
98. M. Wilhelm*, et al.*, Mass-spectrometry-based draft of the human proteome, *Nature*, 2014, **509**, 582-587.
99. A. Bateman*, et al.*, UniProt: The universal protein knowledgebase, *Nucleic Acids Research*, 2017, **45**, D158-D169.
100. A. Shevchenko*, et al.*, In-gel digestion for mass spectrometric characterization of proteins and proteomes, *Nature Protocols*, 2007, **1**, 2856-2860.
101. J. R. Wiśniewski*, et al.*, Universal sample preparation method for proteome analysis, *Nature Methods*, 2009, **6**, 359-362.
102. S. Camerini and P. Mauri, The role of protein and peptide separation before mass spectrometry analysis in clinical proteomics, *Journal of Chromatography A*, 2015, **1381**, 1-12.

103. N. Nagaraj*, et al.*, System-wide perturbation analysis with nearly complete coverage of the yeast proteome by single-shot ultra HPLC runs on a bench top orbitrap, *Molecular and Cellular Proteomics*, 2012, **11**, M111.013722.
104. H. Kočová Vlčková*, et al.*, Current state of bioanalytical chromatography in clinical analysis, *Analyst*, 2018, **143**, 1305-1325.
105. T. Köcher*, et al.*, Analysis of protein mixtures from whole-cell extracts by single-run nanolc-ms/ms using ultralong gradients, *Nature Protocols*, 2012, **7**, 882-890.
106. J. Šesták, D. Moravcová and V. Kahle, Instrument platforms for nano liquid chromatography, *Journal of Chromatography A*, 2015, **1421**, 2-17.
107. H. Liu*, et al.*, Effects of column length, particle size, gradient length and flow rate on peak capacity of nano-scale liquid chromatography for peptide separations, *Journal of Chromatography A*, 2007, **1147**, 30-36.
108. J. C. Medina, N. Wu and M. L. Lee, Comparison of empirical peak capacities for high-efficiency capillary chromatographic techniques, *Analytical Chemistry*, 2001, **73**, 1301-1306.
109. J. P. Chervet, M. Ursem and J. P. Salzmann, Instrumental requirements for nanoscale liquid chromatography, *Analytical Chemistry*, 1996, **68**, 1507-1512.
110. J. Rappsilber, M. Mann and Y. Ishihama, Protocol for micro-purification, enrichment, pre-fractionation and storage of peptides for proteomics using StageTips, *Nature Protocols*, 2007, **2**, 1896-1906.
111. Agilent Technologies, Infinitely better for microfluidic nanospray LC/MS, 2010, 5990-6221EN.
112. D. A. Wolters, M. P. Washburn and J. R. Yates Iii, An automated multidimensional protein identification technology for shotgun proteomics, *Analytical Chemistry*, 2001, **73**, 5683-5690.
113. D. L. Swaney, G. C. McAlister and J. J. Coon, Decision tree-driven tandem mass spectrometry for shotgun proteomics, *Nature Methods*, 2008, **5**, 959-964.
114. A. Schmidt, I. Forne and A. Imhof, Bioinformatic analysis of proteomics data, *BMC Systems Biology*, 2014, **8(Suppl 2)**, S3.
115. A. Michalski*, et al.*, Mass spectrometry-based proteomics using Q Exactive, a high-performance benchtop quadrupole Orbitrap mass spectrometer, *Molecular and Cellular Proteomics*, 2011, **10**, M111.011015.
116. A. Makarov, Electrostatic axially harmonic orbital trapping: A high-performance technique of mass analysis, *Analytical Chemistry*, 2000, **72**, 1156-1162.
117. M. Scigelova and A. Makarov, Orbitrap mass analyzer - Overview and applications in proteomics, *Proteomics*, 2006, **1**, 16-21.
118. T. A. Addona*, et al.*, Multi-site assessment of the precision and reproducibility of multiple reaction monitoring-based measurements of proteins in plasma, *Nature Biotechnology*, 2009, **27**, 633-641.
119. P. Picotti and R. Aebersold, Selected reaction monitoring-based proteomics: Workflows, potential, pitfalls and future directions, *Nature Methods*, 2012, **9**, 555-566.
120. A. C. Peterson*, et al.*, Parallel reaction monitoring for high resolution and high mass accuracy quantitative, targeted proteomics, *Molecular and Cellular Proteomics*, 2012, **11**, 1475-1488.
121. J. D. Chapman, D. R. Goodlett and C. D. Masselon, Multiplexed and data-independent tandem mass spectrometry for global proteome profiling, *Mass Spectrometry Reviews*, 2014, **33**, 452-470.
122. Z. Li*, et al.*, Systematic comparison of label-free, metabolic labeling, and isobaric chemical labeling for quantitative proteomics on LTQ orbitrap velos, *Journal of Proteome Research*, 2012, **11**, 1582-1590.
123. T. C. Walther and M. Mann, Mass spectrometry-based proteomics in cell biology, *Journal of Cell Biology*, 2010, **190**, 491-500.
124. W. Wang*, et al.*, Quantification of proteins and metabolites by mass spectrometry without isotopic labeling or spiked standards, *Analytical Chemistry*, 2003, **75**, 4818-4826.
125. B. Zybailov*, et al.*, Statistical analysis of membrane proteome expression changes in Saccharomyces cerevisiae, *Journal of Proteome Research*, 2006, **5**, 2339-2347.
126. B. Titz*, et al.*, Proteomics for systems toxicology, *Computational and Structural Biotechnology Journal*, 2015, **11**, 73-90.
127. M. H. Dias*, et al.*, Proteomics and drug discovery in cancer, *Drug Discovery Today*, 2015, 264-277.
128. C. A. Luber*, et al.*, Quantitative Proteomics Reveals Subset-Specific Viral Recognition in Dendritic Cells, *Immunity*, 2010, **32**, 279-289.

129. J. Malmström, *et al.*, Proteome-wide cellular protein concentrations of the human pathogen Leptospira interrogans, *Nature*, 2009, **460**, 762-765.
130. J. Cox, *et al.*, Andromeda: A peptide search engine integrated into the MaxQuant environment, *Journal of Proteome Research*, 2011, **10**, 1794-1805.
131. D. N. Perkins, *et al.*, Probability-based protein identification by searching sequence databases using mass spectrometry data, *Electrophoresis*, 1999, **20**, 3551-3567.
132. J. Cox and M. Mann, MaxQuant enables high peptide identification rates, individualized p.p.b.-range mass accuracies and proteome-wide protein quantification, *Nature Biotechnology*, 2008, **26**, 1367-1372.
133. A. I. Nesvizhskii and R. Aebersold, Interpretation of shotgun proteomic data: The protein inference problem, *Molecular and Cellular Proteomics*, 2005, **4**, 1419-1440.
134. J. Cox and M. Mann, 1D and 2D annotation enrichment: a statistical method integrating quantitative proteomics with complementary high-throughput data, *BMC Bioinformatics*, 2012, **13 Suppl 16**, S12.
135. A. N. Kettenbach, J. Rush and S. A. Gerber, Absolute quantification of protein and post-translational modification abundance with stable isotope-labeled synthetic peptides, *Nature Protocols*, 2011, **6**, 175-186.
136. L. C. Gillet, *et al.*, Targeted data extraction of the MS/MS spectra generated by data-independent acquisition: A new concept for consistent and accurate proteome analysis, *Molecular and Cellular Proteomics*, 2012, **11**, O111.016717.
137. M. Ashburner, *et al.*, Gene ontology: Tool for the unification of biology, *Nature Genetics*, 2000, **25**, 25-29.
138. D. W. Huang, B. T. Sherman and R. A. Lempicki, Systematic and integrative analysis of large gene lists using DAVID bioinformatics resources, *Nature Protocols*, 2009, **4**, 44-57.
139. D. W. Huang, B. T. Sherman and R. A. Lempicki, Bioinformatics enrichment tools: Paths toward the comprehensive functional analysis of large gene lists, *Nucleic Acids Research*, 2009, **37**, 1-13.
140. M. Kanehisa and S. Goto, KEGG: Kyoto Encyclopedia of Genes and Genomes, *Nucleic Acids Research*, 2000, **28**, 27-30.
141. D. Croft, *et al.*, Reactome: A database of reactions, pathways and biological processes, *Nucleic Acids Research*, 2011, **39**, D691-D697.
142. A. Franceschini, *et al.*, STRING v9.1: Protein-protein interaction networks, with increased coverage and integration, *Nucleic Acids Research*, 2013, **41**, D808-D815.
143. A. P. Li, Preclinical in vitro screening assays for drug-like properties, *Drug Discovery Today: Technologies*, 2005, **2**, 179-185.
144. W. G. Schoonen, W. M. Westerink and G. J. Horbach, High-throughput screening for analysis of in vitro toxicity in *Molecular, Clinical and Environmental Toxicology Experientia Supplementum*, ed. A. Luch, Birkhäuser, Basel, Switzerland, 2009, vol. 99, pp. 401-452.
145. R. Baudoin, *et al.*, Trends in the development of microfluidic cell biochips for in vitro hepatotoxicity, *Toxicology in Vitro*, 2007, **21**, 535-544.
146. L. Kang, *et al.*, Microfluidics for drug discovery and development: from target selection to product lifecycle management, *Drug Discovery Today*, 2008, **13**, 1-13.
147. R. Khamsi, Labs on a chip: Meet the stripped down rat, *Nature*, 2005, **435**, 12-13.
148. B. A. Merrick and F. A. Witzmann, The role of toxicoproteomics in assessing organ specific toxicity in *Molecular, Clinical and Environmental Toxicology Experientia Supplementum*, ed. A. Luch, Birkhäuser, Basel, Switzerland, 2009, vol. 99, pp. 367-400.
149. J. M. Pascoe and J. J. Roberts, Interactions between mammalian cell DNA and inorganic platinum compounds-I. DNA interstrand cross-linking and cytotoxic properties of platinum(II) compounds, *Biochemical Pharmacology*, 1974, **23**, 1345-1357.
150. Z. Adhireksan, *et al.*, Ligand substitutions between ruthenium-cymene compounds can control protein versus DNA targeting and anticancer activity, *Nature Communications*, 2014, **5**, 3462.
151. T. Zou, *et al.*, Chemical biology of anticancer gold(III) and gold(i) complexes, *Chemical Society Reviews*, 2015, **44**, 8786-8801.
152. Y. T. Lai, *et al.*, Integration of fluorescence imaging with proteomics enables visualization and identification of metallo-proteomes in living cells, *Metallomics*, 2017, **9**, 38-47.

153. S. K. Fung*, et al.*, Cyclometalated Gold(III) Complexes Containing N-Heterocyclic Carbene Ligands Engage Multiple Anti-Cancer Molecular Targets, *Angewandte Chemie - International Edition*, 2017, **56**, 3892-3896.
154. R. Ge*, et al.*, A proteomic approach for the identification of bismuth-binding proteins in Helicobacter pylori, *Journal of Biological Inorganic Chemistry*, 2007, **12**, 831-842.
155. M. Stefanopoulou*, et al.*, Cell response of Escherichia coli to cisplatin-induced stress, *Proteomics*, 2012, **11**, 4174-4188.
156. J. Will, W. S. Sheldrick and D. Wolters, Characterisation of cisplatin coordination sites in cellular Escherichia coli DNA-binding proteins by combined biphasic liquid chromatography and ESI tandem mass spectrometry, *Journal of Biological Inorganic Chemistry*, 2008, **13**, 421-434.
157. J. Will*, et al.*, Identification of (η6-arene)ruthenium(II) protein binding sites in E. coli cells by combined multidimensional liquid chromatography and ESI tandem mass spectrometry: Specific binding of [(η6-p-cymene) RuCl2(DMSO)] to stress-regulated proteins and to helicases, *Journal of Biological Inorganic Chemistry*, 2007, **12**, 883-894.
158. M. V. Babak*, et al.*, Target profiling of an antimetastatic RAPTA agent by chemical proteomics: Relevance to the mode of action, *Chemical Science*, 2015, **6**, 2449-2456.
159. J. Wang*, et al.*, In situ Proteomic Profiling of Curcumin Targets in HCT116 Colon Cancer Cell Line, *Scientific Reports*, 2016, **6**, 22146.
160. R. T. Lawrence*, et al.*, The Proteomic Landscape of Triple-Negative Breast Cancer, *Cell Reports*, 2015, **11**, 1-15.
161. E. Martinez-Balibrea*, et al.*, A proteomic approach links decreased pyruvate kinase M2 expression to oxaliplatin resistance in patients with colorectal cancer and in human cell lines, *Molecular Cancer Therapeutics*, 2009, **8**, 771-778.
162. T. Ozdian*, et al.*, Proteomic profiling reveals DNA damage, nucleolar and ribosomal stress are the main responses to oxaliplatin treatment in cancer cells, *Journal of Proteomics*, 2017, **162**, 73-85.
163. Y. Yao*, et al.*, Comparative proteomic analysis of colon cancer cells in response to Oxaliplatin treatment, *Biochimica et Biophysica Acta - Proteins and Proteomics*, 2009, **1794**, 1433-1440.
164. A. Castagna*, et al.*, A proteomic approach to cisplatin resistance in the cervix squamous cell carcinoma cell line A431, *Proteomics*, 2004, **4**, 3246-3267.
165. K. Le Moguen*, et al.*, Comparative proteomic analysis of cisplatin sensitive IGROV1 ovarian carcinoma cell line and its resistant counterpart IGROV1-R10, *Proteomics*, 2006, **6**, 5183-5192.
166. K. Le Moguen*, et al.*, A proteomic kinetic analysis of IGROV1 ovarian carcinoma cell line response to cisplatin treatment, *Proteomics*, 2007, **7**, 4090-4101.
167. X. D. Yan*, et al.*, Identification of platinum-resistance associated proteins through proteomic analysis of human ovarian cancer cells and their platinum-resistant sublines, *Journal of Proteome Research*, 2007, **6**, 772-780.
168. V. Paulitschke*, et al.*, Functional classification of cellular proteome profiles support the identification of drug resistance signatures in melanoma cells, *Journal of Proteome Research*, 2013, **12**, 3264-3276.
169. G. Sathe*, et al.*, Phosphotyrosine profiling of curcumin-induced signaling, *Clinical Proteomics*, 2016, **13**, 13.
170. T. Sato*, et al.*, Phosphoproteomic analysis identifies signaling pathways regulated by curcumin in human colon cancer cells, *Anticancer Research*, 2017, **37**, 4789-4798.
171. J. G. Lee*, et al.*, Identification of anti-metastatic drug and natural compound targets in isogenic colorectal cancer cells, *Journal of Proteomics*, 2015, **113**, 326-336.
172. R. F. S. Lee*, et al.*, Expression proteomics study to determine metallodrug targets and optimal drug combinations, *Scientific Reports*, 2017, **7**, 1590.
173. V. S. Ayyar*, et al.*, Functional proteomic analysis of corticosteroid pharmacodynamics in rat liver: Relationship to hepatic stress, signaling, energy regulation, and drug metabolism, *Journal of Proteomics*, 2017, **160**, 84-105.
174. Z. Firouzi*, et al.*, Proteomics screening of molecular targets of curcumin in mouse brain, *Life Sciences*, 2014, **98**, 12-17.
175. S. Fu*, et al.*, Proteogenomic studies on cancer drug resistance: towards biomarker discovery and target identification, *Expert Review of Proteomics*, 2017, **14**, 351-362.

176. A. E. Kel*, et al.*, Multi-omics "upstream analysis" of regulatory genomic regions helps identifying targets against methotrexate resistance of colon cancer, *EuPA Open Proteomics*, 2016, **13**, 1-13.
177. K. Karaosmanoglu*, et al.*, Assessment of berberine as a multi-target antimicrobial: A multi-omics study for drug discovery and repositioning, *OMICS A Journal of Integrative Biology*, 2014, **18**, 42-53.
178. S. Qiu*, et al.*, Dissect new mechanistic insights for geniposide efficacy on the hepatoprotection using multiomics approach, *Oncotarget*, 2017, **8**, 108760-108770.
179. B. Muqaku*, et al.*, Coffee consumption modulates inflammatory processes in an individual fashion, *Molecular Nutrition and Food Research*, 2016, **60**, 2529-2541.
180. S. Takahashi*, et al.*, An integrated multi-omics study revealed metabolic alterations underlying the effects of coffee consumption, *PLoS ONE*, 2014, **9**, e91134.
181. D. A. Wolters*, et al.*, Combination of metallomics and proteomics to study the effects of the metallodrug RAPTA-T on human cancer cells, *Metallomics*, 2012, **4**, 1185-1196.
182. S. M. Meier*, et al.*, Proteomic and metabolomic analyses reveal contrasting anti-inflammatory effects of an extract of Mucor racemosus secondary metabolites compared to dexamethasone, *PLoS ONE*, 2015, **10**, e0140367.
183. A. Tahir*, et al.*, Combined Proteome and Eicosanoid Profiling Approach for Revealing Implications of Human Fibroblasts in Chronic Inflammation, *Analytical Chemistry*, 2017, **89**, 1945-1954.
184. R. L. Mayer*, et al.*, Proteomics and metabolomics identify molecular mechanisms of aging potentially predisposing for chronic lymphocytic leukemia, *Molecular and Cellular Proteomics*, 2018, **17**, 290-303.
185. C. Pan*, et al.*, Comparative proteomic phenotyping of cell lines and primary cells to assess preservation of cell type-specific functions, *Molecular and Cellular Proteomics*, 2009, **8**, 443-450.
186. A. Slany*, et al.*, Cell characterization by proteome profiling applied to primary hepatocytes and hepatocyte cell lines Hep-G2 and Hep-3B, *Journal of Proteome Research*, 2010, **9**, 6-21.
187. T. Mosmann, Rapid colorimetric assay for cellular growth and survival: application to proliferation and cytotoxicity assays, *Journal of Immunological Methods*, 1983, **65**, 55-63.
188. M. V. Berridge and A. S. Tan, Characterization of the cellular reduction of 3-(4,5-dimethylthiazol-2-yl)-2,5-diphenyltetrazolium bromide (MTT): subcellular localization, substrate dependence, and involvement of mitochondrial electron transport in MTT reduction, *Archives of Biochemistry and Biophysics*, 1993, **303**, 474-482.
189. ATCC - American Type Culture Collection, MTT Cell Proliferation Assay Instruction Guide, 2011, 30-1010K.
190. A. Bileck*, et al.*, Evaluation of inflammation-related signaling events covering phosphorylation and nuclear translocation of proteins based on mass spectrometry data, *Journal of Proteomics*, 2017, **152**, 161-171.
191. D. Koley and A. J. Bard, Triton X-100 concentration effects on membrane permeability of a single HeLa cell by scanning electrochemical microscopy (SECM), *Proceedings of the National Academy of Sciences of the United States of America*, 2010, **107**, 16783-16787.
192. M. Groessl*, et al.*, Proteome profiling of breast cancer biopsies reveals a wound healing signature of cancer-associated fibroblasts, *Journal of Proteome Research*, 2014, **13**, 4773-4782.
193. S. K. Akiyama, Integrins in cell adhesion and signaling, *Human Cell*, 1996, **9**, 181-186.
194. S. Saveliev*, et al.*, Trypsin/Lys-C protease mix for enhanced protein mass spectrometry analysis, *Nature Methods*, 2013, **10**, Advertising Feature: Application Note.
195. L. Käll*, et al.*, Assigning significance to peptides identified by tandem mass spectrometry using decoy databases, *Journal of Proteome Research*, 2008, **7**, 29-34.
196. A. P. Diz, A. Carvajal-Rodriguez and D. O. F. Skibinski, Multiple Hypothesis Testing in Proteomics: A Strategy for Experimental Work, *Molecular and Cellular Proteomics*, 2011, **10**, M110.004374.

2. Results and Discussion

2.1. Response Profiling Using Shotgun Proteomics Enables Global Metallodrug Mechanisms of Action To Be Established

Dominique Kreutz[a], Andrea Bileck[a], Kerstin Plessl[b], Denise Wolrab[a], Michael Groessl[a], Bernhard K. Keppler[c], Samuel M. Meier[a] and Christopher Gerner[a]

Chemistry - A European Journal, **2017**, 23 (8), 1881-1890

[a] Department of Analytical Chemistry, Faculty of Chemistry, University of Vienna, Waehringer Strasse 38, Vienna, Austria

[b] Department of Obstetrics and Fetal-Maternal Medicine, Reproductive Biology Unit, Medical University of Vienna, Waehringer Guertel 18–20, 5Q, Vienna, Austria

[c] Department of Inorganic Chemistry, Faculty of Chemistry, University of Vienna, Waehringer Strasse 42, Vienna, Austria

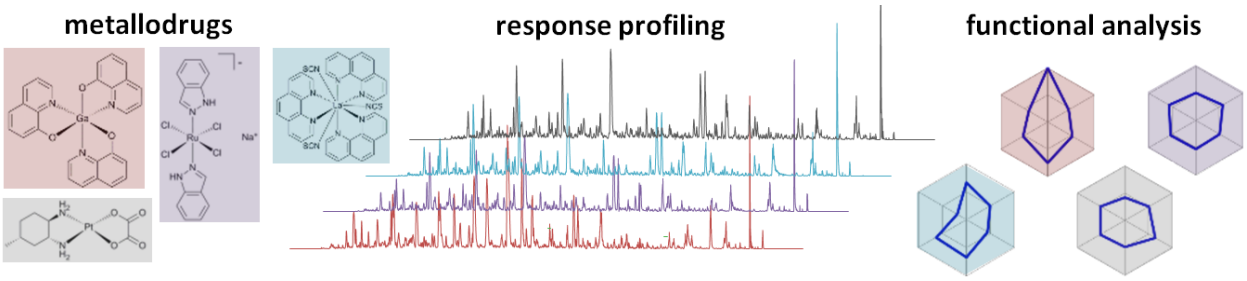

Contributions to this publication:

- Conduction of experiments
- Preparation of figures
- Involved in experimental design, data interpretation and writing of the manuscript

ChemPubSoc Europe

DOI: 10.1002/chem.201604516

CHEMISTRY A European Journal Full Paper

Cancer

Response Profiling Using Shotgun Proteomics Enables Global Metallodrug Mechanisms of Action To Be Established

Dominique Kreutz,[a] Andrea Bileck,[a] Kerstin Plessl,[b] Denise Wolrab,[a] Michael Groessl,[a] Bernhard K. Keppler,[c] Samuel M. Meier,[a] and Christopher Gerner*[a]

Abstract: Response profiling using shotgun proteomics for establishing global metallodrug mechanisms of action in two colon carcinoma cell lines, HCT116 and SW480, has been applied and evaluated with the clinically approved arsenic trioxide. Surprisingly, the complete established mechanism of action of arsenic trioxide was observed by protein regulations in SW480, but not HCT116 cells. Comparing the basal protein expression in the two cell lines revealed an 80% convergence of protein identification, but with significant expression differences, which in turn seem to affect the extent of protein regulation. A clear-cut redox response was observed in SW480 cells upon treatment with arsenic, but hardly in HCT116 cells. Response profiling was then used to investigate four anti-cancer metallodrugs (KP46, KP772, KP1339 and KP1537). Proteome alterations were mapped to selected functional groups, including DNA repair, endocytosis, protection from oxidative stress, protection from endoplasmatic reticulum (ER) stress, cell adhesion and mitochondrial function. The present data suggest that knowledge of the mechanism of action of anti-cancer metallodrugs and improved patient stratification strategies are imperative for the design of clinical studies.

Introduction

Evaluating a drug candidate's prospect of success is an important step in the process of drug discovery and development. Phenotypic assays for assessing cell cycle distribution, viability and death are widely used screening methods in cancer research.[1] However, these tests give little information about global drug effects on a molecular level. Such global molecular profiling methods are particularly sought after in metal-based anti-cancer research because metallodrugs are unspecific according to the general paradigm and it is a formidable challenge to elucidate their mechanisms of action or even direct targets. Because proteins are active players in cellular fate and function, proteome profiling is a powerful tool for identifying specific cellular responses to drug treatments,[2] including induced protein synthesis or proteasomal degradation (i.e., response profiling). Furthermore, chemical proteomics was recently used to profile the potential molecular targets of a ruthenium(II) arene 1,3,5-triaza-7-phosphaadamantane (RAPTA) derivative.[3] Attempts to use proteome profiling for drug screening have already been conducted but those investigations usually combined basal cell states with phenotypic in vitro data.[4,5]

Response profiling is usually based on label-free quantification (LFQ) proteomics, which brings many potential advantages. A broader dynamic range of concentrations can be covered in contrast to label-based methods like SILAC (stable isotope labelling with amino acids) or iTRAQ (isobaric tag for relative and absolute quantitation) and there are fewer sample preparation steps. Additionally, there is no restriction in sample numbers[6] and omitting stable isotope-labelled compounds reduces costs.[7] At the same time, we also sought to increase analytical efficiency by further reducing sample preparation and measurement times to improve the fitness of response profiling for a wide applicability.

The aim of this study was to establish response profiling as a reliable method for assessing the cellular effects of metal-based drug candidates by investigating their global mechanisms of action at a molecular level by using in-depth label-free proteome profiling. The method was evaluated in two colon carcinoma cell lines (i.e., HCT116 and SW480) by using the clinically approved arsenic trioxide (Trisenox, As_2O_3), which is used for treating multiple myeloma and leukaemia and its mechanism of action is largely known.[8,9] The confirmed drug effects of As_2O_3 were then used to construct cancer-related functional groups of proteins for comparative evaluation of four novel metal-based drug candidates belonging to diverse compound families (Figure 1A), including the advanced

[a] D. Kreutz, Dr. A. Bileck, D. Wolrab, Dr. M. Groessl, Dr. S. M. Meier, Prof. Dr. C. Gerner
Department of Analytical Chemistry, Faculty of Chemistry
University of Vienna, Waehringer Strasse 38, 1090 Vienna (Austria)
E-mail: christopher.gerner@univie.ac.at

[b] Dr. K. Plessl
Department of Obstetrics and Fetal-Maternal Medicine
Reproductive Biology Unit, Medical University of Vienna
Waehringer Guertel 18–20, 5Q, 1090 Vienna (Austria)

[c] Prof. Dr. B. K. Keppler
Department of Inorganic Chemistry, Faculty of Chemistry
University of Vienna, Waehringer Strasse 42, 1090 Vienna (Austria)

Supporting information and the ORCID identification number(s) for the author(s) of this article can be found under http://dx.doi.org/10.1002/chem.201604516.

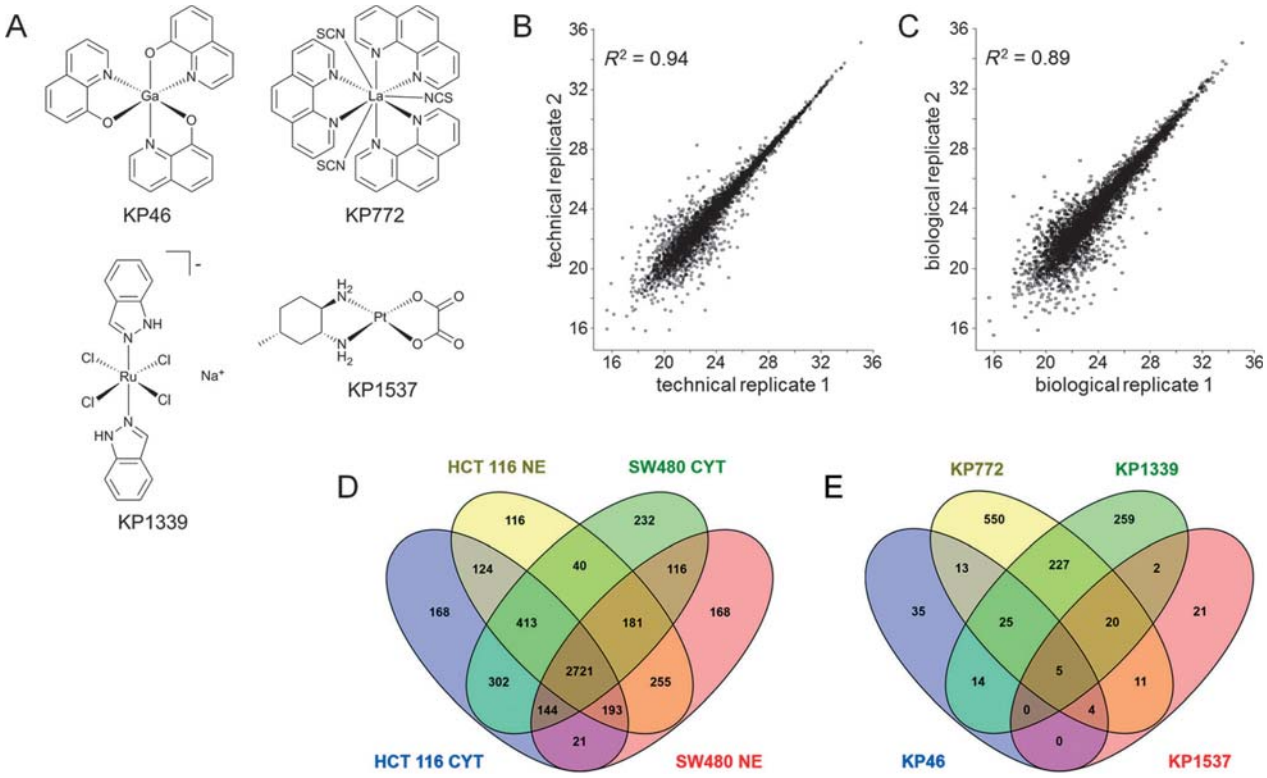

Figure 1. A) Chemical structures of the investigated metal-based drug candidates. Representation of B) technical repeatability and C) biological reproducibility exemplified by the nuclear fractions of SW480 cells treated with KP46. The axes show protein abundances as LFQ values in logarithmic scale to base two. D) Plot of the number of common as well as specific protein identifications in the different fractions (CYT and NE) of HCT116 and SW480. E) An analogous plot exemplifies the numbers of shared as well as unique significant protein regulation events in SW480 nuclear extracts upon treatment with the indicated drug.

sodium *trans*-[tetrachlorobis(1*H*-indazole)ruthenate(III)] (KP1339), tris(8-quinolinolato)gallium(III) (KP46) and the investigational [tris(1,10-phenanthroline)lanthanum(III)] trithiocyanate (KP772) and [(1*R*,2*R*,4*R*)-4-methyl-1,2-cyclohexanediamine] oxalatoplatinum(II) (KP1537).[10]

Results and Discussion

Two colon carcinoma cell lines, HCT116 and SW480, were treated with five metal-based compounds, As_2O_3, which is already used in cancer treatment, and the four anti-cancer drug candidates KP46, KP772, KP1339 and KP1537. Then, the response profiles were investigated by in-depth label-free proteomics. Cells were fractionated into cytoplasmic (CYT) and nuclear extracts (NE). The CYT contains the soluble protein fraction and the NE contains nuclear proteins but also insoluble parts of the cytoplasm, including the cytoskeleton, mitochondria and other organelles. Fractionation was performed because the intracellular platinum distribution was previously determined as an important factor in its mode of action[11] and therefore this might also be relevant for other compound classes. Overall, we identified 5525 non-redundant proteins (i.e., protein groups) in 144 single-injection nano-liquid chromatography (LC)-MS/MS runs, each lasting 135 minutes. Overall, this reduced the measurement time eight-fold compared with previous profiling studies,[2] and at the cost of only 20% protein identifications.

During data evaluation, redundant proteins were joined to protein groups by using MaxQuant.[12] Therefore, the proteins discussed here always correspond to protein groups. The overall measurement time for one metallodrug using response profiling was 54 hours and included control and treated cells, CYT and NE fractions of each state and three biological and two technical replicates. Technical repeatability and biological reproducibility showed average R^2 values of 0.90 and 0.82, respectively (Figure 1B,C), and underlined the stability of the complete workflow from cell culture experiments to in-solution digestion and LC-MS analysis on the proteomic scale. Between 4200 and 5100 proteins were identified per run after applying a false discovery rate (FDR) of 0.01, which generates a data density of three peptide identifications per second over the chromatographic gradient. The detected proteins covered a concentration range of over eight orders of magnitude. Protein regulations were statistically evaluated by performing t-tests, including a permutation-based FDR of 0.05, giving multi-parameter-corrected (mp)-significant changes. Unless otherwise stated, all the protein regulations discussed below were mp-significant.

Response profiling qualifies for tracing metallodrug mechanisms of action

The applicability of response profiling to investigating metallodrug effects was tested by treating the two cell lines with As_2O_3. Although 875 proteins were found significantly regulated in the cytoplasm and 967 proteins in the nuclear extract of SW480 cells, only 3 cytoplasmic and 13 nuclear proteins were found regulated in HCT116 cells (see Table S1 in the Supporting Information). Based on the known mechanism of action,[9] we expected to find a clear reactive oxygen species (ROS) signature. Oxidative stress initiated by As_2O_3 treatment indeed led to an induction of heme oxygenase 1 (HMOX1) and other protection proteins from the Nrf2-Keap1 pathway, for example, thioredoxin or glutathione systems (Figure 2). Moreover, other chaperones, including 78 kDa glucose regulated protein (BiP), heat shock 70 kDa proteins 1A/AB, 1-like, 4, 4L and 6, heat shock cognate 71 kDa protein, heat shock proteins 105 kDa, beta 1, hsp90 alpha and hsp90 beta, were found to be induced (see Table S1), which indicates that massive protein denaturation is caused by the drug.

SW480 cells display cardinal effects of As_2O_3 response

It is also known that As_2O_3 treatment leads to the degradation of the PML-RARα fusion protein by targeting promyelocytic leukemia protein (PML), a tumour suppressor that is involved in various apoptotic pathways.[13] Another postulated direct target of arsenic trioxide is the inhibition of pyruvate dehydrogenase (PDHA1).[9] With the presently applied profiling method, we found that treating SW480 cells with As_2O_3 led to an eight-fold down-regulation of PML in NE (Figure 2). PDHA1 was also affected; a marked increase in the NE (Figure 2) indicated protein translocation that might lead to its inactivation. Response profiling also identified strongly up-regulated redox proteins. For example, HMOX1 and thioredoxin reductase 1 (TXNRD1) were up-regulated 760- and 3-fold, respectively, in CYT after treatment (Figure 2).The role of the former may not be solely cyto-protective, because induction of this protein was also proposed to be responsible for the cytotoxicity of As_2O_3.[9] Heat shock proteins were also induced, as exemplified by HSPA1A and HSPA6 (Figure 2) in both fractions. Similarly, the chaperones α-crystallin B chain and protein Niban were 3800- and 13-fold up-regulated, respectively, in CYT. Therefore, our experiments indicate the occurrence of DNA strand breaks, as characterised by the up-regulation of DNA double-stranded break (DSB) repair proteins, for example, CDCA5. In conclusion, the previously reported proteins that are implicated in the As_2O_3 mechanism of action were successfully identified and their regulations were in full accordance with previous reports.

HCT116 cells show a truncated response upon As_2O_3 treatment

A 15-fold down-degradation of PML was observed in treated HCT116 cells as well as an up-regulation of HMOX1, similarly to SW480 cells. Intriguingly, HCT116 cells lacked a ROS response, as TXNRD1 and other redox proteins were not regulated at all. Moreover, heat shock proteins, DSB repair proteins and PDHA1 were only slightly regulated. Because a strong induction of HMOX1 and down-regulation of PML were observed in both cell types, we denoted them as robust effects of the arsenic treatment, whereas the other proclaimed responses seem to be cell-line specific.

In fact, we found that almost all the proteins specifically induced in SW480 cells show significantly higher basal expres-

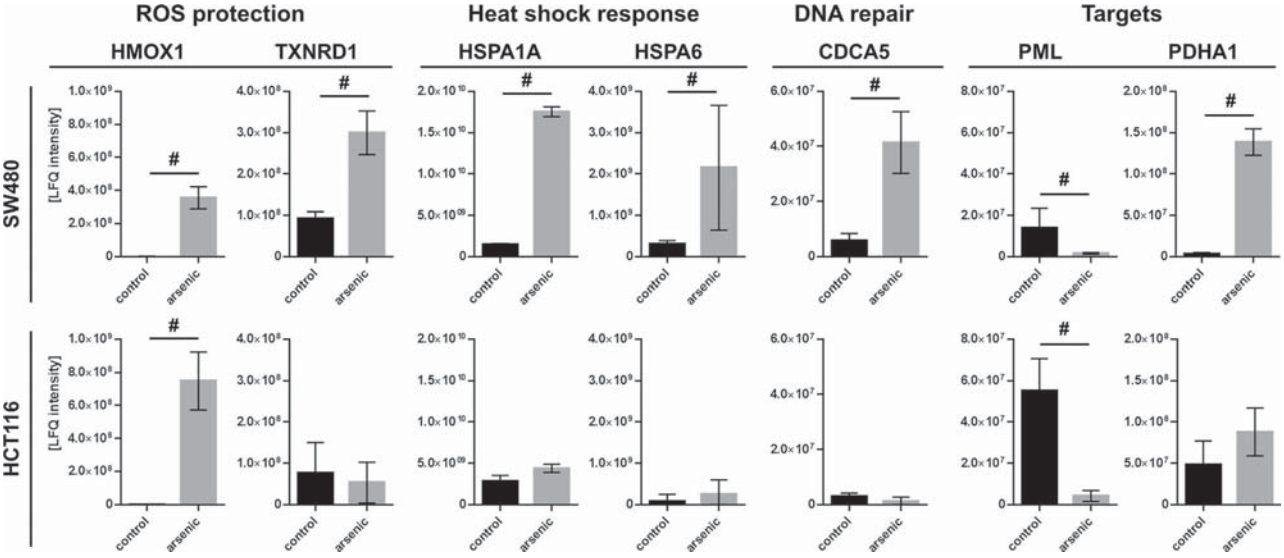

Figure 2. Regulations of proteins upon treatment with As_2O_3 are shown for HCT116 and SW480 cells. The proteins represented are implicated in the known mechanism of action of As_2O_3. Multi-parameter-significant changes in protein abundances are denoted with a hash (p value < 0.05, FDR < 0.01). Proteins involved in ROS protection and heat shock response were determined in the cytoplasmic fraction. Proteins involved in DNA repair as well as targets of arsenic trioxide were determined in the nuclear fraction.

sion levels in HCT116 cells (see Table S1 in the Supporting Information), thereby making the need for additional protein synthesis negligible. This observation suggests that response profiling not only allows the investigation of drug effects, but also supports the prediction of potential drug effects based on the basal protein expression of any kind of cellular system.

Basal protein expression varies significantly in HCT116 and SW480 cells

Genetic variability

There are several known differences between the two investigated cell lines on the genetic level. Although HCT116 and SW480 cells are both KRAS mutant, but BRAF and PTEN wild type, they differ in the mutation status of other genes relevant to cancer. Overall, 359 and 122 genetic mutations were detected in HCT116 and SW480 cells, respectively.[14] The p53 status of HCT116 cells is wild type, whereas for SW480 it is double-mutant. There is a PIK3CA mutation in HCT116 cells that is not present in SW480 cells.[15] In contrast, an APC mutation was demonstrated for SW480 only.[16]

Proteomic variability

Investigating the basal expression of proteins in the two cell lines revealed a convergence of approximately 80% of the protein identifications (Figure 1D). Their relative abundances, however, varied strongly identifying 2486 and 2910 significant protein expression differences in the CYT and NE fractions, respectively. Because identical amounts of protein were analysed, that is, 25 μg per sample, this finding enabled us to correlate basal protein expression with the cell's capacity to cope with stress. The observed fold changes reached 77000-fold higher levels of interleukin-18 in the CYT of HCT116 and 230000-fold higher levels of histone H1.5 in the NE of SW480. The abundance of the adipogenesis regulatory factor was found to be 2400 times higher in the HCT116 cytoplasmic fraction. Overexpression of this protein has been related to *cis*-platinum resistance.[17] The insulin-like growth factor 2 mRNA-binding protein 1, which was 150- and 540-fold enriched in the CYT and NE of SW480 cells, respectively, may protect cells during oxidative stress.[17] Peroxiredoxins were up to 34 times more abundant in HCT116 and are also implicated in the Nrf2-Keap1 pathway of antioxidant effects.[18] Consequently, the two different cell types are clearly equipped with distinct features to deal with ROS.

Data evaluation by using the Database for Annotation, Visualisation and Integrated Discovery (DAVID)[19] revealed DNA repair to be enriched in SW480 nuclear extracts (e.g., nucleotide excision repair, mismatch repair or homologous recombination). In HCT116 nuclear extracts, on the other hand, proteins involved in redox regulating processes such as oxidative phosphorylation, the pentose phosphate pathway or glutathione metabolism were found to be more abundant. Several pathways concerning the metabolism of sugars, including glycolysis/gluconeogenesis and galactose metabolism clustered in HCT116 NE, indicating a higher metabolic turnover.

We also discovered differences in the abundance of integrins, which are important extracellular matrix (ECM) interactors.[20] The laminin receptor integrin β4 was 4 and 14 times more abundant in the CYT and NE of HCT116 cells, respectively. Integrin β5, a receptor for fibronectin, on the other hand, was 42 and 7 times more abundant in the respective SW480 fractions. Also, the integrins β1, α3, α5 and α6 were more abundant in HCT116, whereas integrin αV was the only integrin more abundant in SW480 cells. This might indicate the differential cell adhesion properties of both cell lines. To verify our findings we performed cell adhesion tests with the ECM proteins laminin, collagen and fibronectin with poly-D-lysine as the positive control and bovine serum albumin (BSA) as the negative control (Figure 3).

The drastic differences in the basal expression of numerous proteins in the two cell lines support the hypothesis that they might be causative for cell-specific regulation events detected by response profiling.

Response profiling reveals drug- and cell-line-specific responses to treatment

Following exactly the same procedure as exemplified with As_2O_3, the colon carcinoma cell lines HCT116 and SW480 were also treated with four other metal-based anti-cancer drug candidates, namely KP46, KP772, KP1339 and KP1537. A comparative analysis of all response profiling data revealed that the diversity of cellular responses to the different metallodrugs and between the cell lines was much higher than expected (Table 1).

Table 1. Numbers of multi-parameter-significant protein regulations observed during response profiling after treatment of HCT116 and SW480.

Treatment	HCT116		SW480	
	CYT	NE	CYT	NE
KP46	0	0	0	96
KP772	18	249	706	855
KP1339	0	0	288	552
KP1537	0	0	0	63
As_2O_3	3	13	875	967

The lanthanum-containing KP772 induced the largest number of protein regulations, and KP1537 the least. Proteins in the NE fraction were more strongly regulated compared with the CYT fraction. For example, the exposure of SW480 cells to KP46 induced no protein regulations in CYT, but 96 proteins were found differentially expressed in the NE fraction (Table 1).

The heterogeneity of the drug effects was clearly demonstrated by the fact that only three proteins were found to be similarly regulated by all four compounds in SW480 (Figure 1E), namely the down-regulation of disks large homolog 1, alpha-actinin-1 and alpha-actinin-4. Two other proteins were found to be affected by all the drugs. However, in these cases, KP1537 treatment resulted in the down-regulation, whereas

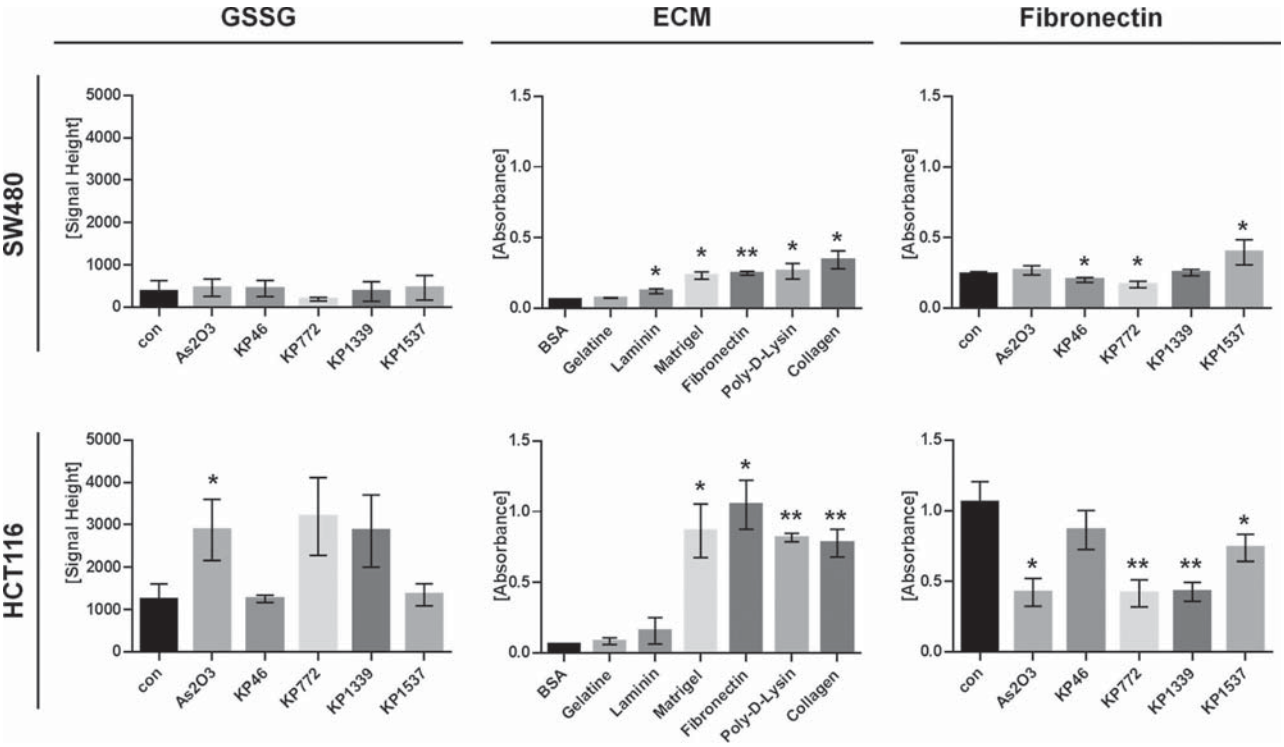

Figure 3. Differences in the detected levels of oxidised glutathione (GSSG) after treatment of the two cell lines with the respective metallodrug and the effects of different extracellular matrices (ECMs) on cell adhesion. A substantial increase in cell adhesion was detected with fibronectin and the effect of metallodrug treatment on the cell adhesion on fibronectin was tested. * = p value < 0.05, ** = p value < 0.005.

the other drugs led to the up-regulation of the general transcription factor IIF subunit 1. KP46 treatment caused an up-regulation of the zinc finger protein 185, as did As_2O_3, whereas the other metallodrugs caused the inverse effect. KP772 treatment led to very specific responses and only 10% of the regulated proteins were found to occur in both cell lines.

Thus, most observed protein-regulation events in the SW480 nuclear extracts were actually specific for a single drug. This observation was rather unexpected as metallodrugs may be expected to generally cause cell stress related to a similar set of stress-responsive proteins.

This implies that a generalisation of all drug effects may hardly be possible. Drugs seem to rather exert many effects in a cell-type specific manner, as desired when treating cancer cells in a patient. Of course, it is important to differentiate between robust drug responses that are similar in many kinds of cells and responses specific to one cell type. Understanding both robust and specific drug responses may provide support for predictions on drug effects in patients, an urgent necessity for appropriate patient stratification and a personalised treatment regimen.

Cancer-related functional groups of proteins

As mentioned above, we significantly reduced the required time for sample preparation and acquisition in comparison with earlier proteome profiling studies by increasing, for example, the data density. However, data evaluation is a bottle-neck in proteomics, through the generation of large protein lists, and usually requires bioinformatic competence for evaluation. To contribute to the establishment of response profiling as an efficient screening method for metallodrug development, we focused on six functional groups of proteins according to which metallodrug effects may be categorised. These functional groups include DNA repair, protection from oxidative stress, protection from ER stress, endocytosis, cell adhesion and mitochondrial function. Each group consists of a number of proteins (see Table S2 in the Supporting Information). The members of these categories were chosen only from proteins, which were found to be significantly regulated by at least one drug. The average fold change was calculated for the proteins that make up each group.

DNA repair

Metal-based drugs are often associated with DNA damage, especially when derived from platinum(II), and this may be their major mode of action.[21] The role of DNA as a potential target for the metallodrug candidates was indirectly examined by evaluating DNA repair proteins.

Protection from oxidative stress

Cancer cells often display higher levels of reactive oxygen species (ROS) than normal cells and are adapted to this situation, for example, with strong antioxidant capacity. However, cancer

cells are only able to cope with this up to a certain extent and a further increase of oxidative stress due to drug treatment may then lead to the induction of apoptosis.[8] Overall, a higher basal expression of redox regulating proteins was detected in HCT116 cells, which indicates a higher redox capacity of these cells. Additionally, we measured oxidised glutathione (GSSG) to evaluate another parameter directly related to oxidative stress upon exposure to the different drugs (Figure 3).

Protection from ER stress

Another promising anti-cancer strategy is the enhancement of ER stress, which may even result in immunogenic cell death.[22,23] Asparagine synthetase (ASNS) and 78 kDa glucose regulated protein are known to increase upon ER stress.[24] These proteins were significantly more highly expressed in HCT116 than in SW480. We examined the regulation of proteins involved in the protection from ER stress.

Endocytosis

Endocytosis can play an important role in drug uptake, because it is responsible for the internalisation of macromolecules,[25] and several metallodrugs have been reported to extensively bind to serum proteins.[21]

Cell adhesion

Integrins are cell adhesion receptors[26] and their differential expression can play an important role in cancer progression.[27] A reduction of cell adhesion supports migratory and invasive phenotypes in cancer cells. We also performed cell adhesion assays to validate integrin regulations after metallodrug treatment (Figure 3).

Mitochondrial function

NADH dehydrogenases are implicated in cellular respiration and indicate the functional state of mitochondria.

Apoptosis

Apoptotic processes were not included in the six groups, because the initiation of the apoptosis machinery would override any other protein signature and interesting mechanistic processes would be obscured. Accordingly, the cells were treated with sub-cytotoxic concentrations (approximately two thirds of the IC_{50} values in SW480). Nonetheless, we identified approximately 70% of the proteins that are listed in the KEGG pathway for apoptosis, including the key players apoptosis regulator BAX, caspases, cellular tumour antigen p53, cytochrome c, tumour necrosis factor receptor superfamily member 6, Bcl-2-like protein 1, inhibitor of nuclear factor κ-B kinase subunit α and transcription factor p65.

Metallodrug effects may be mapped by functional groups of proteins

The spider-web representation allows for an efficient dimension reduction of proteome profiling experiments according to the constructed functional groups of proteins and is used to globally map metallodrug effects on cell lines (Figure 4). Each web shows two hexagons and a centre point. The outer hexagon denotes a +4 average up-regulation, the inner hexagon denotes zero average regulation and the centre point represents a −4 average down-regulation of proteins. For example, KP46 did not show any effects in SW480 cells, whereas KP772 showed a strong DNA mismatch (DMM) response in HCT116 cells. Importantly, the induction of a ROS protection response was confirmed for As_2O_3 in SW480; this response was less pronounced in HCT116 cells according to the basal expression of

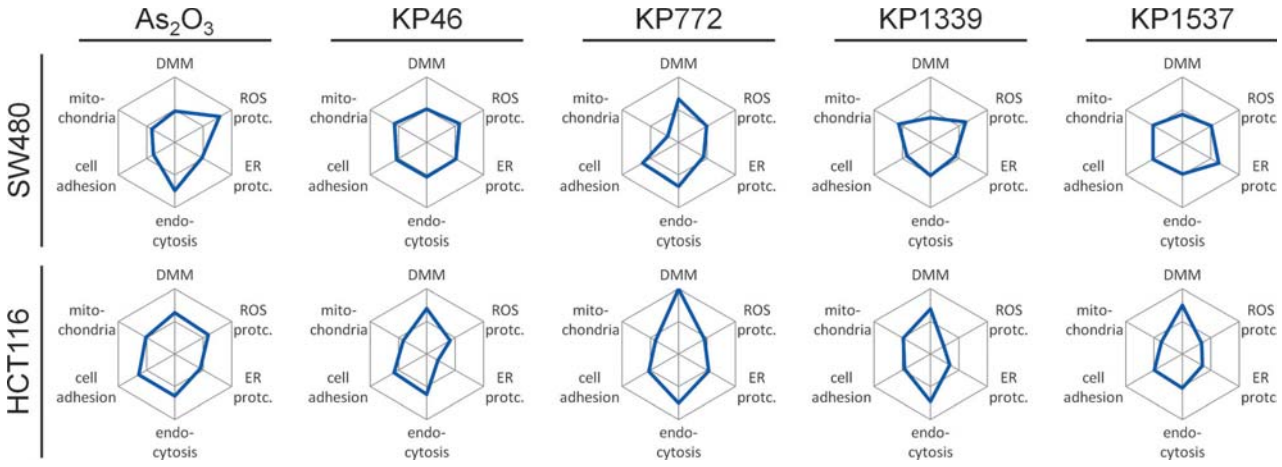

Figure 4. Spider-web plots of the regulation of the functional groups of proteins for each metallodrug in the two cell lines. Each spider web shows two hexagons and a central point. The outer hexagon denotes a +4 average up-regulation, the inner hexagon denotes zero average regulation and the centre point represents a −4 average down-regulation of proteins. DMM (DNA mismatch repair proteins, $n=4$), ROS protc. (proteins involved in the protection from ROS, $n=11$), ER protc. (proteins involved in the protection from ER stress, $n=7$), endocytosis ($n=4$), cell adhesion (integrins, $n=5$) and mitochondria (NADH dehydrogenases, $n=34$).

these proteins. The other functional groups were not significantly affected with the exception of endocytosis. From these representations it is evident that the two colon cell lines respond differently to treatment and that each metallodrug displays characteristic traits that are cell-line-specific.

KP46

In contrast to the SW480 cells, KP46 affected proteins involved in DMM and ER protection and to a lesser extent cell adhesion and endocytosis in HCT116 cells. Although the compound was not reported to affect DNA secondary structure, it seemed to induce a rescue mechanism of DNA repair, in accordance with previous findings.[28] Integrin deregulation was proposed as part of its mode of action,[29] however, we observed only modest effects in HCT116 cells at the applied sub-cytotoxic concentrations.

KP772

The strongest effects of the current data set were observed with KP772 in HCT116 cells and involved DMM as well as endocytic processes. The effects on DMM were accompanied by down-regulation of transcription initiation factors in both cell lines, which is consistent with previous findings of reduced DNA synthesis[30] after treatment. Furthermore, KP772 treatment reportedly led to a higher expression of the transferrin receptor protein 1 (TFRC),[31] and we also found significant up-regulation of TFRC in both cell lines (Figure 5). Interestingly, NADH dehydrogenases were down-regulated in SW480 and suggested altered mitochondrial function.

KP1339

Similarly to As_2O_3, KP1339 was capable of up-regulating ROS protective proteins, which represents a major hallmark. Importantly, KP1339 has already been shown to cause oxidative stress as part of its mechanism of action.[32,33] Furthermore, treatment more strongly affected DMM in HCT116 cells. Extraction experiments of treated cancer cells revealed that KP1339 binds to DNA, however, it is not believed to be a major part in its mode of action.[34] Several receptors were down-regulated in the cytoplasm of KP1339-treated SW480 cells, including C-type mannose receptor 2 (MRC2) and prolow-density lipoprotein receptor-related protein 1 (LRP1). Both receptors are key players in the process of endocytosis.[25] Importantly, KP1339 is assumed to be taken up by the cells through serum proteins by receptor-mediated endocytosis.[34] TFRC was significantly down-regulated in SW480 upon KP1339 exposure (Figure 5). Alpha-actinin-4, one of the proteins down-regulated by all four drugs in SW480 nuclear extracts, might play a role in the efficient recycling of the transferrin receptor 17 and it was strongly influenced by KP1339 exposure. Down-regulation of endocytosis could generally protect cells from further drug uptake.

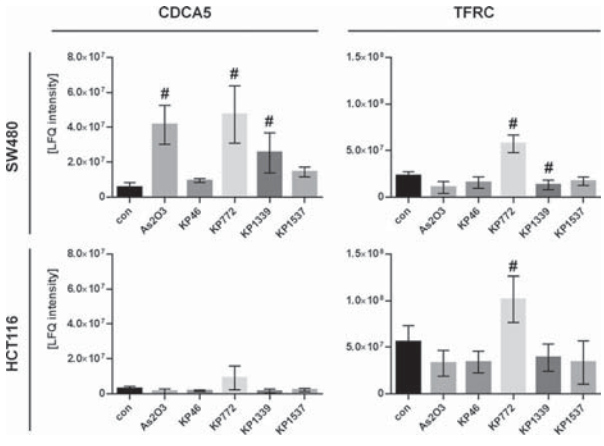

Figure 5. Differences in the protein levels of a selected DNA mismatch repair protein (CDCA5, sororin) and the transferrin receptor (TFRC) upon treatment with the respective metallodrugs and in the two cell lines. A hash denotes a multi-parameter-significant change in protein abundance with respect to the control state (p value < 0.05, FDR < 0.01).

KP1537

The oxaliplatin derivate KP1537 induced the lowest response in protein numbers (Table 1). It seemed to induce a DMM rescue response in HCT116 cells, although its interaction with DNA might not be solely responsible for its anti-cancer effect.[35] In SW480, we observed an up-regulation of ER protective proteins, which indicates that ER stress may also play a role for this compound, for example, ASNS was up-regulated four-fold.

In conclusion, response profiling can be used as a powerful hypothesis-generating tool to aid in the elucidation of unknown mechanisms of action of metallodrugs, which can be further investigated by targeted experiments. Therefore, we set out to validate present findings by analysing oxidised glutathione (GSSG) as a metabolic read-out of glutathione (GSH) consumption upon ROS-induced stress (Figure 3). Importantly, glutathione synthetase and mitochondrial glutathione reductase are expressed at lower levels in SW480 than in HCT116, and indeed we also detected lower levels of GSSG in SW480 cells than in HCT116 cells. However, metallodrug treatment had very little effect in SW480 cells, but more so in HCT116, and this contrasts ROS protection by the induction of proteins. GSSG levels were up-regulated after treatment with KP772 (p value $= 0.051$) and KP1339 (p value $= 0.064$), but only reaching significance with As_2O_3 (p value $= 0.040$; Figure 3). This is in good agreement with the ROS inducing As_2O_3 and KP1339. This is in good agreement with the ROS inducing As_2O_3 and KP1339. KP772 is not yet known to cause ROS, but the higher levels of GSSG are indicative that the cell is forced to consume GSH, which merits further investigations.

In addition, we performed cell adhesion assays as a read-out for integrin activity. An increased adhesion of both cell lines was observed by using Matrigel, fibronectin, poly-D-lysin and collagen (Figure 3), and the increase in cell adhesion was stronger for HCT116 cells than for SW480 cells. The effects of metallodrug treatment on cell adhesion were then investigated on fibronectin because both cell lines showed a strong increase of

adhesion on this matrix. We found that the cell adhesion on fibronectin was significantly affected by treatment with all metallodrugs and led to a reduced adhesion with the exception of KP1537, which led to an increased adhesion in SW480 cells.

Conclusion

The findings of this investigation demonstrate the applicability of response profiling to globally map metallodrug effects with respect to the proteome of cells. This approach may offer new ways to assess the mechanisms of action of anti-cancer metallodrugs in cancer cells, which supports a complex selection process for drug candidates. However, our results also show that drug effects may be cell-type-specific even with regard to cells of the same tissue type. This demonstrates the great need for a detailed molecular characterisation of drug effects and may support an improved stratification strategy for modern personalised medicine.

Experimental Section

Investigated drugs: KP46, KP772, KP1339 and KP1537 were synthesised as described previously.[36–39] KP46 and KP1339 were freshly dissolved in DMSO, KP772 and KP1537 in McCoy's cell culture medium (Life Technologies, UK) at concentrations of 10, 40, 0.5 and 0.5 mM, respectively. As_2O_3 (Sigma–Aldrich, USA) was dissolved at a concentration of 5 mM in NaOH (1.2 mg mL^{-1} in H_2O, the pH was adjusted to 7.0–9.0 with HCl) according to the package insert of Trisenox. Further dilutions to the final concentrations (1 μM KP46, 5 μM KP772, 80 μM KP1339, 0.5 μM KP1537, 5 μM As_2O_3) were conducted with the respective media.

Cell culture: SW480 and HCT116, both colon carcinoma cell lines, were kindly provided by Michael Jakupec (Department of Inorganic Chemistry, University of Vienna, Austria). HCT116 cells were cultured in McCoy's medium (Life Technologies, UK) containing 10% fetal calf serum (FCS; ATCC, USA) and 100 U m^{-} penicillin/streptomycin (ATCC, USA). SW480 cells were cultured in Eagle's minimum essential medium (EMEM; Sigma–Aldrich, USA) supplemented with 10% FCS, 100 U m^{-} penicillin/streptomycin, 0.1 mM non-essential amino acids and 1 mM sodium pyruvate.

Treatment: Concentrations for drug treatment corresponded to approximately two-third IC_{50} values in SW480 cells. Experiments were conducted for 24 h in T25 flasks in triplicate with on average 10^7 cells per flask. Media were changed in control cells and treated cells were given fresh media with the respective drug at the concentrations mentioned above.

Fractionation: Cells were fractionated into cytoplasmic and nuclear extract as previously described.[40] In short, with the combination of an isotonic lysis buffer containing protease inhibitors and shear stress cytoplasmic proteins were solubilised and, after centrifugation, precipitated with ice-cold ethanol at −20 °C overnight. The nuclei were incubated first with a solution containing 500 mM NaCl and then with an NP-40 buffer supplemented with protease inhibitors. The remaining cell material was separated by centrifugation; nuclear proteins were again precipitated with ice-cold ethanol at −20 °C overnight. Precipitated proteins were dissolved in sample buffer (7.5 M urea, 1.5 M thiourea, 4% CHAPS, 0.05% sodium dodecyl sulfate (SDS), 100 mM dithiothreitol (DTT)) and a Bradford assay was employed to determine protein concentrations.

MS sample preparation: Digestions were performed on all samples in solution as previously described.[2] In brief, 25 μg of protein were pre-concentrated on 10 kDa filters (Pall Austria Filter GmbH), reduced with DTT and carbamidomethylated with iodacetamide. To receive peptides, samples were digested with a trypsin/lys-c mixture (Promega, Germany) for 18 h at 37 °C. Eluates were dried and stored at −20 °C until analysis.

LC-MS/MS analysis: For analysis, a nanoLC-system (Dionex Ultimate 3000, Thermo Scientific, Austria) was coupled to a high-resolution QExactive orbitrap mass spectrometer (Thermo Scientific, Austria). Dried samples were resolved in 5 μL of 30% formic acid (FA) containing four synthetic peptides (10 fmol each)[2] and diluted with 40 μL of mobile phase A (98% H_2O, 2% ACN, 0.1% FA). Each sample was recorded twice, 5 μL were injected per analysis.

The LC method and MS parameters were optimised so that an overall 135 min long method was sufficient for single injection analysis. The gradient was 90 min for 8–40% solvent B (80% ACN, 20% H_2O, 0.1% FA) running over a 75 μm × 50 cm C-18 separation column (Dionex, Acclaim PepMap RSCL). The MS method lasted 115 min with the resolution set to 70000 and 17500 with maximum injection time of 50 and 75 ms for MS1 and MS2, respectively. The *m/z* range of 400–1400 was scanned and a top 8 method was chosen for MS/MS analysis.

Data analysis: For protein identification and label-free quantification the freely available MaxQuant software, which includes the Andromeda search engine, was employed.[12] For a positive identification using Swissprot entries only (results will be non-redundant and without isoforms) at least two peptides with at least one unique had to be present. The first and main search peptide tolerance were set to 50 and 25 ppm, respectively, and the FTMS MS/MS match tolerance to 20 ppm. A match between runs was performed with a 7 min match time and a 15 min alignment time window. The false discovery rate (FDR) was fixed to 0.01 on the peptide and protein level. The mass spectrometry based proteomics data have been deposited at the ProteomeXchange Consortium[41] through the PRIDE partner repository with the dataset identifiers PXD004764 to PXD004778 and PXD004788 to PXD004796 (see Table S3 in the Supporting Information), accessible via www.proteomeexchange.org.

Statistical evaluation was performed with the Perseus software accompanying MaxQuant. Label-free quantification (LFQ) values were transformed to the logarithmic scale on the basis of 2. Only proteins that were found at least six times in one cell state and fraction, for example, HCT116 cytoplasm control, were considered for further data evaluation. Permutation-based FDR set to 0.05 for truncation was used for t-tests, which gave multi-parameter-significant changes.

Cell adhesion assay: Cell adhesion experiments were conducted in triplicate in 96-well plates (Eppendorf). For positive control, wells were coated with poly-D-lysin (0.1 mg mL^{-1}, Sigma, USA) for 5 min at 37 °C, washed three times with sterile water and allowed to dry for 2 h. Wells were coated for 2 h at 37 °C with laminin (20 μg mL^{-1}, Sigma, USA) diluted in sterile water, collagen I (2.2 mg mL^{-1}, Corning, Netherlands) diluted in DMEM (Sigma, USA) and sodium bicarbonate (1.5%, Sigma, USA), gelatine (2%, Sigma–Aldrich, USA), Matrigel (1:50, BD Biosciences, Belgium) diluted in serum-free media, fibronectin (20 g mL^{-1}, Millipore, Austria) and BSA (1%, negative control, Cell Signaling, Netherlands) diluted in phosphate-buffered saline (PBS). Wells were washed with PBS and blocked with 0.1% BSA for 1 h at room temperature. SW480 and HCT116 cells were harvested by trypsin, washed twice with PBS and seeded at a density of 20000 cells per well in serum-free media. After 1 h incubation at 37 °C, 5% CO_2 wells were washed

twice with PBS to remove non-adherent cells, and 100 μL media with 10 μL MTT reagent (3-(4,5-dimethylthiazol-2-yl)-2,5-diphenyltetrazolium bromide; THP Medical Products, Austria) were added. Adherent cells were incubated for another 3 h at 37 °C, 5% CO_2, before dissolving the formed crystals in 100 μL DMSO (Sigma–Aldrich) and measuring the absorbance at 570 nm with a microplate reader (Thermo Scientific).

Measurement of oxidised glutathionine (GSSG): L-Glutathione disulfide (GSSG) was purchased from Sigma–Aldrich (USA). T25 flasks containing the cells were flushed with argon and washed with PBS. Then, a cold EDTA suspension (3 mL, 10 mM) was added and the cells were removed by scraping under argon. The cell suspension was transferred into a falcon tube and homogenised with an ultrasonic probe. After further flushing with argon the homogenised cells were centrifuged (4500 g) for 20 min at 4 °C. Cell supernatant (1 mL) was transferred into argon-flushed HPLC vials.

The samples were analysed on a triple quadrupole mass spectrometer (QqQ 6490, Agilent Technologies, Austria) coupled to a 1290 Infinity UHPLC System (Agilent Technologies, Austria) by using a Kinetex 1.7 μm XB-C18 100 Å (50×2.1 mm) column. We used UHPLC-grade mobile aqueous (Sigma–Aldrich, USA, A) and methanolic (MS grade, VWR, Austria, B) phases supplemented with 0.1% formic acid. The gradient was set from 0–2.5% B in 3 min, afterwards washed for 1 min with 80% B and re-equilibrated to 0% B with a total run time of 6 min. The following parameters were used: flow rate 0.5 mL min^{-1}, injection volume 10 μL, column temperature 20 °C, ESI spray voltage 4 kV, nozzle voltage 500 V, gas flow 11 L min^{-1}, sheath gas temperature 400 °C, sheath gas flow 12 L min^{-1}, gas temperature 250 °C and nebuliser gas pressure 35 psi. Multiple reaction monitoring (MRM) was employed for the analysis of GSSG ($[M+2H]^{2+}$ 307.1) with the quantifier 130.1. Additionally, the qualifiers 84.2 and 235.1 were employed. The dwell time was set to 50 ms and positive ion mode was used. The peak height was used for data analysis.

Acknowledgements

S.M.M. thanks Dr. Michael Jakupec for helpful discussions. This work was supported by the Faculty of Chemistry of the University of Vienna.

Keywords: cancer · mechanism of action · metallodrugs · proteomics · response profiling

[1] A. P. Li, *Drug Discovery Today Technol.* **2005**, *2*, 179 – 185.
[2] A. Bileck, D. Kreutz, B. Muqaku, A. Slany, C. Gerner, *J. Proteome Res.* **2014**, *13*, 5989 – 6000.
[3] M. V. Babak, S. M. Meier, K. V. M. Huber, J. Reynisson, A. A. Legin, M. A. Jakupec, A. Roller, A. Stukalov, M. Gridling, K. L. Bennett, J. Colinge, W. Berger, P. J. Dyson, G. Superti-Furga, B. K. Keppler, C. G. Hartinger, *Chem. Sci.* **2015**, *6*, 2449 – 2456.
[4] J. J. Stewart, J. T. White, X. Yan, S. Collins, C. W. Drescher, N. D. Urban, L. Hood, B. Lin, *Molecular & Cellular Proteomics* **2005**, *5*, 433 – 443; Cellular Proteomics **2005**, 5, 433 – 443.
[5] D. P. Fitzpatrick, J. S. You, K. G. Bemis, J. P. Wery, J. R. Ludwig, M. Wang, *Proteomics Clin. Appl.* **2007**, *1*, 246 – 263.
[6] B. Titz, A. Elamin, F. Martin, T. Schneider, S. Dijon, N. V. Ivanov, J. Hoeng, M. C. Peitsch, *Computational and Structural Biotechnology Journal* **2014**, *11*, 73 – 90.
[7] M. H. Dias, E. S. Kitano, A. Zelanis, L. K. Iwai, *Drug Discovery Today* **2016**, *21*, 264 – 277.
[8] C. Gorrini, I. S. Harris, T. W. Mak, *Nat. Rev. Drug Discovery* **2013**, *12*, 931 – 947.
[9] W. H. Miller Jr., H. M. Schipper, J. S. Lee, J. Singer, S. Waxman, *Cancer Res.* **2002**, *62*, 3893 – 3903.
[10] E. Schreiber-Brynzak, E. Klapproth, C. Unger, I. Lichtscheidl-Schultz, S. Göschl, S. Schweighofer, R. Trondl, H. Dolznig, M. A. Jakupec, B. K. Keppler, *Invest. New Drugs* **2015**, *33*, 835 – 847.
[11] A. A. Legin, A. Schintlmeister, M. A. Jakupec, M. Galanski, I. Lichtscheidl, M. Wagner, B. K. Keppler, *Chem. Sci.* **2014**, *5*, 3135 – 3143.
[12] J. Cox, M. Mann, *Nat. Biotechnol.* **2008**, *26*, 1367 – 1372.
[13] Z. G. Wang, D. Ruggero, S. Ronchetti, S. Zhong, M. Gaboli, R. Rivi, P. P. Pandolfi, *Nat. Genet.* **1998**, *20*, 230.
[14] J. Barretina, G. Caponigro, N. Stransky, K. Venkatesan, A. A. Margolin, S. Kim, C. J. Wilson, J. Lehár, G. V. Kryukov, D. Sonkin, A. Reddy, M. Liu, L. Murray, M. F. Berger, J. E. Monahan, P. Morais, J. Meltzer, A. Korejwa, J. Jané-Valbuena, F. A. Mapa, J. Thibault, E. Bric-Furlong, P. Raman, A. Shipway, I. H. Engels, J. Cheng, G. K. Yu, J. Yu, P. Aspesi Jr., M. De Silva, K. Jagtap, M. D. Jones, L. Wang, C. Hatton, E. Palescandolo, S. Gupta, S. Mahan, C. Sougnez, R. C. Onofrio, T. Liefeld, L. MacConaill, W. Winckler, M. Reich, N. Li, J. P. Mesirov, S. B. Gabriel, G. Getz, K. Ardlie, V. Chan, V. E. Myer, B. L. Weber, J. Porter, M. Warmuth, P. Finan, J. L. Harris, M. Meyerson, T. R. Golub, M. P. Morrissey, W. R. Sellers, R. Schlegel, L. A. Garraway, *Nature* **2012**, *483*, 603 – 607.
[15] D. Ahmed, P. W. Eide, I. A. Eilertsen, S. A. Danielsen, M. Eknaes, M. Hektoen, G. E. Lind, R. A. Lothe, *Oncogenesis* **2013**, *2*, e71.
[16] M. Kaur, B. Velmurugan, A. Tyagi, C. Agarwal, R. P. Singh, R. Agarwal, *Neoplasia* **2010**, *12*, 415 – 424.
[17] A. Bateman, M. J. Martin, C. O'Donovan, M. Magrane, R. Apweiler, E. Alpi, R. Antunes, J. Arganiska, B. Bely, M. Bingley, C. Bonilla, R. Britto, B. Bursteinas, G. Chavali, E. Cibrian-Uhalte, A. Da Silva, M. De Giorgi, T. Dogan, F. Fazzini, P. Gane, L. G. Castro, P. Garmiri, E. Hatton-Ellis, R. Hieta, R. Huntley, D. Legge, W. Liu, J. Luo, A. Macdougall, P. Mutowo, A. Nightingale, S. Orchard, K. Pichler, D. Poggioli, S. Pundir, L. Pureza, G. Qi, S. Rosanoff, R. Saidi, T. Sawford, A. Shypitsyna, E. Turner, V. Volynkin, T. Wardell, X. Watkins, H. Zellner, A. Cowley, L. Figueira, W. Li, H. McWilliam, R. Lopez, I. Xenarios, L. Bougueleret, A. Bridge, S. Poux, N. Redaschi, L. Aimo, G. Argoud-Puy, A. Auchincloss, K. Axelsen, P. Bansal, D. Baratin, M. C. Blatter, B. Boeckmann, J. Bolleman, E. Boutet, L. Breuza, C. Casal-Casas, E. De Castro, E. Coudert, B. Cuche, M. Doche, D. Dornevil, S. Duvaud, A. Estreicher, L. Famiglietti, M. Feuermann, E. Gasteiger, S. Gehant, V. Gerritsen, A. Gos, N. Gruaz-Gumowski, U. Hinz, C. Hulo, F. Jungo, G. Keller, V. Lara, P. Lemercier, D. Lieberherr, T. Lombardot, X. Martin, P. Masson, A. Morgat, T. Neto, N. Nouspikel, S. Paesano, I. Pedruzzi, S. Pilbout, M. Pozzato, M. Pruess, C. Rivoire, B. Roechert, M. Schneider, C. Sigrist, K. Sonesson, S. Staehli, A. Stutz, S. Sundaram, M. Tognolli, L. Verbregue, A. L. Veuthey, C. H. Wu, C. N. Arighi, L. Arminski, C. Chen, Y. Chen, J. S. Garavelli, H. Huang, K. Laiho, P. McGarvey, D. A. Natale, B. E. Suzek, C. R. Vinayaka, Q. Wang, Y. Wang, L. S. Yeh, M. S. Yerramalla, J. Zhang, *Nucleic Acids Res.* **2015**, *43*, D204 – D212.
[18] A. Hall, P. A. Karplus, L. B. Poole, *FEBS J.* **2009**, *276*, 2469 – 2477.
[19] D. W. Huang, B. T. Sherman, R. A. Lempicki, *Nat. Protoc.* **2008**, *4*, 44 – 57.
[20] J. S. Desgrosellier, D. A. Cheresh, *Nat. Rev. Cancer* **2010**, *10*, 9 – 22.
[21] C. G. Hartinger, M. Groessl, S. M. Meier, A. Casini, P. J. Dyson, *Chem. Soc. Rev.* **2013**, *42*, 6186 – 6199.
[22] D. Y. Wong, W. W. Ong, W. H. Ang, *Angew. Chem. Int. Ed.* **2015**, *54*, 6483 – 6487.
[23] M. J. Chow, C. Licona, G. Pastorin, G. Mellitzer, W. H. Ang, C. Gaiddon, *Chem. Sci.* **2016**, *7*, 4117 – 4124.
[24] a) M. N. Balasubramanian, E. A. Butterworth, M. S. Kilberg, *Am. J. Physiol. – Endocrinology and Metabolism* **2013**, *304*, E789 – E799; b) Y. Kimata, K. Kohno, *Current Opinion in Cell Biology* **2011**, *23*, 135 – 142.
[25] L. M. Bareford, P. W. Swaan, *Adv. Drug Delivery Rev.* **2007**, *59*, 748 – 758.
[26] S. K. Akiyama, *Human Cell* **1996**, *9*, 181 – 186.
[27] D. Hanahan, R. A. Weinberg, *Cell* **2011**, *144*, 646 – 674.
[28] S. M. Valiahdi, P. Heffeter, M. A. Jakupec, R. Marculescu, W. Berger, K. Rappersberger, B. K. Keppler, *Melanoma Res.* **2009**, *19*, 283 – 293.
[29] U. Jungwirth, J. Gojo, T. Tuder, G. Walko, M. Holcmann, T. Schofl, K. Nowikovsky, N. Wilfinger, S. Schoonhoven, C. R. Kowol, R. Lemmens-Gruber, P. Heffeter, B. K. Keppler, W. Berger, *Molecular Cancer Therapeutics* **2014**, *13*, 2436 – 2449.
[30] P. Heffeter, M. A. Jakupec, W. Körner, S. Wild, N. G. Von Keyserlingk, L. Elbling, H. Zorbas, A. Korynevska, S. Knasmüller, H. Sutterlüty, M. Mick-

sche, B. K. Keppler, W. Berger, *Biochemical Pharmacology* **2006**, *71*, 426 – 440.
[31] P. Heffeter, A. Popovic-Bijelic, P. Saiko, R. Dornetshuber, U. Jungwirth, N. Voevodskaya, D. Biglino, M. A. Jakupec, L. Elbling, M. Micksche, T. Szekeres, B. K. Keppler, A. Gräslund, W. Berger, *Current Cancer Drug Targets* **2009**, *9*, 595 – 607.
[32] U. Jungwirth, C. R. Kowol, B. K. Keppler, C. G. Hartinger, W. Berger, P. Heffeter, *Antioxid. Redox Signaling* **2011**, *15*, 1085 – 1127.
[33] S. Kapitza, M. A. Jakupec, M. Uhl, B. K. Keppler, B. Marian, *Cancer Lett.* **2005**, *226*, 115 – 121.
[34] R. Trondl, P. Heffeter, C. R. Kowol, M. A. Jakupec, W. Berger, B. K. Keppler, *Chem. Sci.* **2014**, *5*, 2925 – 2932.
[35] U. Jungwirth, D. N. Xanthos, J. Gojo, A. K. Bytzek, W. Körner, P. Heffeter, S. A. Abramkin, M. A. Jakupec, C. G. Hartinger, U. Windberger, M. Galanski, B. K. Keppler, W. Berger, *Molecular Pharmacology* **2012**, *81*, 719 – 728.
[36] S. A. Abramkin, U. Jungwirth, S. M. Valiahdi, C. Dworak, L. Habala, K. Meelich, W. Berger, M. A. Jakupec, C. G. Hartinger, A. A. Nazarov, M. Galanski, B. K. Keppler, *J. Med. Chem.* **2010**, *53*, 7356 – 7364.
[37] P. Collery, M. A. Jakupec, B. Kynast, B. K. Keppler, *Metal Ions in Biology and Medicine* **2006**, *9*, 521 – 524.
[38] F. A. Hart, F. P. Laming, *J. Inorg. Nucl. Chem.* **1964**, *26*, 579 – 585.
[39] W. Peti, T. Pieper, M. Sommer, B. K. Keppler, G. Giester, *Eur. J. Inorg. Chem.* **1999**, 1551 – 1555.
[40] A. Slany, A. Bileck, D. Kreutz, R. L. Mayer, B. Muqaku, C. Gerner, *Molecular & Cellular Proteomics* **2016**, *15*, 1982 – 1997; Cellular Proteomics **2016**, 15, 1982 – 1997.
[41] J. A. Vizcaíno, E. W. Deutsch, R. Wang, A. Csordas, F. Reisinger, D. Rios, J. A. Dianes, Z. Sun, T. Farrah, N. Bandeira, P. A. Binz, I. Xenarios, M. Eisenacher, G. Mayer, L. Gatto, A. Campos, R. J. Chalkley, H. J. Kraus, J. P. Albar, S. Martinez-Bartolome, R. Apweiler, G. S. Omenn, L. Martens, A. R. Jones, H. Hermjakob, *Nat. Biotechnol.* **2014**, *32*, 223 – 226.

Manuscript received: September 23, 2016
Accepted Article published: November 7, 2016
Final Article published: January 10, 2017

CHEMISTRY
A European Journal

Supporting Information

Response Profiling Using Shotgun Proteomics Enables Global Metallodrug Mechanisms of Action To Be Established

Dominique Kreutz,[a] Andrea Bileck,[a] Kerstin Plessl,[b] Denise Wolrab,[a] Michael Groessl,[a] Bernhard K. Keppler,[c] Samuel M. Meier,[a] and Christopher Gerner*[a]

chem_201604516_sm_miscellaneous_information.pdf

Supplementary Table S1

Protein regulation upon the treatment of HCT114 and SW480 cells with As_2O_3 and the metal-based compounds KP1339, KP1537, KP46 and KP772 was analyzed independently for the cytoplasmic (cyt) and nuclear (ne) cell fractions. T-test (tt) p-values, tt differences (Diff) as well as indications for multi-parameter significance (tt sign) are listed for each identified protein. Tt differences are reported in a logarithmic scale to the basis 2.

The table can only be accessed online.

Supplementary Table S2

Proteins included in the following functional groups are listed: DNA mismatch repair (DMM), protection from ROS (ROS protc.), protection from ER stress (ER protc.), endocytosis, cell adhesion and mitochondria

DMM

P40692	DNA mismatch repair protein Mlh1
P43246	DNA mismatch repair protein Msh2
P20585	DNA mismatch repair protein Msh3
P52701	DNA mismatch repair protein Msh6

ROS protc.

P09601	Heme oxygenase 1
Q06830	Peroxiredoxin-1
P32119	Peroxiredoxin-2
P30044	Peroxiredoxin-5, mitochondrial
P30041	Peroxiredoxin-6
Q9BYN0	Sulfiredoxin-1
P10599	Thioredoxin
Q16881	Thioredoxin reductase 1, cytoplasmic
Q9NNW7	Thioredoxin reductase 2, mitochondrial
Q99757	Thioredoxin, mitochondrial
O43396	Thioredoxin-like protein 1

ER protc.

O60313	Dynamin-like 120 kDa protein, mitochondrial
O76024	Wolframin
O95881	Thioredoxin domain-containing protein 12
P18031	Tyrosine-protein phosphatase non-receptor type 1
P55145	Mesencephalic astrocyte-derived neurotrophic factor
Q99497	Protein DJ-1
Q9Y4L1	Hypoxia up-regulated protein 1

endocytosis

O14828	Secretory carrier-associated membrane protein 3
MRC2	C-type mannose receptor 2
Q07954	Prolow-density lipoprotein receptor-related protein 1
P02786	Transferrin receptor protein 1

cell adhesion

P17301	Integrin alpha-2
P26006	Integrin alpha-3
P23229	Integrin alpha-6
P05556	Integrin beta-1
P16144	Integrin beta-4

mitochondria

Q9BU61	NADH dehydrogenase [ubiquinone] 1 alpha subcomplex assembly factor 3
Q9P032	NADH dehydrogenase [ubiquinone] 1 alpha subcomplex assembly factor 4
O95299	NADH dehydrogenase [ubiquinone] 1 alpha subcomplex subunit 10, mitochondrial
Q86Y39	NADH dehydrogenase [ubiquinone] 1 alpha subcomplex subunit 11
Q9UI09	NADH dehydrogenase [ubiquinone] 1 alpha subcomplex subunit 12
Q9P0J0	NADH dehydrogenase [ubiquinone] 1 alpha subcomplex subunit 13
O43678	NADH dehydrogenase [ubiquinone] 1 alpha subcomplex subunit 2
O95167	NADH dehydrogenase [ubiquinone] 1 alpha subcomplex subunit 3
Q16718	NADH dehydrogenase [ubiquinone] 1 alpha subcomplex subunit 5
P56556	NADH dehydrogenase [ubiquinone] 1 alpha subcomplex subunit 6
O95182	NADH dehydrogenase [ubiquinone] 1 alpha subcomplex subunit 7
P51970	NADH dehydrogenase [ubiquinone] 1 alpha subcomplex subunit 8
Q16795	NADH dehydrogenase [ubiquinone] 1 alpha subcomplex subunit 9, mitochondrial
O75438	NADH dehydrogenase [ubiquinone] 1 beta subcomplex subunit 1

O96000	NADH dehydrogenase [ubiquinone] 1 beta subcomplex subunit 10
Q9NX14	NADH dehydrogenase [ubiquinone] 1 beta subcomplex subunit 11, mitochondrial
O43676	NADH dehydrogenase [ubiquinone] 1 beta subcomplex subunit 3
O95168	NADH dehydrogenase [ubiquinone] 1 beta subcomplex subunit 4
O43674	NADH dehydrogenase [ubiquinone] 1 beta subcomplex subunit 5, mitochondrial
O95139	NADH dehydrogenase [ubiquinone] 1 beta subcomplex subunit 6
P17568	NADH dehydrogenase [ubiquinone] 1 beta subcomplex subunit 7
O95169	NADH dehydrogenase [ubiquinone] 1 beta subcomplex subunit 8, mitochondrial
Q9Y6M9	NADH dehydrogenase [ubiquinone] 1 beta subcomplex subunit 9
O95298	NADH dehydrogenase [ubiquinone] 1 subunit C2
Q7L592	NADH dehydrogenase [ubiquinone] complex I, assembly factor 7
P49821	NADH dehydrogenase [ubiquinone] flavoprotein 1, mitochondrial
P19404	NADH dehydrogenase [ubiquinone] flavoprotein 2, mitochondrial
O75306	NADH dehydrogenase [ubiquinone] iron-sulfur protein 2, mitochondrial
O75489	NADH dehydrogenase [ubiquinone] iron-sulfur protein 3, mitochondrial
O43181	NADH dehydrogenase [ubiquinone] iron-sulfur protein 4, mitochondrial
O43920	NADH dehydrogenase [ubiquinone] iron-sulfur protein 5
O75380	NADH dehydrogenase [ubiquinone] iron-sulfur protein 6, mitochondrial
O75251	NADH dehydrogenase [ubiquinone] iron-sulfur protein 7, mitochondrial
O00217	NADH dehydrogenase [ubiquinone] iron-sulfur protein 8, mitochondrial

Supplementary Table S3: Assignment of PRIDE Identifiers to the corresponding data set

Data Identifier	Sample Type
PXD004764	cytoplasmic proteins of untreated HCT 116 epithelial cells
PXD004765	cytoplasmic proteins of KP46-treated HCT 116 epithelial cells
PXD004766	cytoplasmic proteins of KP772-treated HCT 116 epithelial cells
PXD004767	cytoplasmic proteins of KP1339-treated HCT 116 epithelial cells
PXD004768	cytoplasmic proteins of KP1537-treated HCT 116 epithelial cells
PXD004769	cytoplasmic proteins of arsenic trioxide-treated HCT 116 epithelial cells
PXD004770	nuclear proteins of untreated HCT 116 epithelial cells
PXD004771	nuclear proteins of KP46-treated HCT 116 epithelial cells
PXD004772	nuclear proteins of KP772-treated HCT 116 epithelial cells
PXD004773	nuclear proteins of KP1339-treated HCT 116 epithelial cells
PXD004774	nuclear proteins of KP1537-treated HCT 116 epithelial cells
PXD004775	nuclear proteins of arsenic trioxide-treated HCT 116 epithelial cells
PXD004776	cytoplasmic proteins of untreated SW480 epithelial cells
PXD004777	cytoplasmic proteins of KP46-treated SW480 epithelial cells
PXD004778	cytoplasmic proteins of KP1339-treated SW480 epithelial cells
PXD004788	cytoplasmic proteins of KP1537-treated SW480 epithelial cells
PXD004789	cytoplasmic proteins of arsenic trioxide-treated SW480 epithelial cells
PXD004790	nuclear proteins of untreated SW480 epithelial cells
PXD004791	nuclear proteins of KP46-treated SW480 epithelial cells
PXD004792	nuclear proteins of KP772-treated SW480 epithelial cells
PXD004793	nuclear proteins of KP1339-treated SW480 epithelial cells
PXD004794	nuclear proteins of KP1537-treated SW480 epithelial cells
PXD004795	nuclear proteins of arsenic trioxide-treated SW480 epithelial cells
PXD004796	cytoplasmic proteins of KP772-treated SW480 epithelial cells

2.2. Curcumin exerts its antitumor effects in a context dependent fashion

Dominique Kreutz[a], Chomdao Sinthuvanich[b], Andrea Bileck[a], Lukas Janker[a], Astrid Slany[a], Christopher Gerner[a]

Journal of Proteomics, **2018**, 182, 65-72

[a] Department of Analytical Chemistry, Faculty of Chemistry, University of Vienna, Waehringer Strasse 38, Vienna, Austria

[b] Department of Biochemistry, Faculty of Science, Kasetsart University, 50 Ngam Wong Wan Road, Lat Yao, Chatuchak, Bangkok, Thailand 10900

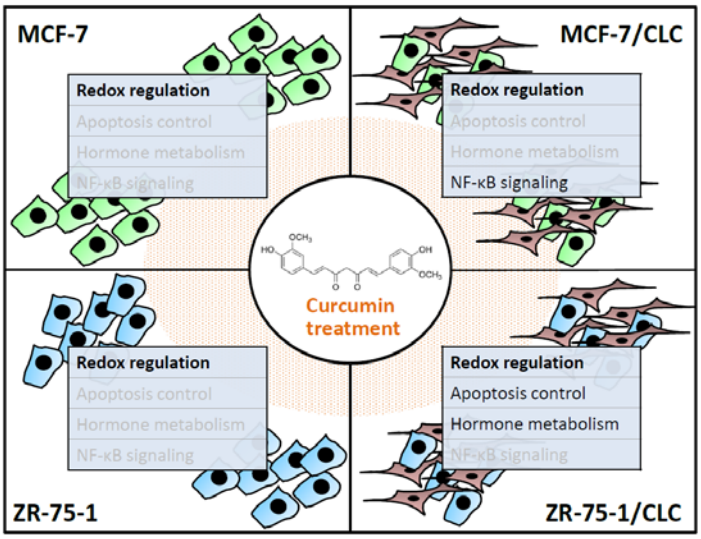

Contributions to this publication:

- Conduction of experiments
- Preparation of figures
- Involved in experimental design, data interpretation and writing of the manuscript

Journal of Proteomics 182 (2018) 65–72

Contents lists available at ScienceDirect

Journal of Proteomics

journal homepage: www.elsevier.com/locate/jprot

Curcumin exerts its antitumor effects in a context dependent fashion

Dominique Kreutz[a], Chomdao Sinthuvanich[b], Andrea Bileck[a], Lukas Janker[a], Besnik Muqaku[a], Astrid Slany[a], Christopher Gerner[a,*]

[a] Department of Analytical Chemistry, Faculty of Chemistry, University of Vienna, Vienna, Austria
[b] Department of Biochemistry, Faculty of Science, Kasetsart University, Bangkok, Thailand

ARTICLE INFO

Keywords:
Cancer-associated fibroblasts
Breast cancer co-culture
Curcumin
Mass spectrometry
Proteome response profiling

ABSTRACT

Proteome profiling profoundly contributes to the understanding of cell response mechanisms to drug actions. Such knowledge may become a key to improve personalized medicine. In the present study, the effects of the natural remedy curcumin on breast cancer model systems were investigated. MCF-7, ZR-75-1 and TGF-β1 pretreated fibroblasts, mimicking cancer-associated fibroblasts (CAFs), were treated independently as well as in tumor cell/CAF co-cultures. Remarkably, co-culturing with CAF-like cells (CLCs) induced different proteome alterations in MCF-7 and ZR-75-1 cells, respectively. Curcumin significantly induced HMOX1 in single cell type models and co-cultures. However, other curcumin effects differed. In the MCF-7/CLC co-culture, curcumin significantly down-regulated RC3H1, a repressor of inflammatory signaling. In the ZR-75-1/CLC co-culture, curcumin significantly down-regulated PEG10, an anti-apoptotic protein, and induced RRAGA, a pro-apoptotic protein involved in TNF-alpha signaling. Furthermore, curcumin induced AKR1C2, an important enzyme for progesterone metabolism. None of these specific curcumin effects were observed in single cell type cultures. All high-resolution mass spectrometry data are available via ProteomeXchange with the identifier PXD008719. The present data demonstrate that curcumin induces proteome alterations, potentially accounting for its known antitumor effects, in a strongly context-dependent fashion.

Biological significance: Better means to understand and potentially predict individual variations of drug effects are urgently required. The present proteome profiling study of curcumin effects demonstrates the massive impact of the cell microenvironment on cell responses to drug action. Co-culture models apparently provide more biologically relevant information regarding curcumin effects than single cell type cultures.

1. Introduction

Curcumin is a naturally occurring polyphenol present in the Indian spice turmeric, exhibiting strong antioxidative activity which manifests itself, for example, in the up-regulation of heme oxygenase 1 (HMOX1) [1]. Furthermore, this compound has anti-inflammatory effects and displays promising chemo-preventive and antitumor activity; it can affect cancer cell proliferation and induce apoptosis [2], while being pharmacologically safe [3]. These features make curcumin a valuable drug candidate for the treatment of cancer, worthy for detailed examinations.

Accounting for 30% of all female cancer cases, breast cancer is one of the most common causes of cancer death for women worldwide [4]. Many studies concerning the potential of curcumin have concentrated on the antitumor effects of this compound on breast cancer cells. In this way, the modulation of the NF-κB signaling pathway by curcumin in MCF-7 cells has been observed [5]. Furthermore, fatty acid synthase inhibition [6] and modulation of the estrogen receptor and the p53 signaling pathway [7] were described as consequences of curcumin application on breast cancer cells. Similarly, changes in the mTORC1 pathway were observed in colon cancer cells [8]. A potential activity of curcumin on the focal adhesion kinase pathway influencing proliferation and migration was observed by Sathe et al. in head and neck cancer [9]. Moreover, a cancer-preventive role of the compound has been described as well, as mammary stem cells, which are considered as the source of breast cancer cells, were selectively affected by curcumin which altered their lipid metabolism and consequently disturbed their self-renewal potential [10]. Finally, curcumin is apparently able to inhibit epithelial-to-mesenchymal transition (EMT) in breast cancer cell lines [11]. Buhrmann et al. [12] observed similar effects in a co-culture model system of colorectal cancer cells and fibroblasts, where curcumin was impeding EMT by suppressing the crosstalk between these cells.

Abbreviations: CAFs, cancer-associated fibroblasts; CLCs, CAF-like cells; EMT, epithelial-to-mesenchymal transition; FDR, false discovery rate; IRDS, interferon-related DNA damage resistance signature; LC, liquid chromatography; LFQ, label free quantification; MRM, multiple reaction monitoring; MS, mass spectrometry; MS/MS, tandem mass spectrometry

* Corresponding author at: Department of Analytical Chemistry, Faculty of Chemistry, University of Vienna, Waehringer Strasse 38, 1090 Vienna, Austria.
E-mail address: christopher.gerner@univie.ac.at (C. Gerner).

https://doi.org/10.1016/j.jprot.2018.05.007
Received 29 January 2018; Received in revised form 29 April 2018; Accepted 4 May 2018
Available online 09 May 2018
1874-3919/

Tumor-stroma interactions have a strong influence on tumor development, progression [13] and drug response [14]. While healthy stromal cells are supposed to prevent tumor development, emerging cancer cells can initiate their transformation into tumor-supporting cells [15]. Cancer-associated fibroblasts (CAFs), an important part of the tumor micro-environment, appear to be more aggressive than naive fibroblasts, having the ability to initiate angiogenesis, promote tumor progression and support invasiveness [15,16]. These cells are rather predominant in the tumor microenvironment and, in case of breast cancer, typically display a wound healing signature [17]. Based on the interplay between tumor cells and CAFs in vivo, co-culture models of cancer and stromal cells may hold great potentials to investigate drugs potentially affecting both normal and tumor cells [18]. As demonstrated recently by us, proteome profiling represents a qualified approach to investigate tumor-CAFs interactions, despite the complexity and challenging interpretation of the resulting data [19–22].

Differing individual responses to anti-cancer drugs may represent one of the most urgent scientific challenges of our modern society, as also successfully designed targeted drugs may exert unexpected responses in a large number of patients. The establishment of resistance mechanisms may be considered to be a typical response pattern which we need to better understand. Response profiling by proteomics actually represents a very powerful method to investigate host responses and mechanisms of drug action [23,24]. Several proteomic studies on curcumin effects have already been conducted on various types of cancer including neuroblastoma [25], gastric [26], prostate [27], colorectal [28,29] and breast cancer [30]. In the present study, we applied proteome profiling to investigate the effects of the natural compound curcumin on breast cancer cells MCF-7 or ZR-75-1 and appropriate co-culture models mimicking in vivo tumor-stroma interactions with mammary fibroblasts. Here we describe that curcumin displayed pronounced and previously unrecognized antitumor effects in a surprisingly strong context-dependent fashion.

2. Materials and methods

2.1. Cell culture

The investigated human breast carcinoma cell lines MCF-7 and ZR-75-1 were kindly provided by Dr. Walter Jaeger (Department of Clinical Pharmacy and Diagnostics, University of Vienna). Cells were cultured in phenol red free DMEM and RPMI (LifeTech, Austria), respectively, containing 10% FCS (ATCC, USA) and 100 U/mL penicillin/streptomycin (ATCC, USA). Human mammary fibroblasts (HMF, ScienCell Research Laboratories, Carlsbad, CA) were cultured in FBM (Lonza, Switzerland) supplemented with the FGM Bullet Kit, including 10% FCS, and 100 U/mL penicillin/streptomycin. The cells were stimulated with TGF-β1 (2 ng/mL; Sigma-Aldrich, Austria) for seven days in order to obtain cancer-associated fibroblast-like cells (CLCs) [17] and used up to passage 5. Experiments were conducted at 37 °C and 5% CO_2 in 6-well-plates in triplicates.

For co-culture models representing the in vivo situation the cancer cells – 1×10^6 and 3×10^5 cells per well of ZR-75-1 and MCF-7, respectively – were incubated with 10% of CLCs with a 1:1 mixture of the respective media. After 24 h of incubation, co-cultures as well as MCF-7, ZR-75-1 and CLCs alone were treated with 30 μM curcumin (Sigma-Aldrich, Austria) for 24 h. Medium was changed in control cells. The treatment concentration was chosen as two third of the IC_{50}-value of fibroblasts (data not shown) which were the most sensitive cells of the investigated ones. After 24 h treatment, cells were controlled for cell death using the Trypan blue exclusion protocol (Thermo Scientific, Austria) with consistently > 95% viable cells, washed with cold PBS and 200 μL sample buffer (7.5 M urea, 1.5 M thiourea, 4% CHAPS, 0.05% SDS, 100 mM dithiothreitol) were added. Cells were scraped off and lysed by means of an ultrasonic stick. Bradford assay (Bio-Rad-Laboratories, Germany) was employed to determine protein concentrations.

2.2. Sample preparation

Whole cell lysates were digested in solution as described previously [31]. Briefly, 20 μg proteins were concentrated on a 10 kDa cut-off filter (Pall Austria Filter GmbH, Austria), reduced with dithiothreitol, carbamidomethylated with iodoacetamide and finally digested with a trypsin/lys-c mixture (Promega, Germany) overnight at 37 °C. This was followed by a clean-up on C-18 spin columns (Pierce,Thermo Scientific). Therefor peptide samples were acidified with trifluoroacetic acid (TFA) (1% final concentration) and transferred on the prewashed and equilibrated spin columns. The column bound peptides were washed (5% acetonitrile ACN, 0.5% TFA) and finally eluted (50% ACN, 0.1% TFA). Dried eluates were stored at −20 °C until analysis.

2.3. LC-MS/MS analysis

As described previously [23] for shotgun proteomics analysis a Dionex Ultimate 3000 nano-HPLC system (Thermo Scientific, Austria) was coupled to a high resolution QExactive orbitrap mass spectrometer (Thermo Scientific, Austria). Samples were dissolved in 5 μL 30% formic acid (FA) containing 10 fmol each of four synthetic peptides as internal standard for LC-MS quality control. After dilution with 40 μL mobile phase A (98% H_2O, 2% ACN, 0.1% FA), 5 μL of the sample were injected. At a flow rate of 10 μL/min of mobile phase A the samples were loaded on a 2 cm × 75 μM C-18 Pepmap100 pre-column (Thermo Scientific, Austria). Peptides were separated over a 75 μm × 50 cm C-18 separation column (Thermo Scientific, Austria) with a 90 min gradient from 8 to 40% solvent B (80% ACN, 20% H_2O, 0.1% FA) at a flow rate of 300 nL/min. The MS parameters were set to resolution 70′000 and 17′500 at 200 *m/z*, AGC targets to 3e6 and 2e4, maximum ion filling time to 50 ms and 100 ms for MS^1 and MS^2, respectively. The *m/z* range was set to 400–1400 in this 115 min long top 8 method with a dynamic exclusion window of 45 s and an isolation window of 2 *m/z*. Peptide match and isotope exclusion were turned on. For MS^2 analysis, HCD fragmentation with 30 eV was applied. Only peptides with charges of +2, +3 and + 4 were considered. Samples were measured in replicates. Lock mass was chosen at 445.12003 m/z.

Multiple reaction monitoring (MRM) method was developed based on shotgun data and using Skyline software (v. 4.1) [32], as described previously [33,34] (Supplementary Table S4). Targeted MRM analysis was conducted on an Agilent 6490 triple quadrupole mass spectrometer coupled with a nano-Chip-LC Agilent Infinity Series HPLC1290 system. Digested sample were reconstituted in 25 μL of 30% formic acid solution containing equimolar concentration of 4 standard peptides (10 fmol/μL). Each time 2 μL of sample were injected and peptides were separated by applying 19 min gradient from 8% to 30% acetonitrile. Skyline software [32] was used for data evaluation and total peak area of each peptide was normalized to standard peptides (global standards).

2.4. Data analysis

The freely available MaxQuant software [35] version 1.6.0.1 was employed for protein identification and label-free quantification (LFQ). Protein identification was achieved searching against the UniProt Database [36] (organism: *Homo sapiens*, reviewed: yes, version 11/2015 with 20,193 entries) Peptide tolerances for first and main search were set to 50 and 25 ppm, respectively. Two peptides with at least one unique peptide were the minimum requirements for a positive identification. Match and alignment time windows were set to 10 and 20 min, respectively, false discovery rates (FDR) to 0.01 for peptides as well as for proteins.

Perseus [37], freely available software for data analysis of MaxQuant outputs, was used for statistical evaluations. Protein groups only identified by site as well as reverse and potential contaminants were

excluded. Label-free quantification values were transformed to the logarithmic scale on the basis of 2. Protein groups had to be identified in at least 70% of the samples of one group for positive identification. Technical replicates were averaged for *t*-tests with a permutation based FDR of 0.05 for truncation, S_0 set to 0.2 revealing multi-parameter significant changes.

All data are available via the public data repository PRIDE at www.proteomexchange.org [38] with the identifier PXD008719.

3. Results

3.1. Differential basal protein composition in cancer cells

Applying high resolution MS/MS hyphenated with nano-LC to investigate proteome profiles of whole cell lysates of in vitro model systems consisting of MCF-7, ZR-75-1 breast carcinoma cells and mammary fibroblasts, cultured alone and in co-cultures, untreated and treated with curcumin, we identified 5780 protein groups (FDR < 0.01, Supplementary Table S1). When comparing MCF-7 and ZR-75-1 cells, 2409 protein groups were found differentially expressed (FDR < 0.05; Fig. 1), demonstrating profound differences in the proteome profile of these two breast cancer cell lines.

Proteome differences were related to tumor aggressiveness, as exemplified by proteins S100P, TUBB3, DKK1 and FABP5 [39–42]; all of these proteins were significantly higher in MCF-7. In contrast, ZR-75-1 expressed proteins related to less aggressive tumors such as AGR3 [43] and the tumor invasion suppressor PDCD4 [44]. In addition, metabolic

Fig. 1. Differential expression of proteins in MCF-7 and ZR-75-1. LFQ values of selected proteins, determined in three biological replicates of MCF-7 and ZR-75-1, respectively, are represented as heat maps. Gene names as well as processes in which the proteins may be involved are indicated.

enzymes such as LDHB, glutamine synthetase GLUL and the signaling molecule PIK3CA were more abundant in ZR-75-1, whereas enzymes regulating lipid metabolism and signaling such as FASN and GNA11, and the pentose phosphate pathway regulator G6PD were more abundant in MCF-7 cells.

Another intriguing difference was apparent with respect to proteins of the interferon-related DNA damage resistance signature (IRDS) described by Weichselbaum et al. [45]. The IRDS signature molecules IFIT1 and IFIT3, ISG15, OAS1 and STAT1 were all more abundant in MCF-7. Both investigated cancer cell lines were estrogen (ERS1) and progesterone receptor (PGR) positive. However, while, cytochrome P450 1B1 (CYP1B1), a protein involved in estrogen metabolism, was found at higher levels in MCF-7, PGR and FKBP5, which play important roles in progesterone metabolism, were more abundant in ZR-75-1.

3.2. Proteome alterations induced upon co-culturing

Human mammary fibroblasts were pretreated with TGF-β1 in order to induce CAF-like cells (CLCs) with a wound-healing signature mimicking the in vivo situation found in human mammary tumors [17]. The breast cancer cells ZR-75-1 and MCF-7 were co-cultured with CLCs, again mimicking plausible in vivo conditions of tumor tissues. Abundance changes of protein groups were evaluated between co-cultures compared to the respective cancer cells cultured alone (Fig. 2, Supplementary Table S1). Caused by the addition of fibroblasts, a large number of fibroblast-derived proteins becomes listed as apparently up-regulated, including mesenchymal markers like VIM, FN1, COL1A2 and THY1 [46] as well as proteins known to be involved in cancer such as S100A4, TGM2, SPARC and ANXA1. However, co-culturing also significantly affected the expression of various proteins specifically derived from the cancer cells.

In MCF-7/CLC co-cultures (Fig. 2A), the glycolytic enzyme LDHB, the cell death promoting protein FADD, the interferon responsive protein MX1 and the tumor promoting protein GDF15 were found up-regulated. The enzyme DHCR7 involved in cholesterol synthesis, the negative mTOR regulator DEPTOR and the tumor-associated serine hydrolase RBBP9 were found down-regulated.

In the ZR-75-1/CLC co-cultures (Fig. 2B), rather different events were observed. Here, the metastasis-associated protein ROR2 and the interferon responsive protein IFITM3 were found up-regulated. The cell growth suppressor protein BUD31, the chemoattractant CXCL12 as well as the metastasis suppressor CD82, the anti-metastatic protein HTT and the calcium uniporter protein MCU were down-regulated.

Proteins found to be significantly regulated upon co-cultivation were further submitted to the oPOSSUM software (version 3.0) [47]. This allowed the detection of over-represented conserved transcription factor binding sites in the corresponding sets of genes (Supplementary Fig. S1, Supplementary Table S3). Significantly regulated proteins in MCF-7/CLC co-cultures revealed that transcriptional targets of the transcription factors FOXA1 and CEBPA are down- and of SOX2 are up-regulated. ZR-75-1/CLC co-cultures displayed a rather different picture. Here, CTCF, SP1 and KLF4-target proteins were down-, whereas proteins associated with the transcription factor NFATC2, a promoter of invasive migration, were up-regulated.

3.3. Cell type-specific responses to curcumin treatment

In order to investigate a realistic scenario which may be representative for a typical in vivo situation, we chose curcumin at the moderate dose of 30 μM for cell treatment. Both, single cell type models as well as co-cultures, were used. The most robust proteome alteration in all cell model systems was the induction of the NF-κB target gene HMOX1 (Figs. 3 and 4), which was also observed in other studies [48]. HMOX1 has been described to exert antitumor effects via inhibiting epithelial-to-mesenchymal transition (EMT), as demonstrated recently in TGF-β1 treated MCF-7 cells [49]. Significant protein regulations

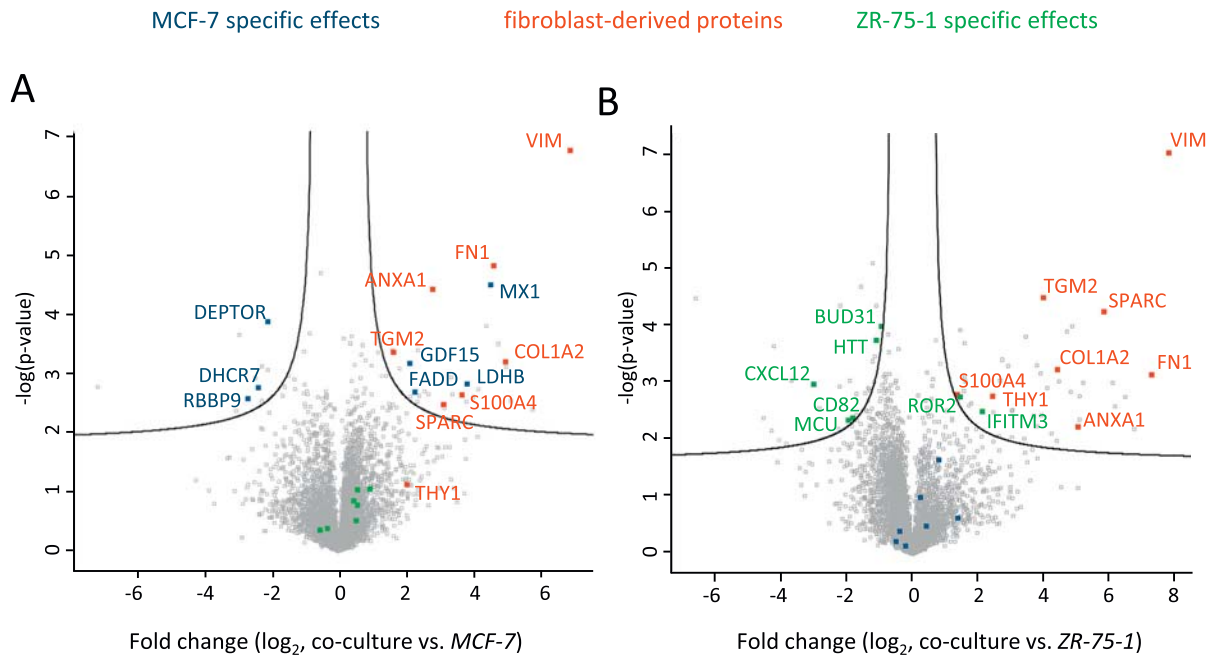

Fig. 2. Proteins significantly regulated in MCF-7 (A) and ZR-75-1 (B) upon co-culturing with CLCs. Fold-changes of LFQ values (log_2 scale) and corresponding p-values (−log scale) are represented by means of volcano plots. Significantly regulated proteins, with an FDR ≤ 0.05 applying multi-parameter correction and s0 ≥ 0.2, are delineated in the upper right region of the plots for up-regulated and upper left region for down-regulated proteins.

upon curcumin treatment in the single cell type models are listed in Supplementary Table S2.

In the co-cultures, protein regulations upon curcumin treatment differed with regard to the breast carcinoma cells. RC3H1, a modulator of IKK/NF-κB activity [50], was strongly down-regulated in MCF-7/CLC co-cultures only (Fig. 4D). As specific was the down-regulation of the anti-apoptotic protein PEG10 in ZR-75-1/CLC co-cultures (Fig. 4E). In this co-culture model, the mTOR regulating protein RRAGA and the enzyme AKR1C2 involved in the progesterone metabolism were found specifically up-regulated upon curcumin treatment (Fig. 4F and G). All of these proteins were not significantly altered when single cell type models were treated with curcumin separately (Fig. 3A–C).

To verify the results of the shotgun analysis, we applied targeted proteomics analysis using multiple reaction monitoring (Fig. 4H–L). While not all single observations reached statistical significance, actually all observations were reproduced independently.

4. Discussion

4.1. Proteome profiling reproduces known curcumin effects

A classical motivation for proteome profiling experiments is to get an unbiased overview of cellular responses to any cellular challenge or perturbation [51]. Cellular responses may provide rich information regarding the effects of drugs [23], also supporting the identification of the molecular mode of action [24]. Dependent on the investigated drug and the employed model systems, few up to several hundred significant protein regulation events may be observed [23]. Regarding the pleiotropic effects of curcumin reported in the literature, the number of regulated proteins identified in the present study was rather small (Fig. 4). However, the oxidant stress response most consistently reported in numerous studies was clearly detectable by the robust induction of HMOX1 (Fig. 4C). In the co-culture model with MCF7, a strong modulation of the NF-kB pathway by downregulating RC3H1 was observed (Fig. 4D), which is in accordance with Liu et al. [5]. The induction of RRAGA (Fig. 4F) in the ZR-75-1 model indicates an influence of the mTOR signaling pathway, supporting previous observations of Sato et al. [8].

4.2. Proteome profiling identifies novel anti-tumor effects of curcumin

All above-mentioned effects are in accordance with described anti-tumor activities of curcumin affecting regulation of apoptosis, metabolism and survival signaling representing important hallmarks of cancer [52]. Actually, the significant regulation of AKR1C2 (Fig. 4G) indicates a strong regulatory function of curcumin in hormone signaling, well known to be crucial for breast cancer [53]. The curcumin-induced up-regulation of this enzyme, active in progesterone metabolism [54], represents a novel finding, independently supporting the notion of potential anti-cancer activities of curcumin. This protein is frequently down-regulated in breast cancer cells, resulting in higher levels of progesterone, tumor growth and progression [54,55]. We consider the effect of curcumin up-regulating this enzyme as very important to understand how this drug may act in vivo.

4.3. Curcumin effects are context-dependent

Generally, drugs are meant to cause rather uniform effects on cells mediated by specific molecular interaction partners and the associated consequences. However, there is ample clinical evidence for strong individual variations in the response to any given therapy as well as context-dependent responses of cells to defined drugs [56]. We have speculated previously whether specific treatment of CAFs could represent a valid strategy to improve anti-cancer therapy [18]. The present data demonstrate that cellular responses observed in single cell type cultures may dramatically differ from responses observed when cells interact with other cells. Rather unexpectedly, most significant curcumin effects presently observed in the co-culture models were apparently context dependent. The influence of curcumin on progesterone metabolism was evident in the ZR-75-1 model where progesterone-associated proteins were found highly expressed (Fig. 1), but not in the MCF-7 model. The effect of curcumin on NF-κB signaling mediated via RC3H1 was observed in the MCF7 model only, which specifically displays an interferon-related DNA-damage resistance proteome signature

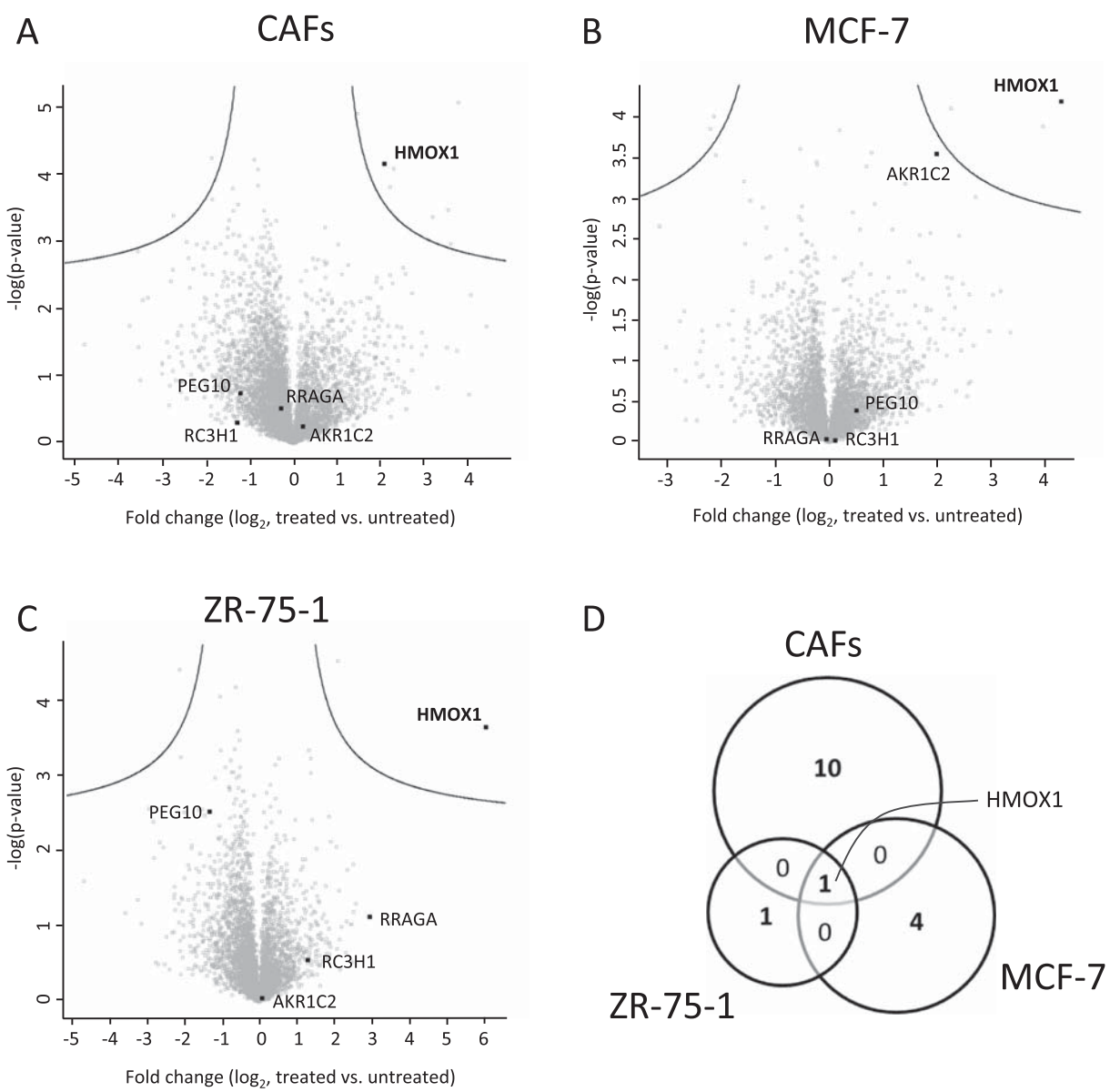

Fig. 3. Proteins significantly regulated in CLCs (A), MCF-7 (B) and ZR-75-1 (C) upon treatment with curcumin; regulatory events summarized in (D) as Venn diagram. Fold-changes of LFQ values (log_2 scale) and corresponding p-values (− log scale) are represented by means of volcano plots. Significantly regulated proteins, with an FDR ≤ 0.05 applying multi-parameter correction and s0 ≥ 0.2, are delineated in the upper right region of the plots for up-regulated (e.g. HMOX1) and upper left region for down-regulated proteins. All other proteins specified in the plots were not found significantly regulated here, however in the co-cultured cells upon treatment with curcumin (Fig. 4).

(Fig. 1). Here we can only speculate whether interferon signaling typically associated with virus defense may modulate NF-κB signaling representing the canonical inflammatory signaling cascade. Fact is that curcumin effects observed in one model were absent in the other and vice versa, demonstrating a very strong context dependent mode of action of curcumin. Already the co-culturing of breast cancer cells with 10% CLCs led to cell-type specific responses (Fig. 2, Supplementary Fig. S1). Bioinformatic analysis with the oPOSSUM software indicated that co-culture induced proteins, which are targets of transcription factors highly relevant for cell de/differentiation, cell cycle and energy metabolism (Supplementaty Fig. 1, Supplementary Table S3). Although co-culturing conditions were identical, the different sets of regulated proteins were also found to be related to different transcription factors. While we typically assume that regulatory events may indicate cell responses of the cells showing positive protein expression already initially, it should be noted that is assumption remains unproven. Anyhow, the main observation of context-dependent co-culture and curcumin effects remains unaffected by this notion.

Our observations may fuel the discussion with regard to individual therapeutic responses mentioned above. Only if we better understood the influencing parameters contained in the genome, proteome and metabolome of diseased cells and their microenvironment, we may be able to predict drug actions in an individualized fashion and better support patient stratification.

5. Conclusions

The present study clearly demonstrates that cells respond to a defined challenge in a strongly context-dependent fashion. Investigation of co-culture models as employed in the present study might provide the opportunity to elaborate the unknown determining parameters in a systematic fashion. Identification of such molecular parameters may be

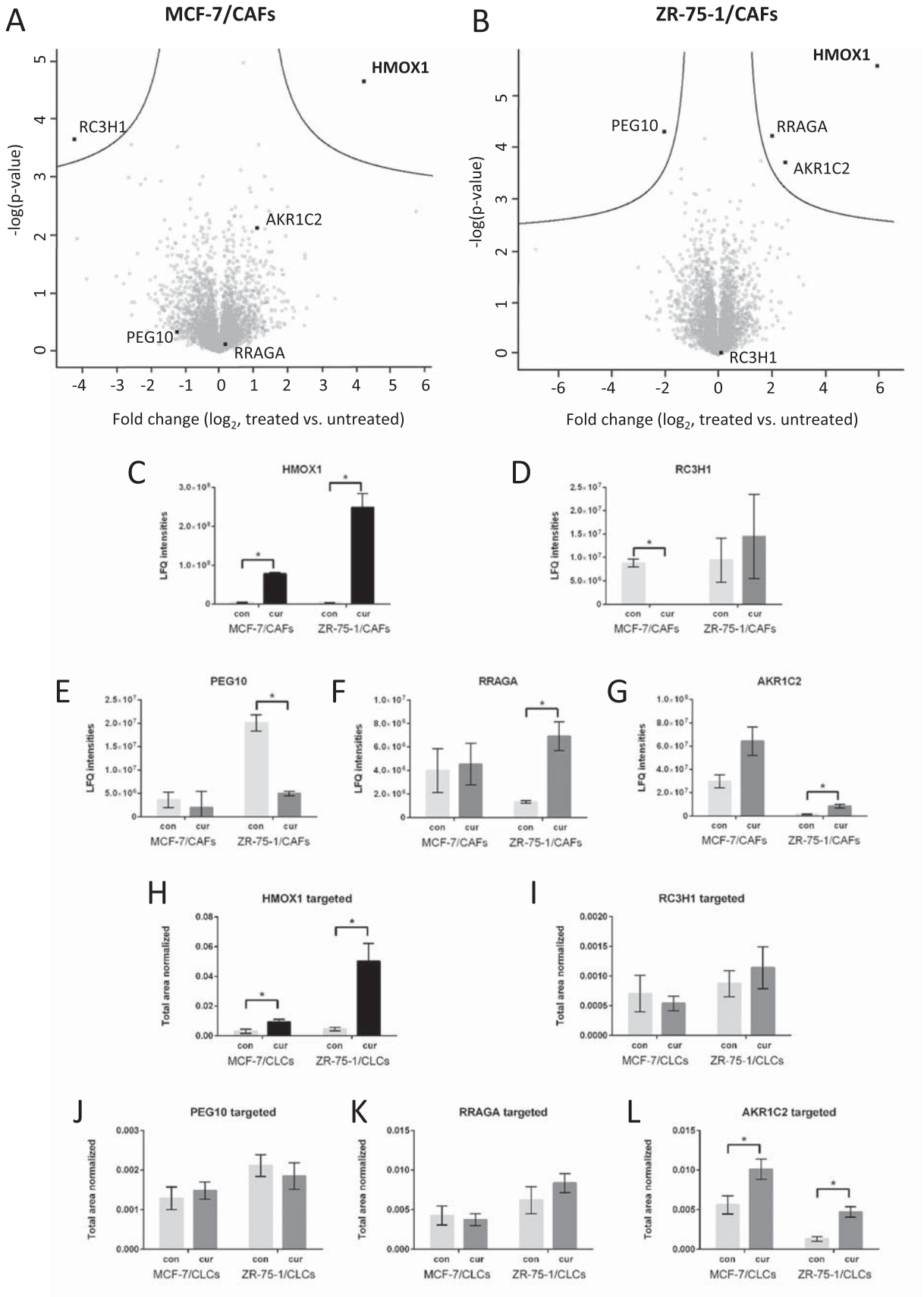

(caption on next page)

Fig. 4. Proteins significantly regulated in MCF-7/CLC (A) and ZR-75-1/CLC (B) co-cultures upon treatment with curcumin. Fold-changes of LFQ values (log_2 scale) and corresponding p-values (− log scale) are represented by means of volcano plots. Significantly regulated proteins, with an FDR ≤ 0.05 applying multi-parameter correction and s0 ≥ 0.2, are delineated in the upper right region of the plots for up-regulated and upper left region for down-regulated proteins. C–G. Levels of proteins specified in (A) or (B) are further represented in bar graphs, asterisks indicating significant differences with an FDR ≤ 0.05 applying multi-parameter correction and s0 ≥ 0.2. H–L. Levels of proteins specified in (A) or (B) measured by MRM represented in bar graphs, total area was normalized to global standards and with respect to best ionization quality, asterisks indicate significant differences.

a key strategy to improve patient stratification and patient-tailored anti-cancer therapy.

Supplementary data to this article can be found online at https://doi.org/10.1016/j.jprot.2018.05.007.

Availability of data

Protein data was submitted to the ProteomeXchange Consortium via the PRIDE partner repository and can be accessed via http://www.proteomeexchange.org with the identifier PXD008719.

Conflicts of interests

The authors declare no conflicts of interests.

Acknowledgements

CS wants to acknowledge Ernst Mach Grant -ASEA-UNINET supported by Federal Ministry of Science, Research and Economy, Austria as well as the Faculty of Chemistry of the University of Vienna for funding.

References

[1] R. Motterlini, R. Foresti, R. Bassi, C.J. Green, Curcumin, an antioxidant and anti-inflammatory agent, induces heme oxygenase-1 and protects endothelial cells against oxidative stress, Free Radic. Biol. Med. 28 (2000) 1303–1312.
[2] D. Liu, Z. Chen, The effect of curcumin on breast cancer cells, J. Breast Cancer 16 (2013) 133–137.
[3] H.P.T. Ammon, M.A. Wahl, Pharmacology of Curcuma longa, Planta Med. 57 (1991) 1–7.
[4] R.L. Siegel, K.D. Miller, A. Jemal, Cancer statistics, 2017, CA Cancer J. Clin. 67 (2017) 7–30.
[5] J.L. Liu, Y.Y. Pan, O. Chen, Y. Luan, X. Xue, J.J. Zhao, L. Liu, H.Y. Jia, Curcumin inhibits MCF-7 cells by modulating the NF-κB signaling pathway, Oncol. Lett. 14 (2017) 5581–5584.
[6] H. Fan, Y. Liang, B. Jiang, X. Li, H. Xun, J. Sun, W. He, H.T. Lau, X. Ma, Curcumin inhibits intracellular fatty acid synthase and induces apoptosis in human breast cancer MDA-MB-231 cells, Oncol. Rep. 35 (2016) 2651–2656.
[7] K. Hallman, K. Aleck, B. Dwyer, V. Lloyd, M. Quigley, N. Sitto, A.E. Siebert, S. Dinda, The effects of turmeric (curcumin) on tumor suppressor protein (p53) and estrogen receptor (ERα) in breast cancer cells, Breast Cancer 9 (2017) 153–161.
[8] T. Sato, Y. Higuchi, Y. Shibagaki, S. Hattori, Phosphoproteomic analysis identifies signaling pathways regulated by curcumin in human colon cancer cells, Anticancer Res. 37 (2017) 4789–4798.
[9] G. Sathe, S.M. Pinto, N. Syed, V. Nanjappa, H.S. Solanki, S. Renuse, S. Chavan, A.A. Khan, A.H. Patil, R.S. Nirujogi, B. Nair, P.P. Mathur, T.S.K. Prasad, H. Gowda, A. Chatterjee, Phosphotyrosine profiling of curcumin-induced signaling, Clin. Proteomics 13 (2016).
[10] J.A. Colacino, S.P. McDermott, M.A. Sartor, M.S. Wicha, L.S. Rozek, Transcriptomic profiling of curcumin-treated human breast stem cells identifies a role for stearoyl-coa desaturase in breast cancer prevention, Breast Cancer Res. Treat. 158 (2016) 29–41.
[11] M. Gallardo, G.M. Calaf, Curcumin inhibits invasive capabilities through epithelial mesenchymal transition in breast cancer cell lines, Int. J. Oncol. 49 (2016) 1019–1027.
[12] C. Buhrmann, P. Kraehe, C. Lueders, P. Shayan, A. Goel, M. Shakibaei, Curcumin suppresses crosstalk between colon cancer stem cells and stromal fibroblasts in the tumor microenvironment: potential role of EMT, PLoS One 9 (2014).
[13] N.A. Bhowmick, E.G. Neilson, H.L. Moses, Stromal fibroblasts in cancer initiation and progression, Nature 432 (2004) 332–337.
[14] M.R. Junttila, F.J. De Sauvage, Influence of tumour micro-environment heterogeneity on therapeutic response, Nature 501 (2013) 346–354.
[15] M.M. Mueller, N.E. Fusenig, Friends or foes - bipolar effects of the tumour stroma in cancer, Nat. Rev. Cancer 4 (2004) 839–849.
[16] A. Klein-Goldberg, S. Maman, I.P. Witz, The role played by the microenvironment in site-specific metastasis, Cancer Lett. 352 (2014) 54–58.
[17] M. Groessl, A. Slany, A. Bileck, K. Gloessmann, D. Kreutz, W. Jaeger, G. Pfeiler, C. Gerner, Proteome profiling of breast cancer biopsies reveals a wound healing signature of cancer-associated fibroblasts, J. Proteome Res. 13 (2014) 4773–4782.
[18] A. Slany, A. Bileck, B. Muqaku, C. Gerner, Targeting breast cancer-associated fibroblasts to improve anti-cancer therapy, Breast 24 (2015) 532–538.
[19] D. Drev, A. Bileck, Z.N. Erdem, T. Mohr, G. Timelthaler, A. Beer, C. Gerner, B. Marian, Proteomic profiling identifies markers for inflammation-related tumor-fibroblast interaction, Clin. Proteomics 14 (2017).
[20] V. Paulitschke, R. Kunstfeld, T. Mohr, A. Slany, M. Micksche, J. Drach, C. Zielinski, H. Pehamberger, C. Gerner, Entering a new era of rational biomarker discovery for early detection of melanoma metastases: Secretome analysis of associated stroma cells, J. Proteome Res. 8 (2009) 2501–2510.
[21] A. Slany, V. Haudek-Prinz, A. Meshcheryakova, A. Bileck, W. Lamm, C. Zielinski, C. Gerner, J. Drach, Extracellular matrix remodeling by bone marrow fibroblast-like cells correlates with disease progression in multiple myeloma, J. Proteome Res. 13 (2014) 844–854.
[22] A. Slany, V. Haudek-Prinz, H. Zwickl, S. Stättner, B. Grasl-Kraupp, C. Gerner, Myofibroblasts are important contributors to human hepatocellular carcinoma: evidence for tumor promotion by proteome profiling, Electrophoresis 34 (2013) 3315–3325.
[23] D. Kreutz, A. Bileck, K. Plessl, D. Wolrab, M. Groessl, B.K. Keppler, S.M. Meier, C. Gerner, Response profiling using shotgun proteomics enables global metallodrug mechanisms of action to be established, Chem. Eur. J. 23 (2017) 1881–1890.
[24] S.M. Meier, D. Kreutz, L. Winter, M.H.M. Klose, K. Cseh, T. Weiss, A. Bileck, B. Alte, J.C. Mader, S. Jana, A. Chatterjee, A. Bhattacharyya, M. Hejl, M.A. Jakupec, P. Heffeter, W. Berger, C.G. Hartinger, B.K. Keppler, G. Wiche, C. Gerner, An Organoruthenium anticancer agent shows unexpected target selectivity for Plectin, Angew. Chem. 56 (2017) 8267–8271.
[25] S. D'Aguanno, I. D'Agnano, M. De Canio, C. Rossi, S. Bernardini, G. Federici, A. Urbani, Shotgun proteomics and network analysis of neuroblastoma cell lines treated with curcumin, Mol. BioSyst. 8 (2012) 1068–1077.
[26] X.Z. Cai, W.Y. Huang, Y. Qiao, S.Y. Du, Y. Chen, D. Chen, S. Yu, R.C. Che, N. Liu, Y. Jiang, Inhibitory effects of curcumin on gastric cancer cells: a proteomic study of molecular targets, Phytomedicine 20 (2013) 495–505.
[27] M. Rivera, Y. Ramos, M. Rodríguez-Valentín, S. López-Acevedo, L.A. Cubano, J. Zou, Q. Zhang, G. Wang, N.M. Boukli, Targeting multiple pro-apoptotic signaling pathways with curcumin in prostate cancer cells, PLoS One 12 (2017).
[28] J.G. Lee, K.Q. McKinney, A.J. Pavlopoulos, J.H. Park, S. Hwang, Identification of anti-metastatic drug and natural compound targets in isogenic colorectal cancer cells, J. Proteome 113 (2015) 326–336.
[29] J. Wang, J. Zhang, C.J. Zhang, Y.K. Wong, T.K. Lim, Z.C. Hua, B. Liu, S.R. Tannenbaum, H.M. Shen, Q. Lin, In situ proteomic profiling of curcumin targets in HCT116 Colon Cancer cell line, Sci. Rep. 6 (2016).
[30] H.Y. Fang, S.B. Chen, D.J. Guo, S.Y. Pan, Z.L. Yu, Proteomic identification of differentially expressed proteins in curcumin-treated MCF-7 cells, Phytomedicine 18 (2011) 697–703.
[31] A. Bileck, D. Kreutz, B. Muqaku, A. Slany, C. Gerner, Comprehensive assessment of proteins regulated by dexamethasone reveals novel effects in primary human peripheral blood mononuclear cells, J. Proteome Res. 13 (2014) 5989–6000.
[32] B. MacLean, D.M. Tomazela, N. Shulman, M. Chambers, G.L. Finney, B. Frewen, R. Kern, D.L. Tabb, D.C. Liebler, M.J. MacCoss, Skyline: an open source document editor for creating and analyzing targeted proteomics experiments, Bioinformatics 26 (2010) 966–968.
[33] B. Muqaku, M. Eisinger, S.M. Meier, A. Tahir, T. Pukrop, S. Haferkamp, A. Slany, A. Reichle, C. Gerner, Multi-omics analysis of serum samples demonstrates reprogramming of organ functions via systemic calcium mobilization and platelet activation in metastatic melanoma, Mol. Cell. Proteomics 16 (2017) 86–99.
[34] B. Muqaku, A. Slany, A. Bileck, D. Kreutz, C. Gerner, Quantification of cytokines secreted by primary human cells using multiple reaction monitoring: evaluation of analytical parameters, Anal. Bioanal. Chem. 407 (2015) 6525–6536.
[35] J. Cox, M. Mann, MaxQuant enables high peptide identification rates, individualized p.p.b.-range mass accuracies and proteome-wide protein quantification, Nat. Biotechnol. 26 (2008) 1367–1372.
[36] A. Bateman, M.J. Martin, C. O'Donovan, M. Magrane, E. Alpi, R. Antunes, B. Bely, M. Bingley, C. Bonilla, R. Britto, B. Bursteinas, H. Bye-Ajee, A. Cowley, A. Da Silva, M. De Giorgi, T. Dogan, F. Fazzini, L.G. Castro, L. Figueira, P. Garmiri, G. Georghiou, D. Gonzalez, E. Hatton-Ellis, W. Li, W. Liu, R. Lopez, J. Luo, Y. Lussi, A. MacDougall, A. Nightingale, B. Palka, K. Pichler, D. Poggioli, S. Pundir, L. Pureza, G. Qi, S. Rosanoff, R. Saidi, T. Sawford, A. Shypitsyna, E. Speretta, E. Turner, N. Tyagi, V. Volynkin, T. Wardell, K. Warner, X. Watkins, R. Zaru, H. Zellner, I. Xenarios, L. Bougueleret, A. Bridge, S. Poux, N. Redaschi, L. Aimo, G. ArgoudPuy, A. Auchincloss, K. Axelsen, P. Bansal, D. Baratin, M.C. Blatter, B. Boeckmann, J. Bolleman, E. Boutet, L. Breuza, C. Casal-Casas, E. De Castro, E. Coudert, B. Cuche, M. Doche, D. Dornevil, S. Duvaud, A. Estreicher, L. Famiglietti, M. Feuermann, E. Gasteiger, S. Gehant, V. Gerritsen, A. Gos, N. Gruaz-Gumowski, U. Hinz, C. Hulo, F. Jungo, G. Keller, V. Lara, P. Lemercier, D. Lieberherr, T. Lombardot, X. Martin, P. Masson, A. Morgat, T. Neto, N. Nouspikel, S. Paesano, I. Pedruzzi, S. Pilbout, M. Pozzato, M. Pruess, C. Rivoire,

B. Roechert, M. Schneider, C. Sigrist, K. Sonesson, S. Staehli, A. Stutz, S. Sundaram, M. Tognolli, L. Verbregue, A.L. Veuthey, C.H. Wu, C.N. Arighi, L. Arminski, C. Chen, Y. Chen, J.S. Garavelli, H. Huang, K. Laiho, P. McGarvey, D.A. Natale, K. Ross, C.R. Vinayaka, Q. Wang, Y. Wang, L.S. Yeh, J. Zhang, UniProt: the universal protein knowledgebase, Nucleic Acids Res. 45 (2017) D158–D169.

[37] J. Cox, M. Mann, 1D and 2D annotation enrichment: a statistical method integrating quantitative proteomics with complementary high-throughput data, BMC Bioinformatics 13 (Suppl. 16) (2012) S12.

[38] J.A. Vizcaino, E.W. Deutsch, R. Wang, A. Csordas, F. Reisinger, D. Rios, J.A. Dianes, Z. Sun, T. Farrah, N. Bandeira, P.A. Binz, I. Xenarios, M. Eisenacher, G. Mayer, L. Gatto, A. Campos, R.J. Chalkley, H.J. Kraus, J.P. Albar, S. Martinez-Bartolome, R. Apweiler, G.S. Omenn, L. Martens, A.R. Jones, H. Hermjakob, ProteomeXchange provides globally coordinated proteomics data submission and dissemination, Nat. Biotechnol. 32 (2014) 223–226.

[39] D. Kanojia, R.A. Morshed, L. Zhang, J.M. Miska, J. Qiao, J.W. Kim, P. Pytel, I.V. Balyasnikova, M.S. Lesniak, A.U. Ahmed, βIII-tubulin regulates breast cancer metastases to the brain, Mol. Cancer Ther. 14 (2015) 1152–1161.

[40] K. Mariz, J.B. Ingolf, H. Daniel, N.J. Teresa, S. Erich-Franz, The Wnt inhibitor dickkopf-1: a link between breast cancer and bone metastases, Clin. Exp. Metastasis 32 (2015) 857–866.

[41] C.A. Powell, M.W. Nasser, H. Zhao, J.C. Wochna, X. Zhang, C. Shapiro, K. Shilo, R.K. Ganju, Fatty acid binding protein 5 promotes metastatic potential of triple negative breast cancer cells through enhancing epidermal growth factor receptor stability, Oncotarget 6 (2015) 6373–6385.

[42] G. Wang, A. Platt-Higgins, J. Carroll, S. De Silva Rudland, J. Winstanley, R. Barraclough, P.S. Rudland, Induction of metastasis by S100P in a rat mammary model and its association with poor survival of breast cancer patients, Cancer Res. 66 (2006) 1199–1207.

[43] J. Obacz, V. Brychtova, J. Podhorec, P. Fabian, P. Dobes, B. Vojtesek, R. Hrstka, Anterior gradient protein 3 is associated with less aggressive tumors and better outcome of breast cancer patients, OncoTargets Ther. 8 (2015) 1523–1532.

[44] Q. Wang, J. Zhu, Y.W. Wang, Y. Dai, Y.L. Wang, C. Wang, J. Liu, A. Baker, N.H. Colburn, H.S. Yang, Tumor suppressor Pdcd4 attenuates Sin1 translation to inhibit invasion in colon carcinoma, Oncogene 36 (2017) 6225–62354.

[45] R.R. Weichselbaum, H. Ishwaran, T. Yoon, D.S.A. Nuyten, S.W. Baker, N. Khodarev, A.W. Su, A.Y. Shaikh, P. Roach, B. Kreike, B. Roizman, J. Bergh, Y. Pawitan, M.J. Van De Vijver, A.J. Minn, An interferon-related gene signature for DNA damage resistance is a predictive marker for chemotherapy and radiation for breast cancer, Proc. Natl. Acad. Sci. U. S. A. 105 (2008) 18490–18495.

[46] A. Slany, V. Paulitschke, V. Haudek-Prinz, A. Meshcheryakova, C. Gerner, Determination of cell type-specific proteome signatures of primary human leukocytes, endothelial cells, keratinocytes, hepatocytes, fibroblasts and melanocytes by comparative proteome profiling, Electrophoresis 35 (2014) 1428–1438.

[47] S.J. Ho Sui, J.R. Mortimer, D.J. Arenillas, J. Brumm, C.J. Walsh, B.P. Kennedy, W.W. Wasserman, oPOSSUM: identification of over-represented transcription factor binding sites in co-expressed genes, Nucleic Acids Res. 33 (2005) 3154–3164.

[48] M.J. Morgan, Z.G. Liu, Crosstalk of reactive oxygen species and NF-κB signaling, Cell Res. 21 (2011) 103–115.

[49] X. Zhu, S. Huang, L. Zeng, J. Ma, S. Sun, F. Zeng, F. Kong, X. Cheng, HMOX-1 inhibits TGF-β-induced epithelial-mesenchymal transition in the MCF-7 breast cancer cell line, Int. J. Mol. Med. 40 (2017) 411–417.

[50] Y. Murakawa, M. Hinz, J. Mothes, A. Schuetz, M. Uhl, E. Wyler, T. Yasuda, G. Mastrobuoni, C.C. Friedel, L. Dölken, S. Kempa, M. Schmidt-Supprian, N. Blüthgen, R. Backofen, U. Heinemann, J. Wolf, C. Scheidereit, M. Landthaler, RC3H1 post-transcriptionally regulates A20 mRNA and modulates the activity of the IKK/NF-κ B pathway, Nat. Commun. 6 (2015).

[51] A.M. Szász, B. Győrffy, G. Marko-Varga, Cancer heterogeneity determined by functional proteomics, Semin. Cell Dev. Biol. 64 (2017) 132–142.

[52] D. Hanahan, R.A. Weinberg, Hallmarks of cancer: the next generation, Cell 144 (2011) 646–674.

[53] K.M. McNamara, H. Sasano, The intracrinology of breast cancer, J. Steroid Biochem. Mol. Biol. 145 (2015) 172–178.

[54] Q. Ji, C. Aoyama, Y.D. Nien, P.I. Liu, P.K. Chen, L. Chang, F.Z. Stanczyk, A. Stolz, Selective loss of AKR1C1 and AKR1C2 in breast cancer and their potential effect on progesterone signaling, Cancer Res. 64 (2004) 7610–7617.

[55] A. Wenners, F. Hartmann, A. Jochens, A.M. Roemer, I. Alkatout, W. Klapper, M. van Mackelenbergh, C. Mundhenke, W. Jonat, M. Bauer, Stromal markers AKR1C1 and AKR1C2 are prognostic factors in primary human breast cancer, Int. J. Clin. Oncol. 21 (2016) 548–556.

[56] F.T. Unger, I. Witte, K.A. David, Prediction of individual response to anticancer therapy: historical and future perspectives, Cell. Mol. Life Sci. 72 (2015) 729–757.

Supplementary Information

Supplemantary Figure S1. Transcription factors responsible for regulation of proteins identified by oPOSSUM. Z-score vs GC content plots of relevant transcription factors. Cut off was set to mean + 2 times standard devation. (A) and (B) represent transcription factors associated with proteins up-regulated or down-regulated in MCF-7/CLC co-cultures, respectively. (C) and (D) represent transcription factors associated with proteins up-regulated or down-regulated in ZR-75-1/CLC co-cultures, respectively.

Supplementary Table S1. List of identified proteins including identification parameters, differentially regulated proteins with regard to MCF-7 compared to ZR-75-1 and co-cultures compared to single cell type culture models. Protein names and gene names are listed according to UniProt, fold change values are listed on a logarithmic scale on the base of 2, protein regulation events meeting an FDR < 0.05 are marked. Identification parameters include the number of total and unique peptides identified via mass spectrometry per protein, the corresponding sequence coverage, q-value, score, intensity and number of MS/MS counts. Note that all MS data are fully available via ProteomeXchange with the identifier PXD008719.

The table can only be accessed online.

Supplementary Table S2. Proteins significantly regulated in CLCs, MCF-7 and/or ZR-75-1 upon treatment with curcumin. Fold-changes of LFQ values and corresponding q-values are listed for all proteins significantly regulated upon treatment with curcumin in CLCs, MCF-7 and/or ZR-75-1, applying an FDR ≤ 0.05, multi-parameter correction and s0 ≥ 0.2. Significant regulatory events are highlighted in bold.

Supplementary Table S3. List of transcription factors responsible for regulation of proteins identified by oPOSSUM. Detailed information about relevant transcription factors to all up- and down-regulated proteins including class, family, GC content and calculated *Z*-score. General settings for the oPOSSUM search are included.

Supplementary Table S4. MRM method: List of proteins, peptides and transitions applied for MRM measurements.

Supplementary Figure S1

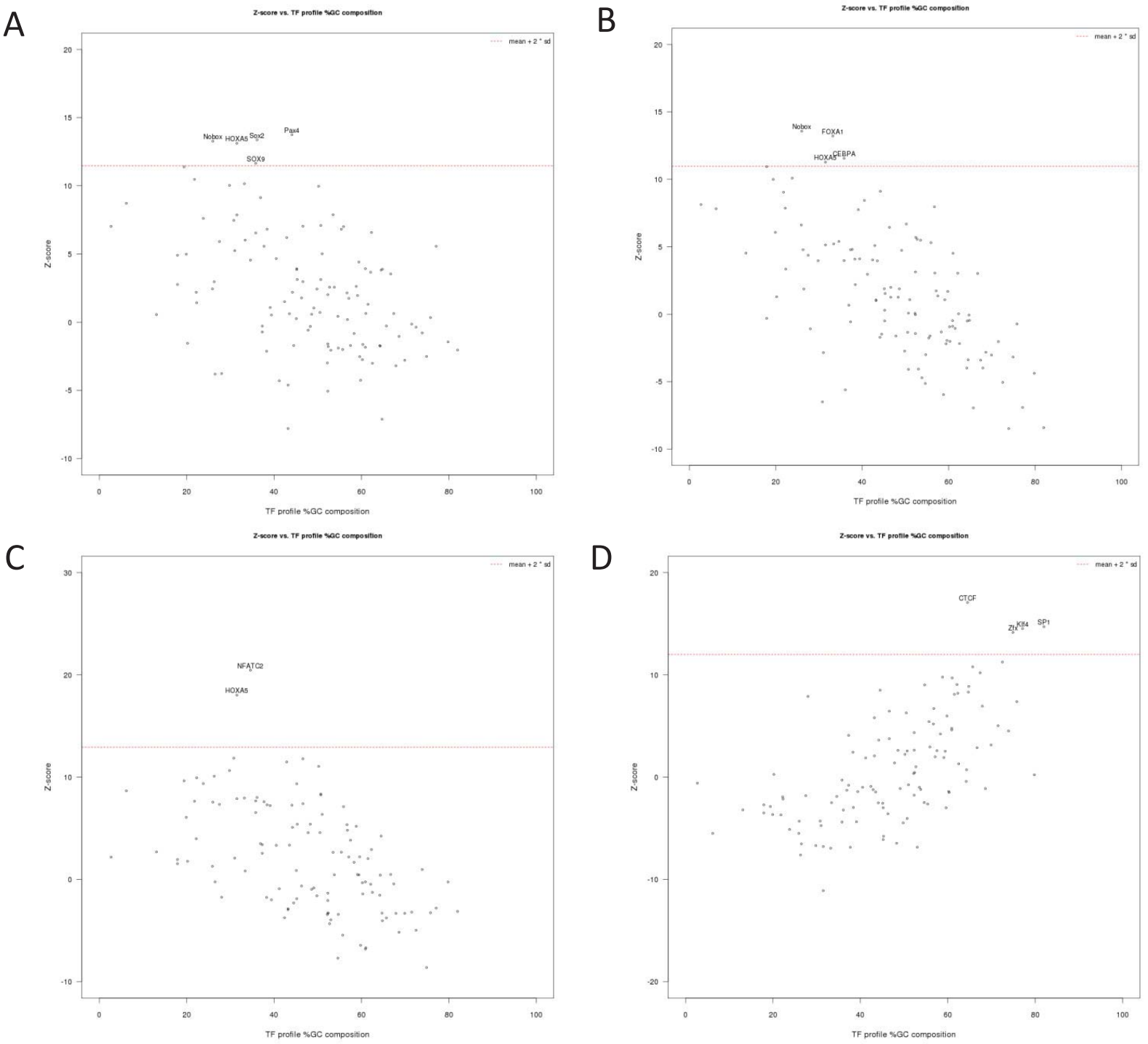

Supplementary Table S2

Gene names	CLCs		MCF-7		ZR-75-1	
	fold change	q-value	fold change	q-value	fold change	q-value
HMOX1	**4.24**	**4.9E-02**	**19.78**	**1.4E-01**	**66.10**	**0.0E+00**
ISLR	**-11.73**	**4.9E-02**	nd	na	nd	na
SEMA7A	**-3.60**	**4.5E-02**	1.48	1.0E+00	1.41	9.7E-01
MMP2	**9.07**	**6.0E-02**	2.82	6.9E-01	-1.58	9.3E-01
SPARC	**4.91**	**3.9E-02**	1.84	1.0E+00	-1.26	9.8E-01
CDKN1A	**12.10**	**4.7E-02**	1.81	1.0E+00	1.06	1.0E+00
GSDMD	**2.76**	**4.2E-02**	nd	na	-1.46	6.9E-01
RND3	**13.65**	**0.0E+00**	1.19	1.0E+00	-1.10	1.0E+00
FKBP5	**4.62**	**5.0E-02**	-1.08	1.0E+00	-1.17	9.3E-01
ADAMTSL1	**-3.63**	**4.3E-02**	1.50	1.0E+00	nd	na
GDF15	**11.70**	**5.8E-02**	3.70	2.0E-01	3.33	5.4E-01
ECE2	1.41	6.6E-01	**15.71**	**7.0E-02**	1.22	9.4E-01
IFIT1	1.06	9.4E-01	**-4.56**	**2.8E-02**	nd	1.0E+00
TTI2	2.28	1.5E-01	**4.82**	**4.7E-02**	-3.66	8.2E-01
MUC5B	nd	na	**-4.34**	**3.5E-02**	nd	na
GCLM	1.54	2.1E-01	1.71	6.7E-01	**4.31**	**4.0E-02**

Supplementary Table S3: Transcription factors responsible for regulation of proteins

ccMCF7 vs MCF7_only significantly up-regulated proteins submitted to oPOSSUM

TF	Class	Family	IC	GC Content	Target gene hits	Target TFBS hits	Z-score
PAX4	Helix-Turn-Helix	Homeo	11.004	0.441	1	1	13.749
SOX2	Other Alpha-Helix	High Mobility Group	12.951	0.361	5	11	13.370
NOBOX	Helix-Turn-Helix	Homeo	9.573	0.260	18	123	13.272
HOXA5	Helix-Turn-Helix	Homeo	8.759	0.315	21	283	13.117
SOX9	Other Alpha-Helix	High Mobility Group	9.079	0.358	17	69	11.648

ccMCF7 vs MCF7_only significantly down-regulated proteins submitted to oPOSSUM

TF	Class	Family	IC	GC Content	Target gene hits	Target TFBS hits	Z-score
NOBOX	Helix-Turn-Helix	Homeo	9.573	0.260	9	71	13.573
FOXA1	Winged Helix-Turn-Helix	Forkhead	12.533	0.332	8	56	13.218
CEBPA	Zipper-Type	Leucine Zipper	8.712	0.358	9	50	11.552
HOXA5	Helix-Turn-Helix	Homeo	9.573	0.260	11	149	11.276

ccZR-75-1 vs ZR-75-1_only significantly up-regulated proteins submitted to oPOSSUM

TF	Class	Family	IC	GC Content	Target gene hits	Target TFBS hits	Z-score
NFATC2	Ig-fold	Rel	9.859	0.346	37	363	20.451
HOXA5	Helix-Turn-Helix	Homeo	9.573	0.260	40	654	18.013

ccZR-75-1 vs ZR-75-1_only significantly down-regulated proteins submitted to oPOSSUM

TF	Class	Family	IC	GC Content	Target gene hits	Target TFBS hits	Z-score
CTCF	Zinc-coordinating	BetaBetaAlpha-zinc finger	17.205	0.645	14	16	17.068
SP1	Zinc-coordinating	BetaBetaAlpha-zinc finger	11.129	0.820	27	176	14.703
KLF4	Zinc-coordinating	BetaBetaAlpha-zinc finger	12.618	0.771	26	192	14.518
ZFX	Zinc-coordinating	BetaBetaAlpha-zinc finger	13.077	0.749	20	79	14.142

General settings for oPOSSUM search

JASPAR collection(s):	CORE
Taxonomic supergroup(s):	vertebrates (Homo sapiens)
Minimum profile specificity:	8 bits
Conservation cutoff:	0.40
Matrix score threshold:	85%
Upstream sequence length:	5000
Downstream sequence length:	5000
Results returned:	All results sorted by Z-score

Supplementary Table S4: MRM method. List of proteins, peptides and transitior

Protein Accession	Protein Name	Protein Description	Gene Name	Peptide Sequence	Precursor Mz	Precursor Charge	Product Mz	Product Charge	Fragment Ion	Collision Energy
global standards	global standards	global standards		VLETKSLYVR	403.239684	3	554.821681	2	y9	9.7
global standards	global standards	global standards		VLETKSLYVR	403.239684	3	498.279649	2	y8	9.7
global standards	global standards	global standards		EGVNDNEEGFFSAR	785.842058	2	684.346386	1	y6	23.5
global standards	global standards	global standards		EGVNDNEEGFFSAR	785.842058	2	480.256508	1	y4	23.5
global standards	global standards	global standards		VLETK[+42]SLYVR	625.36117	2	1037.562586	1	y8	17.7
global standards	global standards	global standards		VLETK[+42]SLYVR	625.36117	2	908.519993	1	y7	17.7
global standards	global standards	global standards		TTPAVLDSDGSYFLYSK	932.454181	2	1394.647438	1	y12	28.8
global standards	global standards	global standards		TTPAVLDSDGSYFLYSK	932.454181	2	831.406503	2	y15	28.8
P09601	HMOX1	Heme oxygenase 1	HMOX1	ESPVFAPVYFPEELHR	639.656226	3	1090.53162	1	y8	18.2
P09601	HMOX1	Heme oxygenase 1	HMOX1	ESPVFAPVYFPEELHR	639.656226	3	927.468292	1	y7	18.2
P09601	HMOX1	Heme oxygenase 1	HMOX1	ESPVFAPVYFPEELHR	639.656226	3	780.399878	1	y6	18.2
P09601	HMOX1	Heme oxygenase 1	HMOX1	TEPELLVAHAYTR	500.59994	3	817.431512	1	y7	13.2
P09601	HMOX1	Heme oxygenase 1	HMOX1	TEPELLVAHAYTR	500.59994	3	718.363098	1	y6	13.2
P09601	HMOX1	Heme oxygenase 1	HMOX1	TEPELLVAHAYTR	500.59994	3	510.267073	1	y4	13.2
P09601	HMOX1	Heme oxygenase 1	HMOX1	YLGDLSGGQVLK	625.342977	2	973.531286	1	y10	17.7
P09601	HMOX1	Heme oxygenase 1	HMOX1	YLGDLSGGQVLK	625.342977	2	688.398815	1	y7	17.7
P09601	HMOX1	Heme oxygenase 1	HMOX1	YLGDLSGGQVLK	625.342977	2	601.366787	1	y6	17.7
Q5TC82	RC3H1	Roquin	RC3H1	GC[+57]QFLGPAMQEEALK	839.900008	2	1186.613635	1	y11	25.4
Q5TC82	RC3H1	Roquin	RC3H1	GC[+57]QFLGPAMQEEALK	839.900008	2	1016.508108	1	y9	25.4
Q5TC82	RC3H1	Roquin	RC3H1	GC[+57]QFLGPAMQEEALK	839.900008	2	848.41823	1	y7	25.4
Q5TC82	RC3H1	Roquin	RC3H1	GC[+57]QFLGPAMQEEALK	839.900008	2	589.319168	1	y5	25.4
Q7L523	RRAGA	Ras-related GTP-binding protein A	RRAGA	LGATIDVEHSHVR	478.588035	3	978.475168	1	y8	12.4
Q7L523	RRAGA	Ras-related GTP-binding protein A	RRAGA	LGATIDVEHSHVR	478.588035	3	635.337218	1	y5	12.4
Q7L523	RRAGA	Ras-related GTP-binding protein A	RRAGA	LGATIDVEHSHVR	478.588035	3	596.807093	2	y10	12.4
Q7L523	RRAGA	Ras-related GTP-binding protein A	RRAGA	TSIWDETLYK	628.313885	2	954.456724	1	y7	17.8
Q7L523	RRAGA	Ras-related GTP-binding protein A	RRAGA	TSIWDETLYK	628.313885	2	768.377411	1	y6	17.8
Q86TG7	PEG10	Retrotransposon-derived protein PEG10	PEG10	DGLITPTIAPNGAQVLQVK	645.701835	3	714.450851	1	y6	18.4
Q86TG7	PEG10	Retrotransposon-derived protein PEG10	PEG10	DGLITPTIAPNGAQVLQVK	645.701835	3	718.417008	2	y14	18.4
Q86TG7	PEG10	Retrotransposon-derived protein PEG10	PEG10	DGLITPTIAPNGAQVLQVK	645.701835	3	527.306198	2	y10	18.4
P52895	AK1C2	Aldo-keto reductase family 1 member C2	AKR1C2	YKPVC[+57]NQVEC[+57]HPYFNQR	560.509745	4	824.404963	1	y6	15.4
P52895	AK1C2	Aldo-keto reductase family 1 member C2	AKR1C2	YKPVC[+57]NQVEC[+57]HPYFNQR	560.509745	4	727.352199	1	y5	15.4
P52895	AK1C2	Aldo-keto reductase family 1 member C2	AKR1C2	YKPVC[+57]NQVEC[+57]HPYFNQR	560.509745	4	564.288871	1	y4	15.4
P52895	AK1C2	Aldo-keto reductase family 1 member C2	AKR1C2	DIVLVAYSALGSHR	500.943818	3	961.485004	1	y9	13.2
P52895	AK1C2	Aldo-keto reductase family 1 member C2	AKR1C2	DIVLVAYSALGSHR	500.943818	3	890.447891	1	y8	13.2
P52895	AK1C2	Aldo-keto reductase family 1 member C2	AKR1C2	DIVLVAYSALGSHR	500.943818	3	727.384562	1	y7	13.2
P52895	AK1C2	Aldo-keto reductase family 1 member C2	AKR1C2	DIVLVAYSALGSHR	500.943818	3	569.31542	1	y5	13.2

2.3. Comprehensive assessment of proteins regulated by dexamethasone reveals novel effects in primary human peripheral blood mononuclear cells

Andrea Bileck[a], Dominique Kreutz[a], Besnik Muqaku[a], Astrid Slany[a], Christopher Gerner[a]

Journal of Proteome Research, **2014**, 13 (12), 5989-6000

[a] Department of Analytical Chemistry, Faculty of Chemistry, University of Vienna, Waehringer Strasse 38, Vienna, Austria

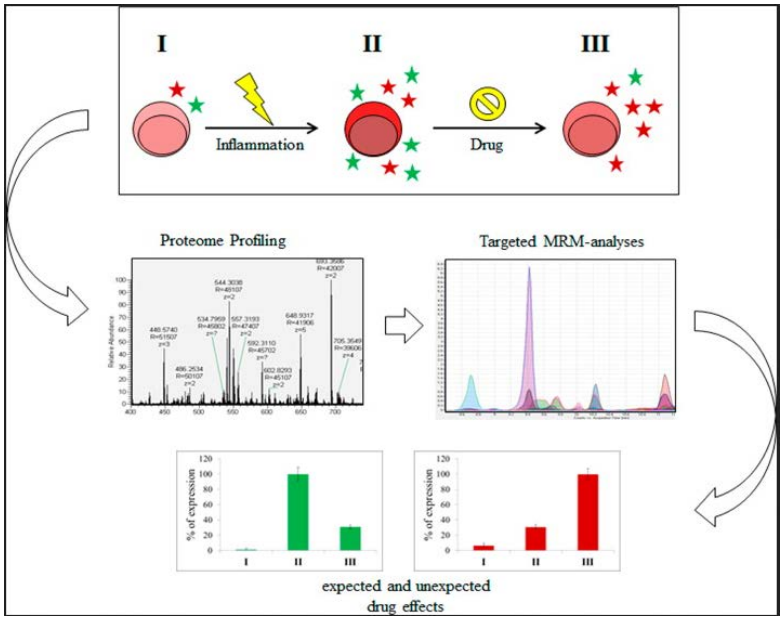

Contributions to this publication:

- Conduction of experiments
- Involved in data interpretation and writing of the manuscript

Summary of "Comprehensive assessment of proteins regulated by dexamethasone reveals novel effects in primary human peripheral blood mononuclear cells"

Human peripheral blood mononuclear cells (PBMCs) from three healthy donors were inflammatory activated *in vitro* and subsequently treated with the antiphlogistic drug dexamethasone. High-resolution mass spectrometry (MS) analysis yielded comprehensive proteome profiles of cytoplasmic, nuclear and secreted protein fractions of the three cell states. Overall 6886 proteins were identified, with 469 regulatory effects observed upon inflammatory activation. A successful stimulation of the PBMCs was demonstrated by the up-regulation of interleukins (ILs) and chemokines. Several proteins were determined with yet unknown involvement in the inflammatory process, *e.g.* zinc-finger proteins and helicase-like transcription factor.

Dexamethasone treatment counter-regulated most of the proteins, which were changed in abundance after inflammatory stimulation. However, the original cell state was not fully reconstituted and some proteins involved in redox regulations such as glutathione reductase and glutathione S-transferase mu 1, were even further up-regulated upon drug treatment. These unexpected effects of inflammatory activation and drug treatment are potentially responsible for adverse effects.

To verify our findings, targeted MS analysis using multiple reaction monitoring (MRM) was conducted on selected proteins. IL-1β, IL-6, C-X-C motif chemokine 2 and growth-regulated alpha protein were found up-regulated by inflammatory activation and successfully down-regulated by dexamethasone treatment using the MRM approach. As opposed to these counter-regulations, pentraxin-related protein PTX3 and tumor necrosis factor-inducible gene 6 protein regulations upon stimulation were even amplified by drug administration. Furthermore, the results revealed strong inter-individual differences in basal protein abundances, but regulatory effects displayed similar trends.

This study showed the great potential of the in-depth analysis of proteome profiles combined with targeted proteomics approaches to investigate drug effects on a molecular level in an individualized fashion.

2.4. An Organoruthenium Anticancer Agent Shows Unexpected Target Selectivity For Plectin

Samuel M. Meier[ab], Dominique Kreutz[a], Lilli Winter[c], Matthias H. M. Klose[bd], Klaudia Cseh[d], Tamara Weiss[e], Andrea Bileck[a], Beatrix Alte[f], Johanna C. Mader[a], Samir Jana[g], Annesha Chatterjee[g], Arindam Bhattacharyya[g], Michaela Hejl[d], Michael A. Jakupec[bd], Petra Heffeter[bf], Walter Berger[bf], Christian G. Hartinger[h], Bernhard K. Keppler[bd], Gerhard Wiche[c] and Christopher Gerner[a]

Angewandte Chemie - International Edition, **2017**, 56 (28), 8267-8271

[a] Department of Analytical Chemistry, Faculty of Chemistry, University of Vienna, Waehringer Strasse 38, Vienna, Austria

[b] Forschungsplattform "Translational Cancer Therapy Research", Universität Wien und Medizinische Universität Wien, Austria

[c] Department of Biochemistry and Cell Biology MFPL, Universität Wien, Dr.-Bohr-Gasse 9, Vienna, Austria

[d] Institut für Anorganische Chemie, Universität Wien, Austria

[e] St. Anna Kinderkrebsforschung, Vienna, Austria

[f] Institut für Krebsforschung, Medizinische Universität Wien, Austria

[g] Department für Zoology, University of Calcutta, 35 Ballygunge Circular Road, India

[h] School of Chemical Science, University of Auckland, New Zealand

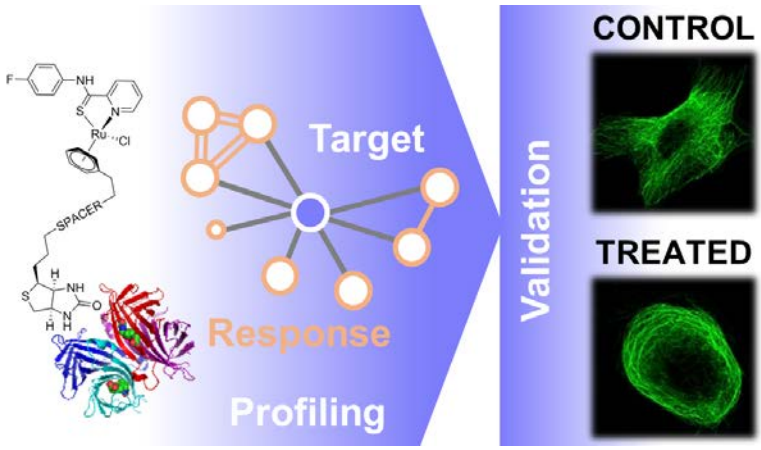

Contributions to this publication:

- Conduction of experiments
- Involved in data interpretation

Anticancer Agents Hot Paper

International Edition: DOI: 10.1002/anie.201702242
German Edition: DOI: 10.1002/ange.201702242

An Organoruthenium Anticancer Agent Shows Unexpected Target Selectivity For Plectin

Samuel M. Meier, Dominique Kreutz, Lilli Winter, Matthias H. M. Klose, Klaudia Cseh, Tamara Weiss, Andrea Bileck, Beatrix Alte, Johanna C. Mader, Samir Jana, Annesha Chatterjee, Arindam Bhattacharyya, Michaela Hejl, Michael A. Jakupec, Petra Heffeter, Walter Berger, Christian G. Hartinger, Bernhard K. Keppler, Gerhard Wiche, and Christopher Gerner**

Abstract: *Organometallic metal(arene) anticancer agents require ligand exchange for their anticancer activity and this is generally believed to confer low selectivity for potential cellular targets. However, using an integrated proteomics-based target-response profiling approach as a potent hypothesis-generating procedure, we found an unexpected target selectivity of a ruthenium(arene) pyridinecarbothioamide (plecstatin) for plectin, a scaffold protein and cytolinker, which was validated in a plectin knock-out model in vitro. Plectin targeting shows potential as a strategy to inhibit tumor invasiveness as shown in cultured tumor spheroids while oral administration of plecstatin-1 to mice reduces tumor growth more efficiently in the invasive B16 melanoma than in the CT26 colon tumor model.*

Metal-based anticancer agents beyond the platinum class offer a largely unexplored chemical space to biology and medicine.[1] A glimpse on their potential can be deduced from the fact that simple ligand modifications on ruthenium organometallics dictate their ability to target either oligonucleotides or proteins in the nucleosome core particle[2] or to catalyze hydride transfer reactions in cells.[3] However, identifying protein targets still represents the main challenge in the field of bioinorganic anticancer drug discovery that is historically governed by serendipity.[4] Although promising validation strategies were recently reported for bismuth[5] and gold porphyrins,[6] no such attempt was carried out for metal-based anticancer agents designed as prodrugs that contain a hydrolytically labile metal–halido bond and which are expected to show rather low specificity according to the current thinking in the field.[4]

We recently discovered the Ru(arene) compound termed plecstatin-1 (Figure 1 A) as a promising metal-based lead structure for the treatment of solid tumors, designed for oral application.[4] Herein, we report on an integrated proteomics-based target-response profiling approach to generate hypotheses on target preferences for such metallodrugs in cells. We identify and validate plectin, a scaffold protein and cytolinker,[7] as the main cellular target of plecstatins with pronounced effects on the organization of non-mitotic microtubules (MTs). Non-mitotic MTs are an underappreciated drug target and their disturbance by plectin-targeting agents affects the motility of cancer cells, which may be harnessed as a promising anticancer strategy.

Crystal-soaking experiments with the nucleosome core particle revealed that plecstatin-1 did only bind to histidines 79 and 106 on histone 2B after hydrolysis.[4] Exposing plasmid DNA to plecstatin-1 at r_b-values of up to 5 did not affect the electrophoretic mobility of the plasmid (Figure S1 A in the Supporting Information), supporting the absence of any DNA interaction.

Plecstatin-1 was selected for a five-dose NCI-60 screen[8] and it showed higher potency in the cell line panel compared to cisplatin and KP1019 (NSC No. 776415, Figure S1 B). COMPARE 170 analysis based on the growth inhibition profile revealed solely correlations below the significance threshold. This indicated that plecstatin-1 follows an unprecedented mode of action.

Plecstatin-1 showed a cellular accumulation of 160 fg cell^{-1} (relative standard deviation, RSD = 36%) comparable to satraplatin (Figure S1 C). Hydrolyzed ruthenium-arene metallodrugs face innumerous potential binding partners intracellularly. Target profiling by affinity purification is suitable to profile for potential targets by immobilizing

[*] Dr. S. M. Meier, M. Sc. D. Kreutz, Dr. A. Bileck, Dr. J. C. Mader, Prof. Dr. C. Gerner
Institut für Analytische Chemie, Universität Wien
Währinger Strasse 38, 1090 Wien (Austria)
E-mail: samuel.meier@univie.ac.at
christopher.gerner@univie.ac.at
Dr. S. M. Meier, M. Sc. M. H. M. Klose, Dr. M. A. Jakupec, Priv.-Doz. Dr. P. Heffeter, Prof. Dr. W. Berger, Prof. Dr. B. K. Keppler
Forschungsplattform "Translational Cancer Therapy Research"
Universität Wien und Medizinische Universität Wien (Austria)
Dr. L. Winter, Prof. Dr. G. Wiche
Department of Biochemistry and Cell Biology MFPL, Universität Wien
Dr.-Bohr-Gasse 9, 1030 Vienna (Austria)
M. Sc. M. H. M. Klose, M. Sc. K. Cseh, M. Hejl, Dr. M. A. Jakupec, Prof. Dr. B. K. Keppler
Institut für Anorganische Chemie, Universität Wien (Austria)
M. Sc. T. Weiss
St. Anna Kinderkrebsforschung, Vienna (Austria)
M. Sc. B. Alte, Priv.-Doz. Dr. P. Heffeter, Prof. Dr. W. Berger
Institut für Krebsforschung
Medizinische Universität Wien (Austria)
M. Sc. S. Jana, Dr. A. Chatterjee, Dr. A. Bhattacharyya
Department für Zoology, University of Calcutta
35 Ballygunge Circular Road (India)
Prof. Dr. C. G. Hartinger
School of Chemical Science, University of Auckland (New Zealand)
Supporting information and the ORCID identification number(s) for the author(s) of this article can be found under https://doi.org/10.1002/anie.201702242.

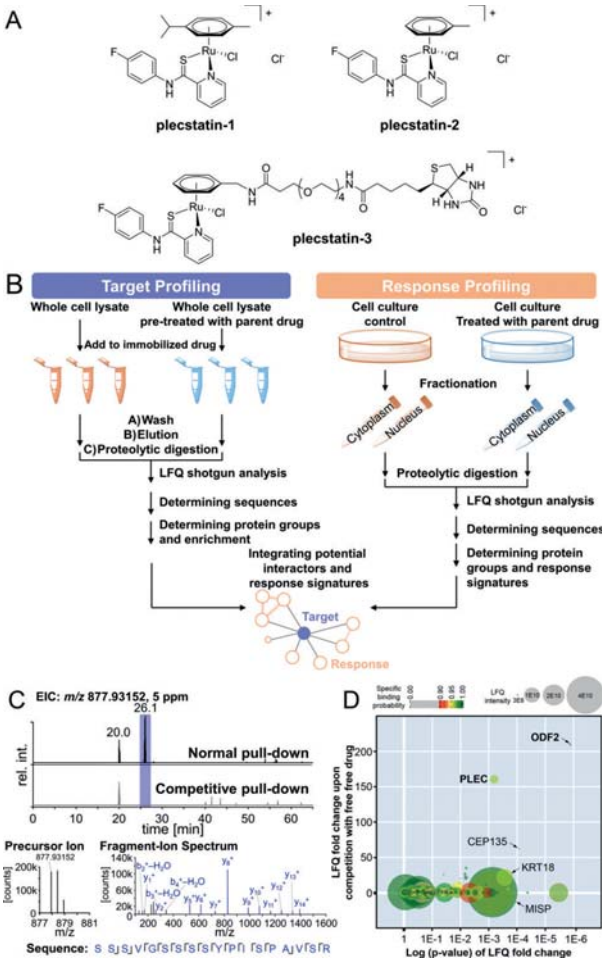

Figure 1. Potential protein targets of plecstatins were obtained by integrated target-response profiling. A) Chemical structures. B) Schematic representation of the integrated target-response profiling workflow. C) Selected chromatograms and mass spectra of a plectin-specific tryptic peptide. D) Plot of the target profiling experiment. PLEC: plectin; ODF2: outer dense fiber protein 2.

a drug on solid support and exposing it to whole cell lysates. Only RAPTA, which is an organoruthenium drug candidate with antimetastatic properties,[9] was assayed in a similar setting

To address non-specific interactions, we performed differential target profiling, whereby the cell lysate is either pre-treated or not pre-treated with the parent metallodrug before adding to the immobilized drug (Figure 1 B). Pre-treatment saturates actual binding sites and results in these proteins not being able to interact with the immobilized drug, which is exemplified in the chromatograms of Figure 1 C.

A derivative of plecstatin-1 with a hydrophilic biotin linker (plecstatin-3, Figure 1 A) was prepared to be immobilized on streptavidin beads. Derivatising the arene is suitable for retaining the target selectivity.[9] Plecstatin-3 was obtained in situ and is stable over 24 h (Figure S1D). The η^6-toluene derivative (plecstatin-2) was also prepared and is used as the parent drug in the proteomics assays. Plecstatin-1 and plecstatin-2 showed very similar in vitro activity profiles (Figure S1 E), with plecstatin-2 being less potent. Whole-cell lysates of HCT116 colon carcinoma cells were generated in this study using a non-denaturing lysis buffer to retain protein tertiary structure. After incubation, the bound proteins were eluted by a combination of chaotropes and acidification in an unmetallated state. After proteolytic digestion, the peptides were analyzed by a label-free quantitative (LFQ) mass-spectrometric shotgun approach (Figure 1 B) using a QExactive Orbitrap. Each run generated approximately 3100 annotated fragment ion spectra, which were searched for protein sequences using MaxQuant (Figure 1 C, Figure S2, see methods in the Supporting Information for details).[10] Enrichment and significance based on LFQ values represent the axes of the target profiling plot (Figure 1 D), while the size of the bubbles represents the LFQ-intensity of a given protein. The specificity of binding was calculated as a percentage using the CRAPome database[11] and was adapted for abundance of MS/MS counts. In Figure 1 D, green represents specific binding probabilities of >0.97. To account for ligand-exchange kinetics in the target profiling experiment, the pre-treated and the not pre-treated cell lysates were incubated with the immobilized drug for 4 h. Roughly 400 proteins were identified of which only outer dense fiber protein 2 (ODF2, 210-fold) and plectin (PLEC, 160-fold) emerged as potential targets with high enrichment factors.

Then, response profiling was carried out as a second dimension by analyzing the proteomic response signatures in living HCT116 cells to drug treatment as recently reported (Figure 1 B).[12] Cells were treated with plecstatin-2 at half IC_{50} concentration and the tryptic digests of fractionated cells were analyzed by LFQ shotgun analysis. Response profiling showed 581 out of 4343 proteins with significant regulation events (false discovery rate, FDR <0.05) in the cytoplasmic and/or nuclear fractions (Figure S3). The data sets of the proteomic experiments are available at the PRIDE repository under PXD005373-PXD005376, PXD005386, and PXD005389 (Table S2).

The significantly regulated proteins were then included to construct the target-response networks for ODF2 and PLEC

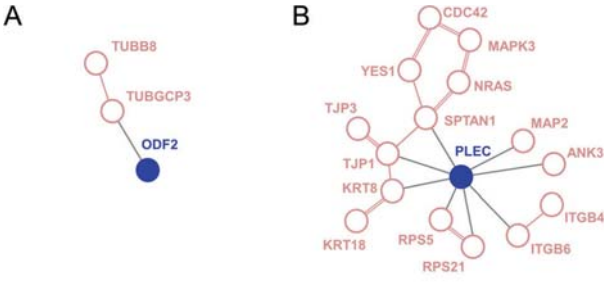

C

Accession	Protein	Intensity	MS/MS counts	Unique Peptides	Coverage	Score	P-value	Ratio N/C
Q15149	Plectin	2.68E+09	253	71	16%	323.3	6.40E-04	160

Figure 2. Target-response profiling network of plecstatins for the two most enriched proteins from HCT116 cells A) ODF2 and B) PLEC. C) Mass spectrometric results for plectin identification from target profiling.

using STRING (Figure 2A,B).[13] This provides a strong target hypothesis because the drug target must be causally linked to its cellular effects.

A small target-response network was observed for ODF2, a component of the centrosomal scaffold (Figure 2A).[14] Inhibiting centrosomal function is expected to lead to a G2/M arrest. Cell cycle analysis by flow cytometry showed an increase (20%) of the G0/G1 fraction at the expense of the S-phase (Figure S4A). The accumulation of cells in the G0/G1 fraction was concentration dependent and also observable in nearly confluent cells (Figure S4B). Therefore, the cell response was unlikely to be related to ODF2.

Plectin is a scaffold protein and an important cytolinker that regulates keratin and tubulin networks.[7,15] Single amino acid mutations in plectin are known to cause a number of diseases among them epidermolysis bullosa simplex (EBS) with muscular dystrophy.[15]

The target-response profiling network revealed several known protein interactors of plectin including receptors, keratins, and the associated signaling machinery (Figure 2B). Plectin was identified with high confidence as an interaction partner of plecstatin-3 (Figures 1C and 2E). Immortalized basal mouse keratinocytes isolated from wild-type ($plec^{+/+}$) or plectin-deficient ($plec^{-/-}$) mice[16] were then used to validate plectin as the actual target for plecstatins by immunofluorescence microscopy (Figure 3 and Figure S4). Treating $plec^{+/+}$ keratinocytes with plecstatin-2 induced an intermediate filament (IF) phenotype manifesting with enlarged network mesh sizes as is characteristic for $plec^{-/-}$ cells.[16b] At the same time, plecstatin-2 seemed to cause a concentration of IFs in the perinuclear regions of $plec^{+/+}$ cells, while no such effect was observed in $plec^{-/-}$ keratinocytes (Figure S4D). The cellular distribution of plectin is not altered upon treatment (Figure 3B) and neither is its abundance as determined in HCT116 cells by response profiling (Figures S3A,B). As clearly revealed by immunolabeling of the MT network, drug-treated $plec^{+/+}$ keratinocytes displayed a significantly smaller perimeter and appeared more rounded compared to control cells (Figure 3C).

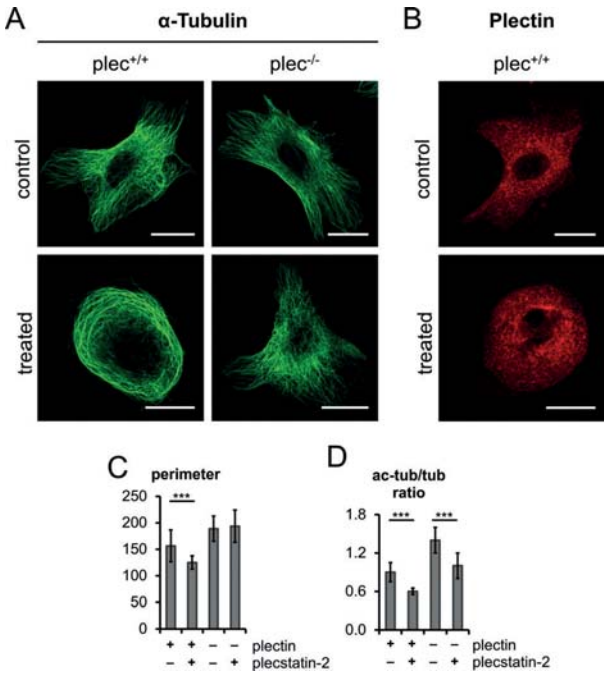

Figure 3. Plecstatin-2 affects cytoarchitecture and shape of keratinocytes by interacting with plectin. A,B) Wild-type ($plec^{+/+}$) or plectin-deficient ($plec^{-/-}$) keratinocytes were treated with half-IC_{50} of plecstatin-2 and analyzed by immunofluorescence microscopy using antibodies to proteins indicated. Scale bars = 20 μm. Diagrams showing average cellular perimeters (C) and acetylated/non-acetylated tubulin (pixel) ratios (D). Number of evaluated cells: $Plec^{+/+}$ control = 90; $Plec^{+/+}$ drug-treated = 104; $Plec^{-/-}$ control = 59; $Plec^{-/-}$ drug-treated = 51. *** p-value < 0.0001.

Another striking observation was that MTs no longer were oriented parallel to the long axis of cells but instead were forming a dense submembraneous network of curved MTs encircling the nucleus, which was observed in the majority (61%) of treated cells, but the nuclei remained intact (Figure S5A–C). $Plec^{-/-}$ keratinocytes did not display such effects upon drug treatment, underlining the necessity of plectin for these phenotypes to be observed. Another characteristic feature of plectin-deficient keratinocytes is the increased acetylation status of their cytoplasmic MTs (Figure 3D).[17] Interestingly, treatment with plecstatin-2 resulted in decreased MT-acetylation in both wild-type and plectin knockout cells (Figure 3D), consistent with the notion that through the drug treatment MTs become less stable and thus more dynamic.

Gene ontology (GO) term analysis of plecstatin-2 treated HCT116 cells from response profiling revealed a down-regulation of mitochondrial proteins (Table S3). Plectin deficiency was reported to affect mitochondria in several cell types.[18] Immunofluorescent staining of $plec^{+/+}$ keratinocytes for cytochrome C (Cyt-C) as a marker for mitochondria revealed that plecstatin-2 treatment did not elongate mitochondria as would be expected of plectin deficiency (Figure S5A–C), but altered their cellular distribution. In parallel, plecstatin-1 induced higher levels of reactive oxygen species (ROS, Figure 4A), while decreasing the mitochondrial membrane potential (MMP, Figure 4B).

Plectin deficiency inhibits migration and invasion in pancreatic,[19] urinary bladder,[20] and colon cancer cells[21] by down-regulating Src/RhoA/CDC42 signaling. In line with these reports, we found down-regulated RhoA signaling in HCT116 cells (i.e. ITGB4, CDC42 and ANK3, Figure 2B) in the response profiling experiment. This strongly supports the hypothesis that plectin-targeting results in reduced mobility and invasiveness of cancer cells. Indeed, an invasion assay using a matrigel-embedded multicellular HCT116 spheroid model showed partial reduction of invasion after plecstatin-2 treatment, which was characterized by a 46–62% lower increase in relative cross-sectional area over 96 h compared to controls (Figure 4C, Figure S6A). Additional interactions with extracellular matrix proteins may also contribute to this effect.[22]

Next, in vivo experiments were performed with a subcutaneously implanted murine colon carcinoma (CT-26) tumor model. Plecstatin-1 was well tolerated orally when applied at 30 mg kg^{-1} for two periods of five consecutive days, that is, at

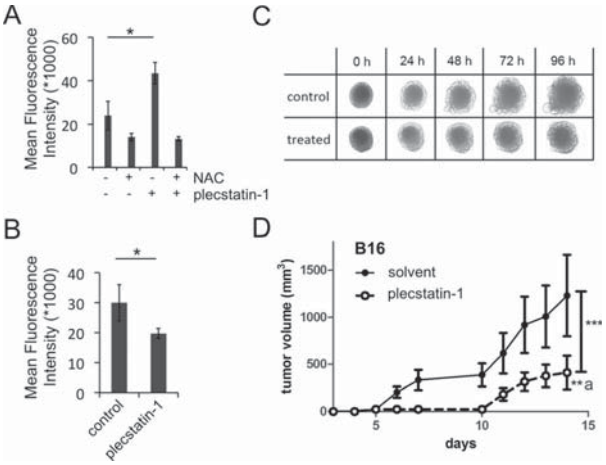

Figure 4. Plecstatins suppress cancer invasion and are tumor-inhibiting in vivo. MDA-MB-231 cells were treated with plecstatin-1 and investigated for A) induction of reactive oxygen species (ROS) and B) reduction of the mitochondrial membrane potential (MMP). * *P*-value <0.05 and NAC is N-acetylcysteine. C) HCT116 were treated in a spheroid invasion assay with plecstatin-2 for 96 h. D) Oral application of plecstatin-1 (30 mg kg^{-1}) effectively inhibits tumor growth in the invasive B16 melanoma tumor model. Doses at days 3–7 and 10–14. **a = $p<0.01$ by Bonferroni Post-test. *** = $p<0.001$ by two-way ANOVA.

days 3–7 and 10–14. With respect to tumor volume, plecstatin-1 showed a significant reduction on the last day.[23] Also, a significant reduction of tumor weight was determined compared to the control group (Figure S6B). Histological staining of the treated tumors did not reveal increased numbers of apoptotic or mitotic cells (Figure S6C). Finally, plecstatin-1 was analogously administered to B6 mice bearing an invasive B16 melanoma. The compound was again well tolerated orally and tumor growth was significantly inhibited (Figure 4D).

In summary, an integrated target-response profiling approach was employed and presented herein for the first time as a hypothesis-generating procedure to identify potential targets of metallodrugs with a labile metal–halido bond in a cellular setting. We found an unexpected selectivity of plecstatins for the structural protein plectin. Plectin-targeting caused the non-mitotic MT network to reorganize in a dense and curved submembraneous network encircling the nucleus, leading to a G0/G1 arrest. Plectin deficiency is responsible for reduced motility of cancer cells in several cancer types and the anti-invasive effect of plecstatin-2 was confirmed in a 3D tumor spheroid model. Plecstatin-1 showed anticancer activity against primary tumors in CT-26 colon and more so in the invasive B16 melanoma tumor model after oral administration. Thus, targeting plectin by plecstatins may be considered as a novel and promising anticancer strategy.

Acknowledgements

S.M.M. and C.G. thank Dieter Prinz of the FACS Core Unit at the St. Anna Kinderkrebsforschung for analyzing samples. G.W. is supported by the Austrian Science Research Fund (FWF, grant I1413-B09).

Conflict of interest

The authors declare no conflict of interest.

Keywords: anticancer agents · plectin · proteomics · ruthenium · target identification

How to cite: *Angew. Chem. Int. Ed.* **2017**, *56*, 8267–8271
Angew. Chem. **2017**, *129*, 8379–8383

[1] E. Meggers, *Curr. Opin. Chem. Biol.* **2007**, *11*, 287–292.
[2] Z. Adhireksan, G. E. Davey, P. Campomanes, M. Groessl, C. M. Clavel, H. Yu, A. A. Nazarov, C. H. Yeo, W. H. Ang, P. Droge, U. Rothlisberger, P. J. Dyson, C. A. Davey, *Nat. Commun.* **2014**, *5*, 3462.
[3] J. J. Soldevila-Barreda, I. Romero-Canelon, A. Habtemariam, P. J. Sadler, *Nat. Commun.* **2015**, *6*, 6582.
[4] S. M. Meier, M. Hanif, Z. Adhireksan, V. Pichler, M. Novak, E. Jirkovsky, M. A. Jakupec, V. B. Arion, C. A. Davey, B. K. Keppler, C. G. Hartinger, *Chem. Sci.* **2013**, *4*, 1837–1846.
[5] L. Hu, T. Cheng, B. He, L. Li, Y. Wang, Y. T. Lai, G. Jiang, H. Sun, *Angew. Chem. Int. Ed.* **2013**, *52*, 4916–4920; *Angew. Chem.* **2013**, *125*, 5016–5020.
[6] D. Hu, Y. Liu, Y. T. Lai, K. C. Tong, Y. M. Fung, C. N. Lok, C. M. Che, *Angew. Chem. Int. Ed.* **2016**, *55*, 1387–1391; *Angew. Chem.* **2016**, *128*, 1409–1413.
[7] G. Wiche, S. Osmanagic-Myers, M. J. Castanon, *Curr. Opin. Cell Biol.* **2015**, *32*, 21–29.
[8] R. H. Shoemaker, *Nat. Rev. Cancer* **2006**, *6*, 813–823.
[9] M. V. Babak, S. M. Meier, K. V. M. Huber, J. Reynisson, A. A. Legin, M. A. Jakupec, A. Roller, A. Stukalov, M. Gridling, K. L. Bennett, J. Colinge, W. Berger, P. J. Dyson, G. Superti-Furga, B. K. Keppler, C. G. Hartinger, *Chem. Sci.* **2015**, *6*, 2449–2456.
[10] J. Cox, M. Mann, *Nat. Biotechnol.* **2008**, *26*, 1367–1372.
[11] D. Mellacheruvu, Z. Wright, A. L. Couzens, J. P. Lambert, N. A. St-Denis, T. Li, Y. V. Miteva, S. Hauri, M. E. Sardiu, T. Y. Low, V. A. Halim, R. D. Bagshaw, N. C. Hubner, A. Al-Hakim, A. Bouchard, D. Faubert, D. Fermin, W. H. Dunham, M. Goudreault, Z. Y. Lin, B. G. Badillo, T. Pawson, D. Durocher, B. Coulombe, R. Aebersold, G. Superti-Furga, J. Colinge, A. J. Heck, H. Choi, M. Gstaiger, S. Mohammed, I. M. Cristea, K. L. Bennett, M. P. Washburn, B. Raught, R. M. Ewing, A. C. Gingras, A. I. Nesvizhskii, *Nat. Methods* **2013**, *10*, 730–736.
[12] D. Kreutz, A. Bileck, K. Plessl, D. Wolrab, M. Groessl, B. K. Keppler, S. M. Meier, C. Gerner, *Chem. Eur. J.* **2017**, *23*, 1881–1890.
[13] A. Franceschini, D. Szklarczyk, S. Frankild, M. Kuhn, M. Simonovic, A. Roth, J. Lin, P. Minguez, P. Bork, C. von Mering, L. J. Jensen, *Nucleic Acids Res.* **2013**, *41*, D808–D815.
[14] K. Kunimoto, Y. Yamazaki, T. Nishida, K. Shinohara, H. Ishikawa, T. Hasegawa, T. Okanoue, H. Hamada, T. Noda, A. Tamura, S. Tsukita, *Cell* **2012**, *148*, 189–200.
[15] L. Winter, G. Wiche, *Acta Neuropathol.* **2013**, *125*, 77–93.
[16] a) K. Andrä, I. Kornacker, A. Jörgl, M. Zörer, D. Spazierer, P. Fuchs, I. Fischer, G. Wiche, *J. Invest. Dermatol.* **2003**, *120*, 189–197; b) S. Osmanagic-Myers, M. Gregor, G. Walko, G. Burgstaller, S. Reipert, G. Wiche, *J. Cell Biol.* **2006**, *174*, 557–568.
[17] R. G. Valencia, G. Walko, L. Janda, J. Novacek, E. Mihailovska, S. Reipert, K. Andrä Marobela, G. Wiche, *Mol. Biol. Cell* **2013**, *24*, 768–784.

[18] a) L. Winter, C. Abrahamsberg, G. Wiche, *J. Cell Biol.* **2008**, *181*, 903 – 911; b) L. Winter, A. V. Kuznetsov, M. Grimm, A. Zeöld, I. Fischer, G. Wiche, *Hum. Mol. Genet.* **2015**, *24*, 4530 – 4544.
[19] S. J. Shin, J. A. Smith, G. A. Rezniczek, S. Pan, R. Chen, T. A. Brentnall, G. Wiche, K. A. Kelly, *Proc. Natl. Acad. Sci. USA* **2013**, *110*, 19414 – 19419.
[20] M. S. Yoneyama, S. Hatakeyama, T. Habuchi, T. Inoue, T. Nakamura, T. Funyu, G. Wiche, C. Ohyama, S. Tsuboi, *Eur. J. Cell Biol.* **2014**, *93*, 157 – 169.
[21] L. McInroy, A. Maatta, *Exp. Cell Res.* **2011**, *317*, 2468 – 2478.
[22] a) J. A. Miyake, M. Benadiba, G. Ribeiro, D. E. O. S. D, A. Colquhoun, *Anticancer Res.* **2014**, *34*, 1901 – 1911; b) A. Levina, A. Mitra, P. A. Lay, *Metallomics* **2009**, *1*, 458 – 470.
[23] M. H. M. Klose, M. Hejl, P. Heffeter, M. A. Jakupec, S. M. Meier, W. Berger, B. K. Keppler, **2016**, https://doi.org/10.1039/C7AN00350A.

Manuscript received: March 1, 2017
Version of record online: May 26, 2017

Angewandte Chemie
Eine Zeitschrift der Gesellschaft Deutscher Chemiker

Supporting Information

An Organoruthenium Anticancer Agent Shows Unexpected Target Selectivity For Plectin

Samuel M. Meier, Dominique Kreutz, Lilli Winter, Matthias H. M. Klose, Klaudia Cseh, Tamara Weiss, Andrea Bileck, Beatrix Alte, Johanna C. Mader, Samir Jana, Annesha Chatterjee, Arindam Bhattacharyya, Michaela Hejl, Michael A. Jakupec, Petra Heffeter, Walter Berger, Christian G. Hartinger, Bernhard K. Keppler, Gerhard Wiche, and Christopher Gerner**

anie_201702242_sm_miscellaneous_information.pdf

Supporting Information

Table of Contents

Experimental Procedures

Instrumentation

All ^{1}H and $^{13}C\{^{1}H\}$ NMR spectra were recorded at 25 °C on a Bruker FT NMR spectrometer Avance III 500 MHz or on a Bruker DRX 400 MHz spectrometer. Protons were numbered according to literature.[1] Elemental analysis was carried out on a Perkin–Elmer 2400 CHNS Elemental Analyzer by the Microanalytical Laboratorys, Faculty of Chemistry, University of Vienna. ESI mass spectra were recorded on a Bruker AmaZon SL ion trap mass spectrometer (Bruker Daltonics GmbH, Bremen, Germany) by direct infusion at a flow rate of 5 µL/min. The following parameters were employed: capillary –4.5 kV, gas flow 8 psi, dry gas 6 L/min, dry temperature 180 °C, end plate offset –500 V, trap drive 64.8 and RF 77%. High resolution mass spectra were recorded on a Maxis UHR ESI time-of-flight mass spectrometer (Bruker Daltonics, Bremen, Germany) employing the following parameters: capillary –4.5 kV, nebulizer 0.4 bar, dry gas 8 L/min, dry temperature 180 °C, 400 Vpp funnel RF, 4 eV quadrupole ion energy and 110 µs transfer time. Samples were diluted with MeOH and injected by direct infusion into the mass spectrometer at a flow rate of 3 µL/min. Generally, spectra were recorded in positive ion mode over 0.5 min and averaged. The Data Analysis 4.0 software package (Bruker Daltonics, Bremen, Germany) was used for processing.

Materials

All reactions were carried out in dry solvents under an inert atmosphere. Chemicals obtained from commercial suppliers were used as received and were of analytical grade. Methanol (HPLC grade) was obtained from Fisher, DMF (extra dry) from Acros, triethylamine from Sigma. Biotin-dPEG4-NHS was obtained from Iris Biotech GmbH.
The precursors $[Ru(\eta^6\text{-benzylammonium})Cl_2]_2Cl_2$,[2] $[Ru(\eta^6\text{-toluene})Cl_2]_2Cl_2$,[3] *N*-(4-fluorophenyl)-2-pyridinecarbothioamide[4] and the compound [chlorido(η^6-p-cymene)(*N*-(4-fluorophenyl)-2-pyridinecarbothioamide)Ru(II)] chloride (plecstatin-1)[1] were prepared following literature procedures.

Synthesis

[Chlorido(η^6-toluene)(*N*-(4-fluorophenyl)-2-pyridinecarbothioamide)ruthenium(II)] chloride (**plecstatin-2**)**.** The previously published method was followed.[1] N-(4-fluorophenyl)-2-pyridinecarbothioamide (75.6 mg, 0.33 mmol) was dissolved in MeOH (10 mL) under argon and was stirred until a clear solution was obtained. $[Ru(\eta^6\text{-toluene})Cl_2]_2Cl_2$ (86 mg, 0.16 mmol) was suspended in MeOH (5 mL) and was added under argon. The reaction mixture was stirred for 19 h at room temperature in the dark. After several minutes, the suspension turned deep red. The reaction mixture was dried, redissolved in dichloromethane (10 mL) and filtered. Hexane (20 mL) was added for precipitation at 4 °C. Red crystals formed that were filtered, washed with hexane and dried. Yield: 140 mg (86%). Elemental analysis found: C, 43.28; H, 3.44; N, 5.22; S, 6.04, calculated for $C_{19}H_{17}Cl_2FN_2RuS{\cdot}0.5CH_2Cl_2$: C, 43.46; H, 3.37; N, 5.20; S, 5.95. MS (ESI^+): *m/z* 424.99 $[M - HCl]^+$ (m_{theor} = 425.01). ^{1}H NMR (500.1 MHz, d_4-MeOD, 25 °C): δ = 9.72 (d, $^{3}J_{(H1,H2)}$ = 5 Hz, 1H, H-1), 8.43 (d, $^{3}J_{(H3,H4)}$ = 8 Hz, 1H, H-4), 8.31 (t, $^{3}J_{(H2,H3)/(H3,H4)}$ = 8 Hz, 1H, H-3), 7.85 (t, $^{3}J_{(H1,H2)/(H2,H3)}$ = 6.5 Hz, 1H, H-2), 7.66 (m, 2H, H-9/H-11), 7.35 (t, $^{3}J_{(H7,H8)/(H11,H12)}$ = 8 Hz, 2H, H-8/H-12), 6.12 (t, $^{3}J_{(H14,H15)/(H15,H16)}$ = 6 Hz, 1H, H-15), 6.10 (t, $^{3}J_{(H16,H17)/(H17,H18)}$ = 6 Hz, 1H, H-17), 5.95 (d, $^{3}J_{(H17,H18)}$ = 6 Hz, 1H, H-18), 5.81 (t, $^{3}J_{(H15,H16)/(H16,H17)}$ = 6 Hz, 1H, H-16), 5.62 (d, $^{3}J_{(H14,H15)}$ = 6 Hz, 1H, H-14), 2.29 (s, 3H, H-19) ppm. $^{13}C\{^{1}H\}$ NMR (125.8 MHz, d_4-MeOD, 25 °C): δ = 164.12 (C-10), 160.33 (C-1), 155.46 (C-5), 141.15 (C-3), 135.52 (C-7), 130.77 (C-2), 128.88 (C-9/C-11), 125.01 (C-4), 117.75 (C-8/C-12), 107.78 (C-13), 92.77 (C-15), 90.89 (C-17), 88.14 (C-18), 83.84 (C-16), 83.78 (C-14), 19.45 (C-19) ppm.
[Chlorido(η^6-benzylammonium)(*N*-(4-fluorophenyl)-2-pyridinecarbothioamide) ruthenium(II)] dichloride (**R1**)**.** The previously published method was followed.[1] N-(4-fluorophenyl)-2-pyridinecarbothioamide (38 mg, 0.17 mmol) was dissolved in DMF (2 mL) under argon and was stirred until a clear solution was obtained. $[Ru(\eta^6\text{-benzylammonium})Cl_2]_2Cl_2$ (52 mg, 0.09 mmol) was suspended in DMF (1 mL) and was added under argon. The reaction mixture was stirred for 19 h at room temperature in the dark. A clear and dark yellow solution formed. Chloroform (20 mL) was added and then cooled to 4 °C. The brown precipitate was filtered under argon because the product is moisture sensitive and dried *in vacuo*. Yield: 50 mg (56%). Elemental analysis found: C, 39.74; H, 3.63; N, 7.67; S, 5.60, calculated for $C_{19}H_{19}Cl_3FN_3RuS{\cdot}1.5H_2O$: C, 39.70; H, 3.86; N, 7.31; S, 5.58. MS (ESI^+): *m/z* 476.00 $[M - HCl]^+$ (m_{theor} = 475.99), *m/z* 440.03 $[M - 2HCl]^+$ (m_{theor} = 440.02). ^{1}H NMR (500.1 MHz, d_4-MeOD, 25 °C): δ = 9.78 (d, $^{3}J_{(H1,H2)}$ = 6 Hz, 1H, H-1), 8.48

(d, $^3J_{(H3,H4)}$ = 8 Hz, 1H, H-4), 8.35 (t, $^3J_{(H2,H3)/(H3,H4)}$ = 8 Hz, 1H, H-3), 7.89 (t, $^3J_{(H1,H2)/(H2,H3)}$ = 6.5 Hz, 1H, H-2), 7.65 (m, 2H, H-9/H-11), 7.36 (t, $^3J_{(H7,H8)/(H11,H12)}$ = 9 Hz, 2H, H-8/H-12), 6.44 (d, $^3J_{(H14,H15)}$ = 5 Hz, 1H, H-14), 6.34 (t, $^3J_{(H16,H17)/(H17,H18)}$ = 6 Hz, 1H, H-17), 6.17 (t, $^3J_{(H15,H16)/(H16,H17)}$ = 6 Hz, 1H, H-16), 5.95 (d, $^3J_{(H17,H18)}$ = 6 Hz, 1H, H-18), 5.94 (t, $^3J_{(H14,H15)/(H15,H16)}$ = 6 Hz, 1H, H-15), 4.17 (q, $^3J_{(H19,NH)}$ = 14 Hz, 2H, H-19) ppm. $^{13}C\{^1H\}$NMR (125.8 MHz, d_4-MeOD, 25 °C): δ = 162.20 (C-10), 160.75 (C-1), 155.10 (C-5), 141.79 (C-3), 135.57 (C-7), 131.15 (C-2), 128.82 (C-9/C-11), 125.69 (C-4), 118.04 (C-8/C-12),93.20 (C-14), 92.33 (C-17), 89.96 (C-16), 86.42 (C-15), 84.40 (C-18), 43.17 (C-19) ppm.

[Chlorido(biotin-dPEG(4)-amido-η^6-benzyl)(*N*-(4-fluorophenyl)-2-pyridinecarbothioamide) ruthenium(II)] chloride (**plecstatin-3**)**.** The precursor **R1** (2.74 mg, 0.005 mmol) was dissolved in DMF (0.12 mL) and biotin-dPEG(4)-NHS (2.95 mg, 0.005 mmol) dissolved in DMF (0.12 mL) was added. Triethylamine (10 µL) was added and the flask was purged with argon and stirred for 1 h. The *in situ* generated plecstatin-3 was directly immobilized on the streptavidin beads. HR-MS (ESI$^+$): 913.2400 ([M – HCl]$^+$, m_{ex} = 913.2370, 3 ppm), 468.1139 ([M – HCl + Na]$^{2+}$, m_{ex} = 468.1131, 2 ppm).

DNA Interaction Studies

The structural modification of DNA by plecstatin-1 was tested by agarose gel electrophoresis with the plasmid pBR322. TAE (1x) buffer was employed as incubation medium. Stock solutions of 1 mM of plecstatin-1 was prepared in TAE (1x) buffer, diluted with TAE (1x) buffer and stored at -20 °C. The plasmid pBR322 was diluted with TAE (1x) buffer, as well. Incubation mixtures were prepared to yield r_b-values corresponding 0.5 (64 µM compound) and 5.0 (642 µM compound). The agarose gels consisted of 1% agarose in TAE (1×) buffer and the incubation mixtures were subject to 2 h running time at 100 V and 70 mA in a PerfectBlue™ Mini S (PEQLAB) GE chamber. The DNA bands were stained with ethidium bromide (1 µl/mL) and were processed and analyzed with the gel documentation system GenoView UV-source and GenoSoft Version 3.08 C (VWR).

$Na_2EDTA\cdot$(p.a., Fisher Scientific), NaOH (Fluka), tris(hydroxymethyl)aminoethane, glacial acetic acid (p.a., Acros) and MilliQ H_2O (18.2 MΩ, Synergy 185 UV Ultrapure, Millipore, France) were used for the preparation of the TAE buffer. Loading buffer (6x), pBR322 DNA (0.5 µg/µL) and GeneRuler™ 1kb DNA ladder (0.5 µg/µL) were obtained from Fermentas.

Cell Accumulation Experiments

Cell accumulation experiments were performed with the SW480 cell line obtained from ATCC.[5] The cell line was kindly provided by Brigitte Marian, Institute of Cancer Research, Department of Medicine I, Medical University of Vienna. All cell culture media and supplements were purchased from Sigma-Aldrich unless noted otherwise, and plasticware from StarLab. Cells were grown as adherent monolayer cultures in 75 cm^2 culture flasks in Minimal Essential Medium (MEM) supplemented with 10% heat-inactivated fetal bovine serum (Invitrogen), 1 mM sodium pyruvate, 1% *v*/v non-essential amino acids and 4 mM l-glutamine but without antibiotics at 37 °C under a moist atmosphere containing 5% CO_2 and 95% air. For accumulation studies, cells were seeded into 12-well plates in densities of $1.8\cdot10^5$ cells per well in aliquots of 1 mL complete culture medium. For all experiments, samples and corresponding adsorption/desorption controls were located on the same plate; and for determination of the cell number, three wells of a separate plate were seeded in the same manner. Plates were kept at 37 °C for 24 h. Plecstatin-1 was dissolved in complete culture medium and added to the wells (after removal of the medium used for seeding of the cells) in volumes of 2 mL to a final concentrations of 50 µM. During drug exposure (2 h at 37 °C), the cell number in three wells of a parallel plate was determined by trypsinization and counting in a hemocytometer. After exposure, the medium was removed and the cells were washed three times with phosphate buffered saline (PBS).

The cells were then lyzed with 0.4 mL HNO_3 per well for 1 h at room temperature. Aliquots of 400 µL were then diluted to a total volume of 8 mL.

Cytotoxicity Assay

The human HCT116 colon cancer cell line was propagated in 25 cm^2 culture flasks (StarLab) as adherent monolayer cultures in RPMI 1640 medium (Sigma Aldrich) supplemented with 10% heat-inactivated fetal bovine serum (FBS) (Thermo Fisher) and 1 mM sodium pyruvate (Sigma Aldrich) at 37 °C in a humidified atmosphere with 5% CO_2. Cytotoxicity was determined by the Alamar Blue Assay (AB assay; AB = resazurin sodium salt, Sigma Aldrich). For this purpose, cells were harvested from culture flasks by trypsinization and seeded in RPMI 1640 medium into 96-well plates (for monolayers: CytoOne, StarLab; for spheroids: Nunclon Sphera, VWR) in cell densities of $1.5\cdot10^3$ (for monolayers) and $3\cdot10^3$ (for spheroids) cells per well. In case of monolayer culture, cells were allowed for 24 h to settle and resume exponential growth. Spheroids were grown for 7 days to the required diameter. Both monolayers and spheroids were then treated with the test compound dissolved in DMSO to a stock concentration of 80 mM and serially diluted in RPMI 1640 medium. The final concentration of DMSO never exceeded 1%. One hundred microliter of dilution were added to each well, and plates were incubated for 96 h at 37 °C and 5% CO_2. A fresh AB solution of 440 µM (≈ 110 µg/mL) in PBS (Sigma Aldrich) was prepared and 20 µL of AB solution were added to every well for the last 4 h (for monolayers) or 24 h (for spheroids) of drug exposure. Fluorescence (ex. 530/35 nm, em. 620/40 nm) was measured using a microplate reader (Synergy HT, BioTek). The IC_{50} values (concentrations resulting in 50% viable cells compared to untreated controls) were interpolated, and a subcytotoxic concentration for use in the spheroid invasion assay was inferred from the concentration-effect curve.

Metal Quantification by Inductively-Coupled Plasma Mass Spectrometry (ICP-MS)

The ICP-MS measurements were carried out with an *Agilent 7500ce* mass spectrometer (Agilent Technologies, Waldbronn, Germany), which was equipped with a CETAC ASX-520 autosampler (Nebraska, USA) and a MicroMist nebulizer at a sample uptake rate of approx. 0.25 mL/min. The Agilent MassHunter software package (Workstation Software, version B.01.01, Build 123.11, Patch 4, 2012) was used for data processing. The experimental parameters for ICP-MS are summarized in Table S1.

Table S1. ICP MS parameter.

	ICP-MS Agilent 7500ce
RF power (W)	1560
Cone material	Nickel
Carrier gas (L/min)	0.92 – 0.97
Make up gas (L/min)	0.22 – 0.27
Plasma gas (L/min)	15
Monitored isotopes	^{101}Ru, ^{102}Ru, ^{115}In, ^{185}Re, ^{195}Pt
Dwell time (s)	0.3
Number of replicates	10
Number of sweeps	100

Cell Cycle Analysis

The cell cycle distribution of untreated and treated HCT-116 cells was analysed with a CycleTEST PLUS DNA reagent kit (Becton Dickinson Immunocytometry Systems) and flow cytometry (FACS) and the manual of the manufacturer for cell suspensions was followed. In brief, HCT-116 cells were grown similarly as mentioned above in T25 flasks to ~80% confluency. Then, the medium was renewed either without or with plecstatin-2 (4 and 16 µM). The cells were incubated for 24 h at 37 °C in a humidified atmosphere containing 5% carbon dioxide, trypsinized and the suspension transferred into a 15 mL Falcon tube. After centrifugation (300 g, 24 °C, 5 min), the supernatant was removed and washed with 1 mL buffer solution and gently vortexed (sodium citrate, sucrose and DMSO). This step was performed three times. The cells were counted and adjusted to $1x10^6$ cells/mL in PBS and directly stained. For this purpose, the cell suspensions were centrifuged (400 g, 24 °C, 5 min) and the supernatant was decanted. Trypsin buffer was added and gently mixed. The mixture was incubated for 10 min at room temperature. Then, the trypsin inhibitor and RNase buffer was added and gently mixed. The mixture was again incubated for 10 min at room temperature. Finally, cold propidium iodide staining solution was added and incubated for 10 min in the dark on ice. The samples were filtered into 12 × 75-mm FACS-tubes and analysed by flow cytometry. Each condition was run in triplicate.

Preparation Target Profiling

HCT116 cells (purchased from the ATCC, passage 7–24) were cultivated to approximately 10^8 cells per flask for pull-down experiments using McCoy's 5A modified medium (Gibco, Life Technologies, with l-glutamine), supplemented with penicillin, streptamycin and 10% heat-inactivated fetal-calf serum. The cells were washed and pelleted by centrifugation (2300 g, 4 °C, 5 min). Cell pellets were suspended in non-denaturing lysis buffer (1.5 mL) and homogenized by passing through a gauge syringe twenty times. The lysis buffer consisted of NaCl 100 mM, Tris HCl 50 mM, $MgCl_2$ (1.5 mM), NaF (25 mM), NP-40 0.2%, glycerol 5%, DDM 0.2%, TLCK 10 µg/mL, DTT 1 mM, Na_3VO_4 (1 mM), PMSF (1 mM) and pepstatin/leupeptin/aprotinin each 1 µg/mL, at pH 7.4. The suspension was centrifuged (3500 rpm, 5 min, 4 °C) and the supernatant was collected yielding a soluble protein amount of at least 15 mg/sample. In normal pull-downs, the HCT116 whole cell lysate was directly exposed to the immobilized plecstatin-3, whereas the lysate was pre-incubated for 1 h with free drug 2 (20 µM in DMF) for competitive pull-downs.

Pierce Streptavidin UltraLink resins were washed with lysis buffer. The biotin conjugate plecstatin-3 was added and was incubated for 30 min. After washing with lysis buffer, HCT116 whole cell lysate (1.5 mL) was added and incubated independently for 2, 4 or 19 h, respectively. The beads were then transferred into spin columns (MobiSpin Column "F", Mobitec) and washed with lysis buffer and HEPES buffer (pH 8, HEPES-NaOH 50 mM, EDTA 0.5 mM, including PMSF 1 mM, TLCK 10 µg/mL and pepstatin/leupeptin/aprotinin each 1 µg/mL). Proteins were eluted with 250 µL elution buffer (formic acid 50%, urea 2 M) and stored at –20 °C.

Preparation Response Profiling

HCT116 cells were grown in mono-layer culture (T25 flask, $6{\cdot}10^6$ cells and passages 9–31) in McCoy's 5A modified medium (Gibco, Life Technologies, with l-glutamine and serum-free) and supplemented with penicillin, streptomycin and 10% heat-inactivated fetal-calf serum to ~80% confluency. The medium was renewed either without or with compound plecstatin-2 at 4 or 16 µM, respectively, and the cells were incubated for 24 h at 37 °C in a humidified atmosphere containing 5% carbon dioxide.

The cells were separated into cytoplasmic and a nuclear fractions. Cells were lysed. Cytoplasmic proteins were collected and precipitated overnight. The pellet containing the nuclei was swelled in hypertonic solution, diluted 10-fold with NP-40 and after centrifugation, the soluble nuclear proteins were collected and precipitated overnight. The samples were dried and dissolved in sample buffer.

In-Solution Digestion of Proteins

Samples (25 µg protein) were loaded onto molecular weight cut-off filters. The acidic samples of the affinity purification experiments (30 µg protein) were neutralized with ammonium bicarbonate (pH 8). Proteins were reduced with dithiothreitol at 37 °C and alkylated with iodacetamide. Then, proteins were digested with trypsin/LysC and the peptides were collected, purified over C18 spin columns (in the case of proteome profiling samples) and dried.

Hyphenated Mass Spectrometry

Mass Spectrometry. Samples were analysed on a nLC-MS setup consisting of a Dionex 3000 nano-LC hyphenated to a QExactive Orbitrap equipped with a nanoESI source (ThermoFisher Scientific). The instrument was operated with Q Exactive software version 2.3 SP1, build 1788. Experiments were analyzed with Thermo Scientific Qual Browser and Thermo Xcalibur 3.0.63. The instrument was operated in positive ion mode using 2.2 kV ESI+, 300 °C capillary temperature, no sheath/auxiliary/spare gas, maximum spray current 50 nA, probe heater 350 °C, RF-Level 50 and an NSI ion source. A Top12 (response profiling) or Top6 (target proifling) method was used with the following parameters for full MS (0 eV *in source* dissociation, 2 default charge state, 70'000 resolution, AGC target 1e6, 20 ms max. accumulation time in the IT) and fragment MS (AGC target 5e4, Isolation 1 *m/z*, HCD 30% NCE, Intensity threshold 6.7e2, Apex trigger 6–20 s, charge exclusion: 1 and >5, dynamic exclusion 30 s, 250 ms fill time). The resolution was 17'500 at *m/z* = 200.

Chromatrography. The chromatographic separations were conducted using eluents A (water : acetonitrile : formic acid, 98 : 2 : 0.1) and B (water : acetonitrile : formic acid, 80 : 20 : 0.1). Each dried sample was reconstituted with 10 fmol synthetic peptide standard (in 30% FA, 5 µL) and with eluent A (40 µL) and the injection volume was 5 µL. Chromatographic separation was performed with a Pepmap100 precolumn (2 cm x 75 µm, C18, Thermo Fisher Scientific) and Pepmap100 analytical column (50 cm x 75 µm, C18, Thermo Fisher Scientific). For the target proifling, the chromatographic method consisted of a 38 min stepped gradient from 7–35% B and a 85 min total run time. A gradient from 8–40% B over 120 min was used for the cytoplasmic and nuclear fractions of the response profiling experiments.

Protein Identification and Enrichment Analysis

Proteins were searched with MaxQuant (version 1.5.2.8) including the Andromeda search engine for label-free quantification of cytoplasmic fractions, nuclear fractions and affinity pull-down samples. We allowed a maximum of two missed cleavages and at least one (plectin isoforms) or two (rest) unambiguous peptide for identifications. The first search peptide tolerance was 20 ppm and the main search tolerance was set to 5 ppm for this Orbitrap instrument type. Protein and peptide false-discovery rate (FDR) was set to 0.01. We included N-terminal acetylation and methionine oxidation as variable modifications and cysteine carbamidomethylation as a fixed modification. The minimum score was set to 40. Proteins were searched against the human UniProtKB/SwissProt database. Protein isoforms were usually combined into protein groups, except for plectin isoform searches. Data sets were analyzed with Perseus (Version 1.5.1.6). After log(2) transformation of the LFQ-values, rows were filtered based on valid values with a minimum number of 6 values in at least one group. Additional searches were performed using Proteome Discoverer (1.4.0.288) with Mascot and a Mascot Significance Threshold of 0.01 on the peptide level. Here, all proteins were included with >2 peptides and PSMs (peptide-spectrum matches) and a score of >30.

Gene ontology (GO) term analysis was performed with DAVID[6] against the human gene background. The confidence of enrichment of a term is expressed by a Q-value, which is a multiple testing-corrected P-value according to Benjamini-Hochberg.

The bubble plot contains four dimensions. The y-axis represents the enrichment of a protein and is calculated as the ratio of the LFQ-areas of a given protein (two biological and two technical replicas) in the normal pull-down with respect to the competitive pull-down. The x-axis denotes the confidence of the enrichment and is obtained by a p-value of the mentioned LFQ-areas. The size of the bubbles represents the intensity in the mass spectrometric analysis. Finally, the colour represents the specific binding probability (P) and is a measure of specificity of a given protein to bind to the small molecule probe. It is obtained via the CRAPome database[7] and is calculated as follows:

$$P = 1 - (\text{CRAPome N° of samples containing the protein})/(\text{CRAPome total N° of samples}) \cdot (\text{CRAPome average SC})/(\text{Average SC of Pull Down})$$

SC denotes spectral counts. The total number (N°) of samples in the CRAPome database was 411.

Immunofluorescence Staining Procedures and Confocal Microscopy

HCT116 cells were seeded into 8-well chamber slides (SPL) in Opti-MEM medium. When cells reached about 60-70% confluence, they were treated with 16 µM of plecstatin-2 for 24 h. Thereafter, cells were washed with 1x PBS and fixed with Roti-Histofix 4% (ROTH) at 4°C for 15 min, washed twice with 1x PBS and stored in 1x PBS at 4 °C for up to one week. For permeabilization and blocking, cells were treated with 1x PBS + 0.3% TritonX-100 + 5% goat serum for 10 min at RT. Subsequently, cells were incubated with 1st antibodies, either MsαHu-Cytokeratin 8/18 (Thermo Scientific) diluted 1:100 or MsαHu-mitochondria (MTC02) (abcam) diluted 1:100 in 1x PBS + 1% BSA + 1% serum + 0.1% TritonX-100 overnight at 4°C. The next day, cells were washed twice with 1x PBS and incubated with secondary antibody GtαMs-AF594 (Life Technologies) diluted 1:400 in 1x PBS + 2% BSA + 1% goat serum + 0.1% TritonX-100 for 1 h at RT. After washing twice with 1x PBS, cells were incubated with 2 µg/ml DAPI in 1x PBS for 2 min at RT, washed twice with 1x PBS and embedded in Fluoromount-G mounting medium (SouthernBiotech). Images of immunolabeled HCT116 cells were acquired with a confocal laser scanning microscope (LEICA, TCS SP8X) using the Leica LAS AF software. Images are depicted as maximum projection of total z-stacks and brightness and contrast were adjusted in a homogenous manner using Leica LAS AF.

Mouse keratinocytes expressing plec$^{+/+}$/p53$^{-/-}$ or plec$^{-/-}$/p53$^{-/-}$ were cultured in KGM medium (KGM-2 BulletKit w/o Ca^{2+}, Lonza) supplemented with ITS supplement (Sigma) and Ca^{2+}-free FCS. The cells were grown on collagen-1 and finally split in 24 wells on coverslips. They were rinsed and fixed with 2.5% PFA, quenched with 0.1 M glycine, permeabilized with 0.1% Triton X-100 and blocked with 5% BSA in PBS for 1 h at room temperature. Then, the cells were immunolabeled with primary antibodies in PBS for 1.5–3.5 h at room temperature. The following primary antibodies were used for immunofluorescence microscopy: guineapig antiserum to plectin (GP21, Progen), rat monoclonal antibodies (mAbs) to α-tubulin (clone YL1/2, SM2202P, Acris), mouse mAbs to

acetylated tubulin (clone 6-11B-1, T6793, Sigma-Aldrich), mouse mAbs to cytochrome C (BD Pharmingen, #556432), rabbit AS to keratin 5 (Covance, PRB-160P). The cells were then washed with PBS. Primary antibodies were used in combination with donkey anti-guineapig biotin/streptavidin rhodamine red, goat anti-rat IgG Alexa 488, goat anti-mouse IgG Cy5, and goat anti-rabbit IgG Cy5 (all from Jackson ImmunoResearch Laboratories). After incubating for 1 h and washing, the cells were stained with DAPI, washed with deionized water and mounted in mowiol 4-88 onto microscope slides (Wenzel, SuperFrost). Images of immunolabeled cells were acquired at room temperature with a confocal microscope (Zeiss, LSM 510) using the LSM 510 module in the LSM software.

Invasion Assay

Multicellular spheroids from HCT116 cells were grown for 7 days in RPMI 1640 medium in 96-well plates (Nunclon Sphera, Thermo Fisher) and their size was measured with an inverted microscope (Olympus CKX41, 4× objective) and Cell^F software. Spheroids of well comparable size (diameter: ca. 500–600 µm; matched pairs with differences in max. diameter <25 µm within each pair) were selected for the spheroid invasion assay. Growth factor reduced Matrigel (Becton Dickinson) was diluted to a final concentration of 300 µg/mL with or without plecstatin-2. One hundred fifty microliter of these solutions were added to the wells containing spheroids in 50 µL medium. The plate was incubated in a humidified atmosphere with 5% CO_2 in air at 37 °C. Both untreated and treated spheroids were monitored simultaneously with a JuliBr live cell analyzer (NanoEntek) for 96 h.

In vivo Experiments

Six- to eight-week-old female Balb/c (for CT-26) and C57/B6JRj (for B16) mice were kept in a pathogen-free environment and every procedure was performed in a laminar airflow cabinet. Experiments were carried out according to the Austrian and FELASA guidelines (BMWF-66.009/0084-II/3b/2013) for animal care and protection.

CT-26 cells ($5x10^5$ cells) and B16 ($1x10^5$ cells) were injected (in serum-free medium) subcutaneously into the right flank. Therapy was started when tumour nodules were palpable. Animals were treated orally with plecstatin-1 for twice 5 consecutive days (days 3–7 and days 9–14) at a dose of 30 mg/kg. Before administration, plecstatin-1 was dissolved in 10% DMSO. Animals were controlled for distress development every day and tumour size was assessed regularly by calliper measurement and tumour volume was calculated using the formula (length x $(width)^2$)/2. On day 14, (24 h after the last treatment) animals were anesthetized and tissue samples were collected. Samples were stored at –20°C.

Determination of Reactive Oxygen Species (ROS)

MDA-MB-231 cells were seeded in 12-well plates at a density of 2.5 x 10^5 cells per well. The cells were treated with plecstatin-1 (20 µM = IC_{50}) with or without N-acetyl cysteine (NAC) for 48 h. After trypsination, the cells were washed with PBS and incubated for 45 min with DCFDA (5 µM) at 37 °C. Fluorescence was then determined by flow cytometry using the FL-1 filter.

Determination of Mitochondrial Membrane Potential (MMP)

MDA-MB-231 cells were seeded in 12-well plates at 2.5 x 10^5 cells/well. The cells were then treated with plecstatin-1 (20 µM = IC_{50}) for 48 h. After trypsination, the cells were washed with PBS and incubated for 45 min with $DiOC_6$ (50 nM) at 37 °C. Fluorescence was then determined by flow cytometry using the FL-1 filter.

Statistical Calculations

Target profiling was performed in biological duplicates and each in technical duplicates. Response profiling was performed in biological triplicates and each in technical duplicates. Cell experiments were done at least in biological triplicates. A two-sided student t-test was calculated and deemed significant if $p < 0.05$. Proteomic experiments were additionally corrected by a permutation-based false-discovery rate (FDR = 0.05, 250 permutations) and S0 = 0.5 (hyperbolic conversion). A significant protein regulation is obtained when the permutation-based multi-parameter corrected P-value of the LFQ-intensities of a given protein between treated and untreated samples is <0.05. Animal experiments were performed with 4 animals in each group. Significances were calculated by one-way ANOVA with Dunett posttest, two-way ANOVA and Bonferroni post-test. ROS and MMP experiments were repeated at least three times. All data are presented as mean ± standard deviation (SD). Significance was calculated by a two-sided t-test with unequal variance and a P value < 0.05 was considered as statistically significant.

Results and Discussion

A

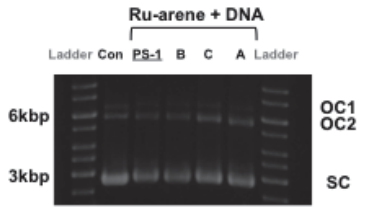

B

	Metal	GI50 (μM)	LC50 (μM)	NSC N°
plecstatin-1	Ru(II)	4.5	62	776415
KP1019	Ru(III)	56	>100	666158
Cisplatin	Pt(II)	15	92	119875

C

	Cellular Accumulation in SW480 (fg/cell)
plecstatin-1	160 (RSD 36%)
satraplatin	129 (RSD 13%)
KP1019	31 (RSD 13%)

D

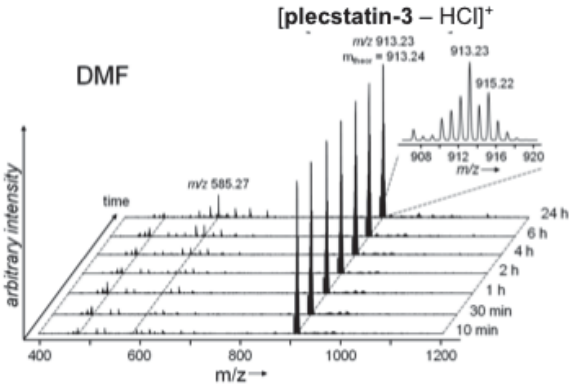

E

	IC50 (μM)			
	CH1 (PA1)	SW480	A549	HCT116
plecstatin-1	4 ± 1	4 ± 1	14 ± 2	10 ± 3
plecstatin-2	18 ± 3	11 ± 1	95 ± 8	29 ± 4

Figure S1. (**A**) DNA interaction studies of plecstatin-1 with pBR322 plasmids. The complex was incubated for 24 h with the plasmid at r_b = 5 and did not result in electrophoretic shifts compared to the control. The experiment was performed with other metal arene 2-pyridinecarbothioamide analogues, namely *N*-phenyl- (A), *N*-4-hydroxyphenyl- (B) and *N*-4-morpholinophenyl-2-pyridinecarbothioamide (C). OC1 and OC2 are nicked circular plasmid and SC is supercoiled plasmid. (**B**) Results of the NCI-60 screen in comparison to KP1019 and cisplatin. Average GI50 (growth inhibition of 50%) and LC50 (lethal concentraction of 50%) are given in μM concentrations. (**C**) Cellular accumulation of plecstatin-1, satraplatin and KP1019[8] in SW480 colon carcinoma cells as determined by inductively-coupled plasma mass spectrometry (ICP-MS). The cells were treated with 50 μM of the respective compounds for 2 h. (**D**) The reaction of P1 with biotin-dPEG(4)-NHS and supplemental triethylamine was monitored in DMF. (**E**) Comparison of the antiproliferative activity as IC_{50}'s (μM) of plecstatin-1 and plecstatin-2 in four cancer cell lines determined by the MTT assay. With the exception of the multidrug-resistant A549, plecstatin-2 is approximately 3-fold less active compared to plecstatin-1 underlining the assumption that both compounds follow a similar mechanism of action.

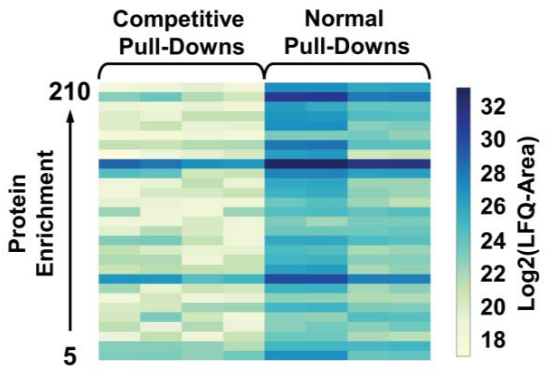

Figure S2. Heat map showing the LFQ-area of each experiment including the biological and technical replicates. Each row represents a protein and the enrichment increases form bottom (5-fold) to top (210-fold). The colour represents the LFQ-intensity.

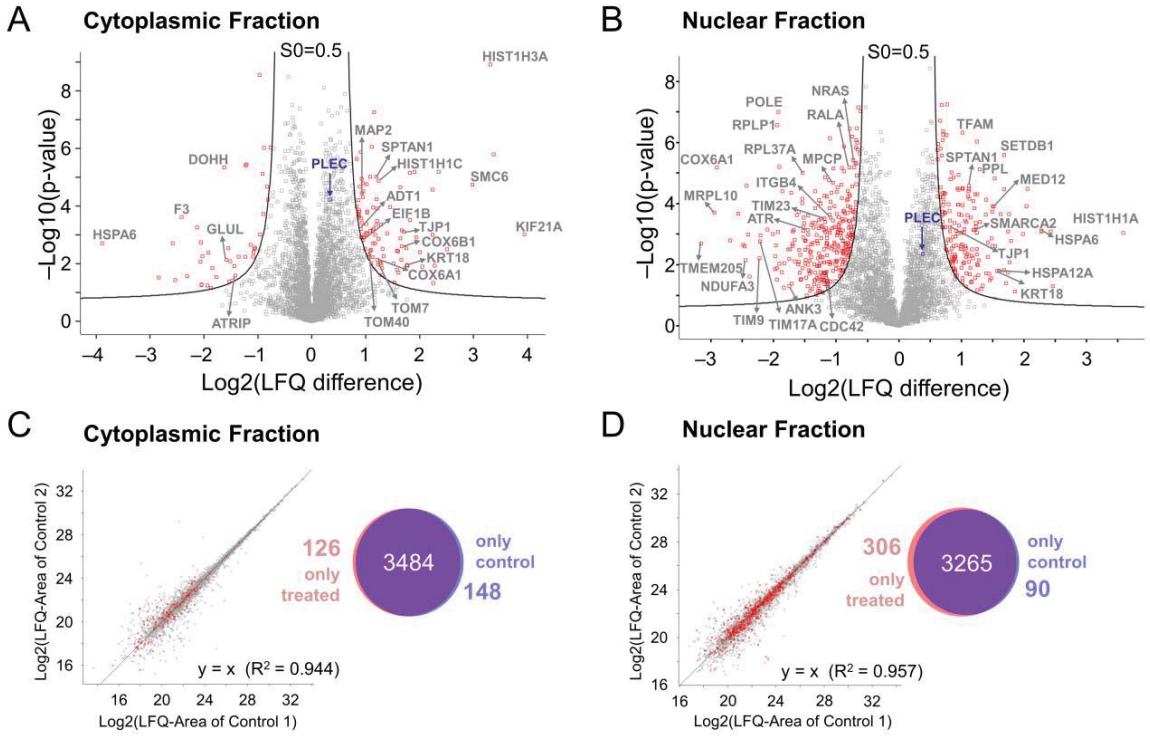

Figure S3. (**A**) Volcano plot of label-free proteome profiling of HCT116 cells treated with plecstatin-2 at half-IC_{50} concentration for 24 h, cytoplasmic fraction. Of the total of 3761 cytoplasmic proteins, 135 were significantly regulated upon treatment. Significantly changed proteins are highlighted in red, plectin (PLEC) in blue. (**B**) Similar volcano plot depicting the nuclear (insoluble) fraction. Of the total of 3665 nuclear proteins, 478 were significantly regulated upon treatment with plecstatin-2. Scatter plots of the label-free proteome profiling depicting the biological replicates control 1 and control 2 of the cytoplasmic (**C**) and nuclear fraction (**D**) of HCT116 cells. Significantly regulated proteins are highlighted in red. Criteria for significant regulation: FDR 0.05, 250 cycles and S=0.5. The correlation coefficient for y = x is given. The Venn diagrams show the proteins identified in the control and the treated cells.

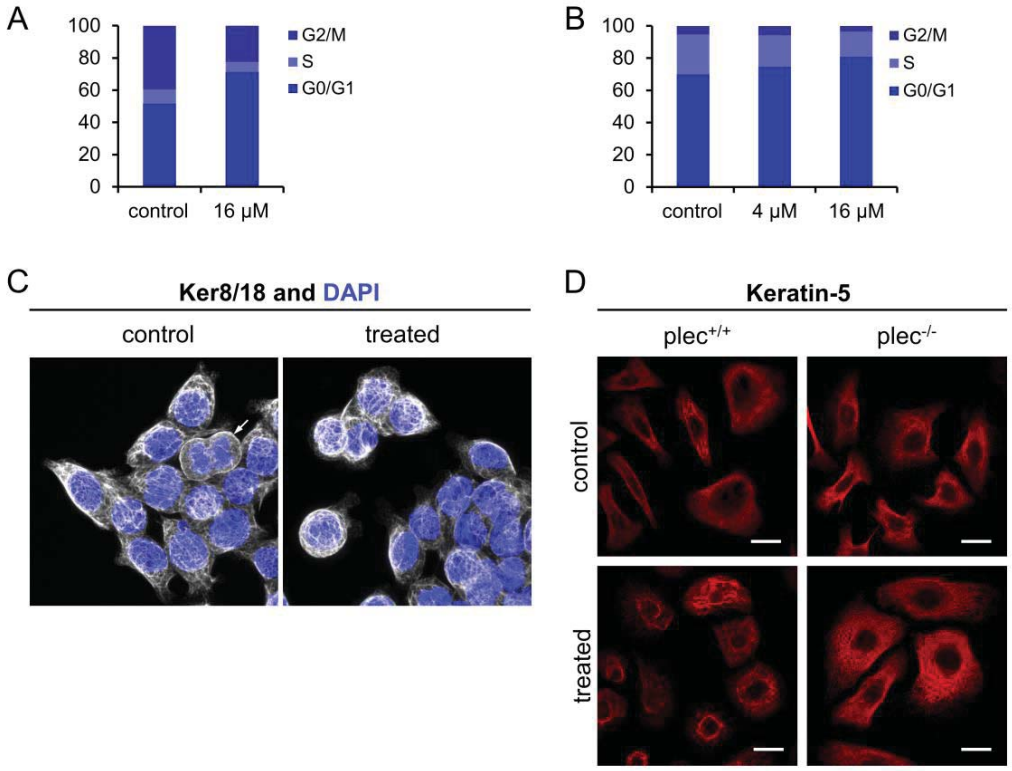

Figure S4. (**A**) Cell cycle analysis of HCT116 cells in exponential growth treated with plecstatin-2 (16 µM). (**B**) Cell cycle analysis of nearly confluent HCT116 cells treated with 4 and 16 µM plecstatin-2. (**C**) Immunofluorescence microscopy of HCT116 cells with Ker8/18 antibody and DAPI, treated with 16 µM plecstatin-2. The keratins are not affected by the drug treatment. (**D**) Wild-type ($plec^{+/+}$) or plectin-deficient ($plec^{-/-}$) keratinocyte cell cultures were treated with half-IC_{50} of plecstatins-2 and subsequently subjected to immunofluorescence microscopy using antibodies to proteins indicated. Untreated cells werved as controls. The scale bars represent 20 µM.

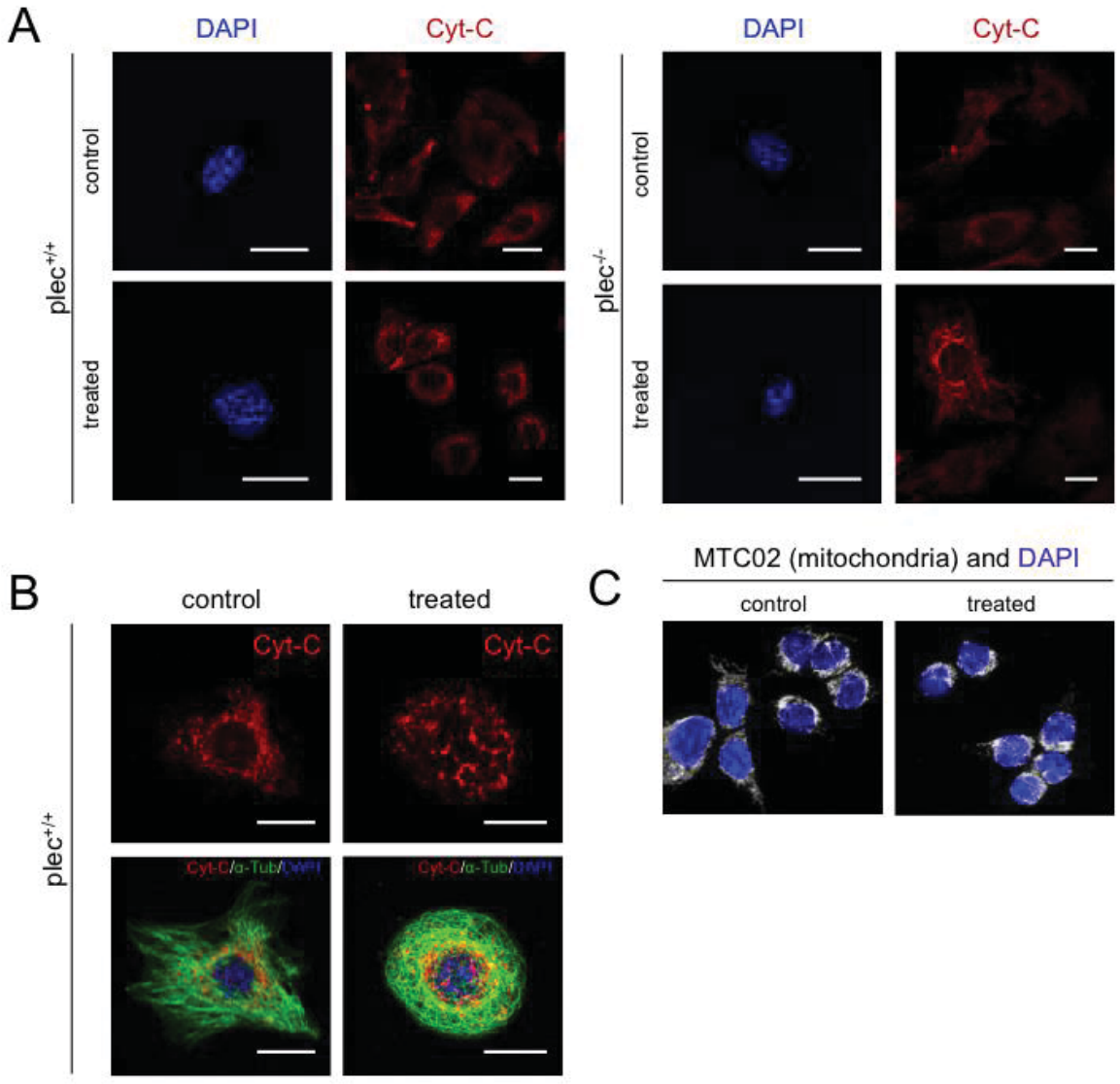

Figure S5. (**A**) Visualization of nuclei and mitochondria in wild-type ($plec^{+/+}$) and plectin knock-out ($plec^{-/-}$) keratinocytes treated with subcytotoxic concentrations of plecstatin-2. Nuclei and mitochondria were labelled with DAPI and antibodies to cytochrome C (Cyt-C), respectively. Control, cells without drug treatment. Scale bars represent 20 µm. (**B**) Triple labeling of control and drug-treated $plec^{+/+}$ keratinocytes visualizing cytochrome C (Cyt-C), MTs (α-Tub), and nuclei (DAPI). Scale bars represent 20 µm. (**C**) Immunofluorescent staining of HCT116 cells with anti-Mitochondria antibody (MTC02) and DAPI in drug-untreated (control) and treated cells. A bundling of mitochondria was observed next to the nuclear envelope.

A

	IC50 (μM) in HCT116	
	AB assay 2D	AB assay 3D
plecstatin-2	68 ± 16	> 400

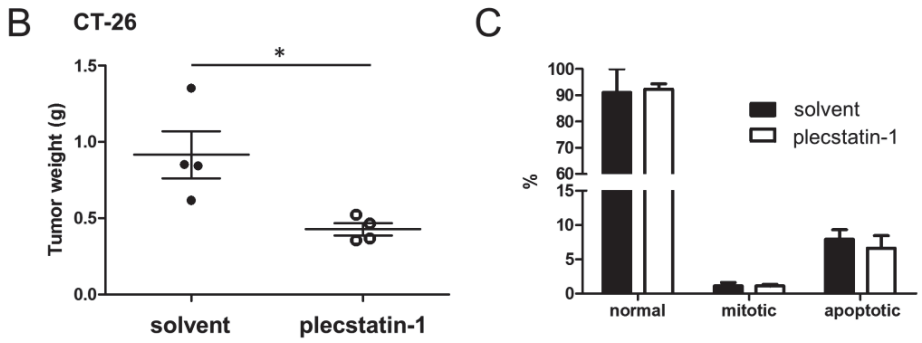

Figure S6. (**A**) The antiproliferative activity of plecstatin-2 was assessed by the AlamarBlue assay in order to relate to the 3D spheroid model. The IC_{50} concentrations in μM are reported in 2D and 3D cell culture. (**B**) Cumulative efficacy of reduction of tumour weight after two-weeks oral treatment in the CT-26 xenograft model. * = Significant reduction of tumour weight by plecstatin-1 (30 mg/kg, days 3–7 and 10–14) with respect to control ($p<0.05$) calculated by one-way ANOVA with Dunet posttest. (**C**) Histological analysis of the CT-26 tumors. The tumors did not show altered fractions of apoptosis or mitosis.

Table S2. Assignment of PRIDE Identifiers to the corresponding data set.

Data Identifier	Sample Type
PXD005373	cytoplasmic proteins of untreated HCT 116 epithelial cells, 24h
PXD005374	cytoplasmic proteins of plecstatin-2 treated HCT 116 epithelial cells, 24h
PXD005375	nuclear proteins of untreated HCT 116 epithelial cells, 24h
PXD005376	nuclear proteins of plecstatin-2 treated HCT 116 epithelial cells, 24h
PXD005389	whole cell lysate of HCT 116 epithelial cells, plecstatin-3 normal pull down 4h
PXD005386	whole cell lysate of HCT 116 epithelial cells, plecstatin-3 competitive pull down 4h

Table S3. Gene Ontology (GO) term analysis of significantly upregulated (258 proteins) and down-regulated (342 proteins) of plecstatin-2 treated HCT116 cells. The counts refer to number of proteins associated with a given protein. The Q-value is a multiple testing corrected P-value according to Benjamini-Hochberg for the enrichment of proteins for a given term. Finally, KEGG pathway analysis was performed with the significantly regulated proteins employing similar metrics.

GO Category	Upregulated LFQ values		
	Term	**Count**	**Q-value**
BP	RNA splicing	29	2.6E-12
	RNA processing	35	6.2E-10
	Chromatin organization	27	1.6E-08
	Histone modification	11	1.6E-03
	Regulation of actin filament depolymerization	5	4.3E-02
CC	Nuclear lumen	78	7.4E-24
	Spliceosome	13	1.4E-05
	Cytoskeleton	41	3.1E-04
	Ribonucleoprotein complex	19	9.1E-03
	Histone acetyltransferase complex	6	1.0E-02
GO Category	**Down-regulated LFQ values**		
	Term	**Count**	**Q-value**
BP	Translation	42	3.2E-18
	Translational elongation	15	8.1E-06
	Mitochondrion organization	14	1.7E-03
	RNA processing	25	3.0E-02
CC	Ribosome	45	7.3E-28
	Mitochondrion	90	4.2E-27
	Cytosolic ribosome	13	3.6E-06

References

[1] S. M. Meier, M. Hanif, Z. Adhireksan, V. Pichler, M. Novak, E. Jirkovsky, M. A. Jakupec, V. B. Arion, C. A. Davey, B. K. Keppler, C. G. Hartinger, *Chem. Sci.* **2013**, *4*, 1837-1846.
[2] F. K. Cheung, C. Lin, F. Minissi, A. L. Criville, M. A. Graham, D. J. Fox, M. Wills, *Org. Lett.* **2007**, *9*, 4659-4662.
[3] M. A. Bennett, A. K. Smith, *J. Chem. Soc. Dalton Trans.* **1974**, 233-241.
[4] W. A. Kinney, N. E. Lee, R. M. Blank, C. A. Demerson, C. S. Sarnella, N. T. Scherer, G. N. Mir, L. E. Borella, J. F. Dijoseph, C. Wells, *J. Med. Chem.* **1990**, *33*, 327-336.
[5] S. Göschl, H. P. Varbanov, S. Theiner, M. A. Jakupec, M. Galanski, B. K. Keppler, *J. Inorg. Biochem.* **2016**, *160*, 264-274.
[6] W. Huang da, B. T. Sherman, R. A. Lempicki, *Nat. Protocols* **2009**, *4*, 44-57.
[7] D. Mellacheruvu, Z. Wright, A. L. Couzens, J. P. Lambert, N. A. St-Denis, T. Li, Y. V. Miteva, S. Hauri, M. E. Sardiu, T. Y. Low, V. A. Halim, R. D. Bagshaw, N. C. Hubner, A. Al-Hakim, A. Bouchard, D. Faubert, D. Fermin, W. H. Dunham, M. Goudreault, Z. Y. Lin, B. G. Badillo, T. Pawson, D. Durocher, B. Coulombe, R. Aebersold, G. Superti-Furga, J. Colinge, A. J. Heck, H. Choi, M. Gstaiger, S. Mohammed, I. M. Cristea, K. L. Bennett, M. P. Washburn, B. Raught, R. M. Ewing, A. C. Gingras, A. I. Nesvizhskii, *Nat. Methods* **2013**, *10*, 730-736.
[8] A. E. Egger, C. Rappel, M. A. Jakupec, C. G. Hartinger, P. Heffeter, B. K. Keppler, *J Anal. At. Spectrom.* **2009**, *24*, 51-61.

Complete References from main text having more than 10 authors:

[2] Z. Adhireksan, G. E. Davey, P. Campomanes, M. Groessl, C. M. Clavel, H. Yu, A. A. Nazarov, C. H. Yeo, W. H. Ang, P. Droge, U. Rothlisberger, P. J. Dyson, C. A. Davey, *Nat. Commun.* **2014**, *5*, 3462.
[4] S. M. Meier, M. Hanif, Z. Adhireksan, V. Pichler, M. Novak, E. Jirkovsky, M. A. Jakupec, V. B. Arion, C. A. Davey, B. K. Keppler, C. G. Hartinger, *Chem. Sci.* **2013**, *4*, 1837-1846.
[9] M. V. Babak, S. M. Meier, K. V. M. Huber, J. Reynisson, A. A. Legin, M. A. Jakupec, A. Roller, A. Stukalov, M. Gridling, K. L. Bennett, J. Colinge, W. Berger, P. J. Dyson, G. Superti-Furga, B. K. Keppler, C. G. Hartinger, *Chem. Sci.* **2015**, *6*, 2449-2456.
[11] D. Mellacheruvu, Z. Wright, A. L. Couzens, J. P. Lambert, N. A. St-Denis, T. Li, Y. V. Miteva, S. Hauri, M. E. Sardiu, T. Y. Low, V. A. Halim, R. D. Bagshaw, N. C. Hubner, A. Al-Hakim, A. Bouchard, D. Faubert, D. Fermin, W. H. Dunham, M. Goudreault, Z. Y. Lin, B. G. Badillo, T. Pawson, D. Durocher, B. Coulombe, R. Aebersold, G. Superti-Furga, J. Colinge, A. J. Heck, H. Choi, M. Gstaiger, S. Mohammed, I. M. Cristea, K. L. Bennett, M. P. Washburn, B. Raught, R. M. Ewing, A. C. Gingras, A. I. Nesvizhskii, *Nat. Methods* **2013**, *10*, 730-736.
[13] A. Franceschini, D. Szklarczyk, S. Frankild, M. Kuhn, M. Simonovic, A. Roth, J. Lin, P. Minguez, P. Bork, C. von Mering, L. J. Jensen, *Nucleic Acids Res.* **2013**, *41*, D808-D815.
[14] K. Kunimoto, Y. Yamazaki, T. Nishida, K. Shinohara, H. Ishikawa, T. Hasegawa, T. Okanoue, H. Hamada, T. Noda, A. Tamura, S. Tsukita, *Cell* **2012**, *148*, 189-200.

Author Contributions

S.M.M., L.W., B.K.K, G.W. and C.G. conceived the study and planned experiments. S.M.M, G.W. and C.G. wrote the manuscript with support from all authors. S.M.M. synthesized the plestatins. D.K., L.W. and A.Bi. performed *in vitro* studies. L.W. performed immunofluorescence microscopy with keratinocytes and T.W. with HCT116 cells. J.C.M. optimized digestion conditions. S.J., A.C. and A.Bh. performed MMP and ROS assays. A.Bi. and S.M.M. performed MS analysis and evaluated data. B.A., P.H. and W.B. planned and performed the *in vivo* experiments. S.M.M. and C.G.H performed the COMPARE analysis. K.C. and M.A.J. planned and performed spheroid invasion assays. M.H.M.K., M.H., M.A.J. and S.M.M. planned and performed uptake studies.

Conclusions

Elucidating drug effects is a challenging, but crucial task in drug discovery and development. Even though many assays are applied during first screening efforts, they often give little information on the molecular level and hence on the underlying mechanism. This doctoral thesis clearly demonstrated the promise of label-free shotgun proteomics to gain insights into drug effects on the level of the proteome, especially with respect to potential novel or unknown mechanisms of next-generation metal-based anticancer agents and natural products. Furthermore, target identification was successfully achieved for the ruthenium-based plecstatin. The established profiling methods allowed analyzing 30.000 peptides per 135 min run on average, amounting to approximately 5.000 protein groups covering a concentration range of 6–8 orders of magnitude. Significant regulatory effects on protein abundance were assessed in a biologically reproducible and technically repeatable way illustrating the stability of cell culture experiments, sample preparation and the MS performance.

The shotgun-proteomics approach presented in this thesis enables the generation of hypotheses about global pharmacological effects of various compounds, which can be further explored in targeted investigations. A strong context-dependency of drug responses was observed in various cell culture models that emphasized the massive impact of the microenvironment on cellular adaptions under stress. Obviously, every system can respond differently to one and the same drug. These cell-type specific drug responses even occur in cells from the same tissue and illustrate the importance of their detailed molecular characterizations. Basal protein abundances characteristic for a given cancer cell line may influence protein regulations upon different kinds of stress, e.g. oxidative stress or DNA damage, better than others. For example, the colon cancer cell line HCT116 displayed a 34-fold higher expression of peroxiredoxins compared to SW480 that are involved in the Nrf2-Keap1 pathway of dealing with redox stress. Moreover, the impact of the microenvironment was investigated in a systematic fashion by employing co-culture models of stromal and cancer cells and shotgun-proteomics turned out to be well suited for such purposes.

Drug responses may vary significantly in individuals. It is therefore important to understand the underlying mechanistic similarities and differences of drug effects to be able to predict drug responses. Specifically, understanding both robust and specific effects could support predictions on drug efficacy in patients. Acute disease symptoms are often controlled with conventional drugs targeting single molecules or mechanisms, e.g. pain is treated with cyclooxygenase-inhibitors.

However, chronic diseases (e.g. cancer) cannot be cured analogously. Label-free shotgun proteomics offers completely new aspects for assessing drug effects.

Effective target identification and a better understanding of mechanisms of action improve the ability to predict a drug's prospect of success during development. Identified sets of proteins from proteomic analyses might be taken to predict sensitivity or resistance toward a drug, and hence may support the development of improved patient stratification strategies and personalized anti-cancer therapies which are urgently needed in the clinics.

4. Abstract

A better understanding of drug targets and the underlying modes of action are of great importance for drug development and application in clinical practice. The traditionally employed and well established phenotypic assays for cell cycle, viability and death analysis give little information about global effects on a molecular basis. Proteins are increasingly identified as drug targets and hold great potential for the elucidation of modes of action since they are the active players within cell, responsible for cellular fate and function. Therefore, a label-free quantification proteomics approach based on liquid chromatography-tandem mass spectrometry (LC-MS/MS) was employed to evaluate protein abundances in treated and untreated cells, *i.e.* response profiling. Drug effects were investigated in different cell culture models by response profiling of (i) the metal-based anticancer drugs As_2O_3, KP46 (gallium), KP772 (lanthanum), NKP-1339 (ruthenium) and KP1537 (platinum) and (ii) the naturally occurring biphenol curcumin.

Colon carcinoma cells were exposed to the metallodrugs and subsequently fractionated into cytoplasmic and nuclear extracts to gain a deeper insight into the regulatory effects. For a better representation of the *in vivo* situation, investigations on curcumin effects executed not only with single cell type cultures but also with tumor-stroma co-culture models of breast cancer and cancer-associated fibroblast-like cells. Whole cell lysates were obtained for this study. Overall, 5525 and 5780 protein groups were identified by LC-MS/MS analysis of in-solution digested colon and breast cancer samples, respectively. Remarkably great differences of basal protein abundances were observed in the diverse cells, even if they derived from the same tissue. This circumstance may substantially affect protein regulations upon drug exposure. Global effects of the investigated metallodrugs on the proteome were characterized and hypotheses on hitherto unrecognized mechanisms were generated. Response profiling of curcumin demonstrated strong context-dependent effects, emphasizing the massive contribution of the microenvironment to drug responses. The findings of this thesis might contribute to the improvement of drug evaluation as well as patient stratification strategies.

5. Zusammenfassung (German Abstract)

Für die Entwicklung eines Wirkstoffes und dessen klinische Anwendung ist ein besseres Verständnis seiner zellulären Targets und Wirkungsweise von enormer Bedeutung. Die derzeit eingesetzten phänotypischen Analysemethoden für Zellzyklus, Viabilität und Zelltod haben sich bewährt, liefern allerdings wenig Informationen über globale Effekte auf molekularer Ebene. Proteine werden zunehmend als Wirkstofftargets identifiziert und aufgrund ihrer Schlüsselfunktionen in zellulären Abläufen, weisen sie großes Potential für die Aufklärung von Wirkmechanismen auf. Deshalb wurde eine auf Flüssigchromatographie (LC) und Tandem-Massenspektrometrie (MS/MS) basierende Label-freie Proteomanalysemethode herangezogen, um Unterschiede in Proteinabundanzen zwischen mit Medikamenten behandelten und unbehandelten Zellen zu evaluieren. In verschiedenen Zellkuturmodellen wurden die Effekte von (i) den Metall-basierenden Antikrebswirkstoffen As_2O_3, KP46 (Gallium), KP772 (Lanthan), NKP-1339 (Ruthenium) und KP1537 (Platin) sowie (ii) dem natürlich vorkommenden Biphenol Kurkumin untersucht.

Colonkarzinomzellen wurden mit den Metallverbindungen behandelt und anschließend in Zytoplasma und Krenextrakt fraktioniert, um einen tieferen Einblick in die stattfindenden regulatorischen Prozesse zu erhalten. Zur besseren Repräsentation der *in vivo* Situation, wurden Kurkumineffekte in Co-Kulturmodellen von Brustkrebszellen mit Krebsassoziierten-Fibroblasten untersucht. Hierfür wurden Gesamtzelllysate analysiert. Insgesamt wurden 5525 beziehungsweise 5780 Proteingruppen in den enzymatisch verdauten Colonkarzinom- und Brustkrebsproben mittels LC-MS/MS identifiziert. Die basalen Proteinkonzentrationen variierten stark zwischen den verschiedenen Zellen, auch wenn sie von dem gleichen Gewebe stammten, wodurch Proteinregulationen durch Wirkstoffbehandlungen entscheidend beeinflusst werden können. Die Untersuchungen der Effekte der Metallverbindungen auf das Proteom ermöglichten die Generierung von Hypothesen bezüglich ihrer Wirkmechanismen, die bis dahin unbekannt waren. Die Proteomanalysen der Kurkumineffekte zeigten, dass die Reaktion auf einen Wirkstoff stark kontextabhängig ist und die Tumormikroumgebung einen massiven Einfluss darauf ausübt. Die Ergebnisse dieser Dissertation könnten zu einer Verbesserung des Wirkstoffevaluierungsprozesses und von Patientenstratifizierungsstrategien führen.

6. Scientific Contributions

6.1. List of Publications

1. Kreutz D, Sinthuvanich C, Bileck A, Janker L, Slany A, Gerner C. „Curcumin exerts its antitumor effects in a context dependent fashion“, *J Proteom*. **2018**, 182:65-72

2. Meier SM, Kreutz D, Winter L, Klose MHM, Cseh K, Weiss T, Bileck A, Alte B, Mader JC, Jana S, Chatterjee A, Bhattacharyya A, Hejl M, Jakupec MA, Heffeter P, Berger W, Hartinger CG, Keppler BK, Wiche G, Gerner C. “An organoruthenium anticancer agent shows unexpected target selectivity for plectin” *Angew Chem Int Ed Engl*. **2017**; 56(28):8267–8271

3. Tahir A, Bileck A, Muqaku B, Niederstaetter L, Kreutz D, Mayer RL, Wolrab D, Meier SM, Slany A, Gerner C. “Combined proteome and eicosanoid profiling approach for revealing implications of human fibroblasts in chronic inflammation” *Anal Chem*. **2017**; 89(3):1945–1954

4. Kreutz D, Bileck A, Plessl K, Wolrab D, Groessl M, Keppler BK, Meier SM, Gerner C. “Response profiling using shotgun proteomics enables global metallodrug mechanisms of action to be established“ *Chemistry*. **2017**; 23(8):1881–1890

5. Bileck A, Mayer RL, Kreutz D, Weiss T, Taschner-Mandl S, Meier SM, Slany A, Gerner C. “Evaluation of inflammation-related signaling events covering phosphorylation and nuclear translocation of proteins based on mass spectrometry data” *J Proteomics*. **2017**; 152:161–171

6. Muqaku B, Tahir A, Klepeisz P, Bileck A, Kreutz D, Mayer RL, Meier SM, Gerner M, Schmetterer K, Gerner C. ”Coffee consumption modulates inflammatory processes in an individual fashion” *Mol Nutr Food Res*. **2016**; 60(12):2529–2541

7. Slany A, Bileck A, Kreutz D, Mayer RL, Muqaku B, Gerner C. “Contribution of human fibroblasts and endothelial cells to the hallmarks of inflammation as determined by proteome profiling” *Mol Cell Proteomics*. **2016**; 15(6):1982–97

8. Meier SM, Muqaku B, Ullmann R, Bileck A, Kreutz D, Mader JC, Knasmüller S, Gerner C. “Proteomic and metabolomic analyses reveal contrasting anti-inflammatory effects of an extract of mucor racemosus secondary metabolites compared to dexamethasone” *PLoS One*. **2015**; 10(10):e0140367

9. Muqaku B, Slany A, Bileck A, Kreutz D, Gerner C. “Quantification of cytokines secreted by primary human cells using multiple reaction monitoring: evaluation of analytical parameters” *Anal Bioanal Chem*. **2015**; 407(21):6525–36

10. Bileck A, Kreutz D, Muqaku B, Slany A, Gerner C. “Comprehensive assessment of proteins regulated by dexamethasone reveals novel effects in primary human peripheral blood mononuclear cells” *J Proteome Res*. **2014**; 13(12):5989–6000

11. Groessl M, Slany A, Bileck A, Gloessmann K, Kreutz D, Jaeger W, Pfeiler G, Gerner C. “Proteome profiling of breast cancer biopsies reveals a wound healing signature of cancer-associated fibroblasts” *J Proteome Res*. **2014**; 13(11):4773–82

6.2. List of Oral Contributions

03/16/2018 Invited guest lecture for Special Research Program SFB-54: "InThro", Medical University of Vienna (Vienna, Austria): *"Investigation of drug effects by in-depth label-free proteome profiling"*

02/20-21/2018 29th MassSpec Forum Vienna (Vienna, Austria): *"Curcumin exerts its antitumor effects in a context dependent fashion"*

09/21-24/2015 16th Austrian Chemistry Days (Innsbruck, Austria): *"Investigation of novel metal-based anticancer drug candidates' mechanisms of action by in-depth proteome profiling"*

08/26-28/2015 13th Austrian Proteomic Research Symposium (Klosterneuburg, Austria): *"Proteome profiling for evaluation of drug effects – a pilot study using a resveratrol derivative"*

06/12-13/2015 11th ASAC JunganalytikerInnenforumm (Innsbruck, Austria): *"Assessment of drug-induced proteome alterations exemplified on four breast cancer cell lines treated with the resveratrol derivative 3,3',4,4',5,5'-hexahydroxystilbene"*

09/02-04/2013 1st International Symposium on Profiling (Lisbon, Portugal): *"Assessment of drug effects exemplified by activated PBMCs treated with Aspirin and Dexamethasone, respectively"*

6.3. List of Poster Contributions

07/20-22/2015 British Society for Proteome Research 2015 Meeting (Reading, United Kingdom): *"Assessment of drug-induced proteome alterations exemplified on four breast cancer cell lines treated with the resveratrol derivative 3,3',4,4',5,5'-hexahydroxystilbene"*

10/05-08/2014 13th Human Proteome Organization World Congress (Madrid, Spain): *"Evaluation of mode of action as well as resistance mechanisms regarding the novel anticancer Ruthenium compound KP1339 by proteome profiling"*

09/22-24/2014 12th Austrian Proteomic Research Symposium (Salzburg, Austria): *"Proteome profiling allows evaluating resistance mechanisms of tumor cells against the anticancer Ruthenium compound KP1339"*

„Ich habe mich bemüht, sämtliche Inhaber der Bildrechte ausfindig zu machen und ihre Zustimmung zur Verwendung der Bilder in dieser Arbeit eingeholt. Sollte dennoch eine Urheberrechtsverletzung bekannt werden, ersuche ich um Meldung bei mir.“

D. Kreutz
Juni, 2018